

ENERGY PATH ANALYSIS OF CIRCULAR CONFINED CONCRETE COLUMNS SUBJECTED TO AXIAL COMPRESSION

Dissertation

Presented to Faculty of Engineering, Kanagawa University in Partial
Fulfillment of the Requirements for the Degree of Doctor of Engineering

Submitted by

Di Yang

Supervised by

Professor **Kazushi Shimazaki**

CONTENTS

ACKNOWLEDGMENTS	i
ABSTRACT	iii
CHAPTER 1. INTRODUCTION	1
1.1. Background.....	1
1.2. Objectives and organization	2
References	4
CHAPTER 2. ENERGY PATH OF CIRCULAR CONCRETE-FILLED STEEL TUBE STUB COLUMNS UNDER AXIAL COMPRESSION	5
2.1. Introduction	5
2.2. Experimental program	7
2.2.1. Definition and determination of the energy path	7
2.2.2. Experimental Setup.....	12
2.2.3. Experimental results	14
2.3. Investigation of the energy path.....	15
2.3.1. Evaluation indices of the energy path.....	15
2.3.2. Parametric analysis of the energy path	17
2.3.3. Comparison of energy path and stress path	19
2.4. Energy path-based load-bearing capacity of CFST columns	23
2.4.1. Effect of energy path on concrete compressive strength	23
2.4.2. Load-bearing capacity of CFST columns and verification	25
2.5. Conclusions	30
CHAPTER 3. ENERGY PATH OF FRP-CONFINED CONCRETE STUB COLUMNS SUBJECTED TO AXIAL COMPRESSION	37
3.1. Introduction	37
3.2. Evaluation method of energy path.....	38
3.2.1. Definition of the energy path.....	38
3.2.2. Evaluation index of the energy path	41
3.3. Experimental programs	42
3.3.1. Details of the specimens and test.....	42
3.3.2. Experimental results	43
3.4. Investigation of energy path.....	45
3.4.1. Theoretical study on energy path	45
3.4.2. Experimental observation of energy path	48
3.4.3. Relationship between energy path and compressive strength.....	51
3.5. Conclusions	52
CHAPTER 4. LOAD-BEARING CAPACITY ANALYSIS BASED ON ENERGY PATH	56
4.1. Introduction	56
4.2. Confining action of the steel tube and FRP jacket	57
4.2.1. Confining action of the CFST column	57
4.2.2. Confining action of the FRP-confined concrete column	58
4.3. The stress path of actively and passively confined concrete.....	59
4.4. Equivalent lateral stress of passively confined concrete	60
4.4.1. Equivalent lateral stress of steel-confined concrete	60
4.4.2. Equivalent lateral stress of FRP-confined concrete	62

1	1.1 Introduction
2	1.2 Objectives of the course
3	1.3 Scope of the course
4	1.4 Prerequisites
5	1.5 Course structure
6	1.6 Assessment
7	1.7 References
8	2.1 Introduction
9	2.2 Objectives of the chapter
10	2.3 Scope of the chapter
11	2.4 Prerequisites
12	2.5 Course structure
13	2.6 Assessment
14	2.7 References
15	3.1 Introduction
16	3.2 Objectives of the chapter
17	3.3 Scope of the chapter
18	3.4 Prerequisites
19	3.5 Course structure
20	3.6 Assessment
21	3.7 References
22	4.1 Introduction
23	4.2 Objectives of the chapter
24	4.3 Scope of the chapter
25	4.4 Prerequisites
26	4.5 Course structure
27	4.6 Assessment
28	4.7 References
29	5.1 Introduction
30	5.2 Objectives of the chapter
31	5.3 Scope of the chapter
32	5.4 Prerequisites
33	5.5 Course structure
34	5.6 Assessment
35	5.7 References
36	6.1 Introduction
37	6.2 Objectives of the chapter
38	6.3 Scope of the chapter
39	6.4 Prerequisites
40	6.5 Course structure
41	6.6 Assessment
42	6.7 References
43	7.1 Introduction
44	7.2 Objectives of the chapter
45	7.3 Scope of the chapter
46	7.4 Prerequisites
47	7.5 Course structure
48	7.6 Assessment
49	7.7 References
50	8.1 Introduction
51	8.2 Objectives of the chapter
52	8.3 Scope of the chapter
53	8.4 Prerequisites
54	8.5 Course structure
55	8.6 Assessment
56	8.7 References
57	9.1 Introduction
58	9.2 Objectives of the chapter
59	9.3 Scope of the chapter
60	9.4 Prerequisites
61	9.5 Course structure
62	9.6 Assessment
63	9.7 References
64	10.1 Introduction
65	10.2 Objectives of the chapter
66	10.3 Scope of the chapter
67	10.4 Prerequisites
68	10.5 Course structure
69	10.6 Assessment
70	10.7 References
71	11.1 Introduction
72	11.2 Objectives of the chapter
73	11.3 Scope of the chapter
74	11.4 Prerequisites
75	11.5 Course structure
76	11.6 Assessment
77	11.7 References
78	12.1 Introduction
79	12.2 Objectives of the chapter
80	12.3 Scope of the chapter
81	12.4 Prerequisites
82	12.5 Course structure
83	12.6 Assessment
84	12.7 References
85	13.1 Introduction
86	13.2 Objectives of the chapter
87	13.3 Scope of the chapter
88	13.4 Prerequisites
89	13.5 Course structure
90	13.6 Assessment
91	13.7 References
92	14.1 Introduction
93	14.2 Objectives of the chapter
94	14.3 Scope of the chapter
95	14.4 Prerequisites
96	14.5 Course structure
97	14.6 Assessment
98	14.7 References
99	15.1 Introduction
100	15.2 Objectives of the chapter
101	15.3 Scope of the chapter
102	15.4 Prerequisites
103	15.5 Course structure
104	15.6 Assessment
105	15.7 References
106	16.1 Introduction
107	16.2 Objectives of the chapter
108	16.3 Scope of the chapter
109	16.4 Prerequisites
110	16.5 Course structure
111	16.6 Assessment
112	16.7 References
113	17.1 Introduction
114	17.2 Objectives of the chapter
115	17.3 Scope of the chapter
116	17.4 Prerequisites
117	17.5 Course structure
118	17.6 Assessment
119	17.7 References
120	18.1 Introduction
121	18.2 Objectives of the chapter
122	18.3 Scope of the chapter
123	18.4 Prerequisites
124	18.5 Course structure
125	18.6 Assessment
126	18.7 References
127	19.1 Introduction
128	19.2 Objectives of the chapter
129	19.3 Scope of the chapter
130	19.4 Prerequisites
131	19.5 Course structure
132	19.6 Assessment
133	19.7 References
134	20.1 Introduction
135	20.2 Objectives of the chapter
136	20.3 Scope of the chapter
137	20.4 Prerequisites
138	20.5 Course structure
139	20.6 Assessment
140	20.7 References
141	21.1 Introduction
142	21.2 Objectives of the chapter
143	21.3 Scope of the chapter
144	21.4 Prerequisites
145	21.5 Course structure
146	21.6 Assessment
147	21.7 References
148	22.1 Introduction
149	22.2 Objectives of the chapter
150	22.3 Scope of the chapter
151	22.4 Prerequisites
152	22.5 Course structure
153	22.6 Assessment
154	22.7 References
155	23.1 Introduction
156	23.2 Objectives of the chapter
157	23.3 Scope of the chapter
158	23.4 Prerequisites
159	23.5 Course structure
160	23.6 Assessment
161	23.7 References
162	24.1 Introduction
163	24.2 Objectives of the chapter
164	24.3 Scope of the chapter
165	24.4 Prerequisites
166	24.5 Course structure
167	24.6 Assessment
168	24.7 References
169	25.1 Introduction
170	25.2 Objectives of the chapter
171	25.3 Scope of the chapter
172	25.4 Prerequisites
173	25.5 Course structure
174	25.6 Assessment
175	25.7 References
176	26.1 Introduction
177	26.2 Objectives of the chapter
178	26.3 Scope of the chapter
179	26.4 Prerequisites
180	26.5 Course structure
181	26.6 Assessment
182	26.7 References
183	27.1 Introduction
184	27.2 Objectives of the chapter
185	27.3 Scope of the chapter
186	27.4 Prerequisites
187	27.5 Course structure
188	27.6 Assessment
189	27.7 References
190	28.1 Introduction
191	28.2 Objectives of the chapter
192	28.3 Scope of the chapter
193	28.4 Prerequisites
194	28.5 Course structure
195	28.6 Assessment
196	28.7 References
197	29.1 Introduction
198	29.2 Objectives of the chapter
199	29.3 Scope of the chapter
200	29.4 Prerequisites
201	29.5 Course structure
202	29.6 Assessment
203	29.7 References
204	30.1 Introduction
205	30.2 Objectives of the chapter
206	30.3 Scope of the chapter
207	30.4 Prerequisites
208	30.5 Course structure
209	30.6 Assessment
210	30.7 References
211	31.1 Introduction
212	31.2 Objectives of the chapter
213	31.3 Scope of the chapter
214	31.4 Prerequisites
215	31.5 Course structure
216	31.6 Assessment
217	31.7 References
218	32.1 Introduction
219	32.2 Objectives of the chapter
220	32.3 Scope of the chapter
221	32.4 Prerequisites
222	32.5 Course structure
223	32.6 Assessment
224	32.7 References
225	33.1 Introduction
226	33.2 Objectives of the chapter
227	33.3 Scope of the chapter
228	33.4 Prerequisites
229	33.5 Course structure
230	33.6 Assessment
231	33.7 References
232	34.1 Introduction
233	34.2 Objectives of the chapter
234	34.3 Scope of the chapter
235	34.4 Prerequisites
236	34.5 Course structure
237	34.6 Assessment
238	34.7 References
239	35.1 Introduction
240	35.2 Objectives of the chapter
241	35.3 Scope of the chapter
242	35.4 Prerequisites
243	35.5 Course structure
244	35.6 Assessment
245	35.7 References
246	36.1 Introduction
247	36.2 Objectives of the chapter
248	36.3 Scope of the chapter
249	36.4 Prerequisites
250	36.5 Course structure
251	36.6 Assessment
252	36.7 References
253	37.1 Introduction
254	37.2 Objectives of the chapter
255	37.3 Scope of the chapter
256	37.4 Prerequisites
257	37.5 Course structure
258	37.6 Assessment
259	37.7 References
260	38.1 Introduction
261	38.2 Objectives of the chapter
262	38.3 Scope of the chapter
263	38.4 Prerequisites
264	38.5 Course structure
265	38.6 Assessment
266	38.7 References
267	39.1 Introduction
268	39.2 Objectives of the chapter
269	39.3 Scope of the chapter
270	39.4 Prerequisites
271	39.5 Course structure
272	39.6 Assessment
273	39.7 References
274	40.1 Introduction
275	40.2 Objectives of the chapter
276	40.3 Scope of the chapter
277	40.4 Prerequisites
278	40.5 Course structure
279	40.6 Assessment
280	40.7 References
281	41.1 Introduction
282	41.2 Objectives of the chapter
283	41.3 Scope of the chapter
284	41.4 Prerequisites
285	41.5 Course structure
286	41.6 Assessment
287	41.7 References
288	42.1 Introduction
289	42.2 Objectives of the chapter
290	42.3 Scope of the chapter
291	42.4 Prerequisites
292	42.5 Course structure
293	42.6 Assessment
294	42.7 References
295	43.1 Introduction
296	43.2 Objectives of the chapter
297	43.3 Scope of the chapter
298	43.4 Prerequisites
299	43.5 Course structure
300	43.6 Assessment
301	43.7 References
302	44.1 Introduction
303	44.2 Objectives of the chapter
304	44.3 Scope of the chapter
305	44.4 Prerequisites
306	44.5 Course structure
307	44.6 Assessment
308	44.7 References
309	45.1 Introduction
310	45.2 Objectives of the chapter
311	45.3 Scope of the chapter
312	45.4 Prerequisites
313	45.5 Course structure
314	45.6 Assessment
315	45.7 References
316	46.1 Introduction
317	46.2 Objectives of the chapter
318	46.3 Scope of the chapter
319	46.4 Prerequisites
320	46.5 Course structure
321	46.6 Assessment
322	46.7 References
323	47.1 Introduction
324	47.2 Objectives of the chapter
325	47.3 Scope of the chapter
326	47.4 Prerequisites
327	47.5 Course structure
328	47.6 Assessment
329	47.7 References
330	48.1 Introduction
331	48.2 Objectives of the chapter
332	48.3 Scope of the chapter
333	48.4 Prerequisites
334	48.5 Course structure
335	48.6 Assessment
336	48.7 References
337	49.1 Introduction
338	49.2 Objectives of the chapter
339	49.3 Scope of the chapter
340	49.4 Prerequisites
341	49.5 Course structure
342	49.6 Assessment
343	49.7 References
344	50.1 Introduction
345	50.2 Objectives of the chapter
346	50.3 Scope of the chapter
347	50.4 Prerequisites
348	50.5 Course structure
349	50.6 Assessment
350	50.7 References
351	51.1 Introduction
352	51.2 Objectives of the chapter
353	51.3 Scope of the chapter
354	51.4 Prerequisites
355	51.5 Course structure
356	51.6 Assessment
357	51.7 References
358	52.1 Introduction
359	52.2 Objectives of the chapter
360	52.3 Scope of the chapter
361	52.4 Prerequisites
362	52.5 Course structure
363	52.6 Assessment
364	52.7 References
365	53.1 Introduction
366	53.2 Objectives of the chapter
367	53.3 Scope of the chapter
368	53.4 Prerequisites
369	53.5 Course structure
370	53.6 Assessment
371	53.7 References
372	54.1 Introduction
373	54.2 Objectives of the chapter
374	54.3 Scope of the chapter
375	54.4 Prerequisites
376	54.5 Course structure
377	54.6 Assessment
378	54.7 References
379	55.1 Introduction
380	55.2 Objectives of the chapter
381	55.3 Scope of the chapter
382	55.4 Prerequisites
383	55.5 Course structure
384	55.6 Assessment
385	55.7 References
386	56.1 Introduction
387	56.2 Objectives of the chapter
388	56.3 Scope of the chapter
389	56.4 Prerequisites
390	56.5 Course structure
391	56.6 Assessment
392	56.7 References
393	57.1 Introduction
394	57.2 Objectives of the chapter
395	57.3 Scope of the chapter
396	57.4 Prerequisites
397	57.5 Course structure
398	57.6 Assessment
399	57.7 References
400	58.1 Introduction
401	58.2 Objectives of the chapter
402	58.3 Scope of the chapter
403	58.4 Prerequisites
404	58.5 Course structure
405	58.6 Assessment
406	58.7 References
407	59.1 Introduction
408	59.2 Objectives of the chapter
409	59.3 Scope of the chapter
410	59.4 Prerequisites
411	59.5 Course structure
412	59.6 Assessment
413	59.7 References
414	60.1 Introduction
415	60.2 Objectives of the chapter
416	60.3 Scope of the chapter
417	60.4 Prerequisites
418	60.5 Course structure
419	60.6 Assessment
420	60.7 References
421	61.1 Introduction
422	61.2 Objectives of the chapter
423	61.3 Scope of the chapter
424	61.4 Prerequisites
425	61.5 Course structure
426	61.6 Assessment
427	61.7 References
428	62.1 Introduction
429	62.2 Objectives of the chapter
430	62.3 Scope of the chapter
431	62.4 Prerequisites
432	62.5 Course structure
433	62.6 Assessment
434	62.7 References
435	63.1 Introduction
436	63.2 Objectives of the chapter
437	63.3 Scope of the chapter
438	63.4 Prerequisites
439	63.5 Course structure
440	63.6 Assessment
441	63.7 References

4.5. Application for the equivalent lateral stress and verification	63
4.5.1. Application for the equivalent lateral stress of passively confined concrete.....	63
4.5.2. Verification for the equivalent lateral stress of passively confined concrete	64
4.5.3. The load-bearing capacity model of CFST column based on energy path.....	68
4.6. Conclusions	70
CHAPTER 5. SUMMARIES	73

ACKNOWLEDGMENTS

I wish to extend my deepest gratitude to Professor Yan-Gang Zhao, my guiding light throughout this doctoral voyage. His unwavering support, boundless encouragement, and expert guidance have been the cornerstone of my academic journey, steering me from the genesis to the fruition of this thesis. Under his mentorship, I've not only delved into the depths of scholarly knowledge but also imbibed the art of innovative research—a blend of creative thinking, unwavering dedication, and a meticulous approach. Collaborating with Professor Zhao has been an immense honor and privilege. The lessons gleaned from this association will serve as a beacon, guiding my path forward in academia.

Furthermore, I wish to convey my profound gratitude to Professor Siqi Lin and Xifeng Yan for their invaluable mentorship and support in guiding my academic journey. Their selfless dedication in imparting knowledge, along with their patient guidance in resolving my queries, has been instrumental in shaping my academic growth and understanding.

Then, I would like to express my deep gratitude to Associate Professors Haizhong Zhang and Xiaoyu Yang for their invaluable support and guidance. Their assistance was pivotal in helping me navigate through the challenges encountered in both my research and life in Japan.

Great thanks go to the review committee members: Professor Kazushi Shimazaki, Professor Masanori Fujita, Professor Keisuke Yoshie, Professor Yoshiharu Shumuta, Associate Professors Yuki Shirai, Associate Professors Makoto Nakamura, Associate Professors Tsutomu Ochiai for their valuable comments and suggestions on this work.

Sincere thanks go to the member of Zhao laboratory for their help in solving the met difficulties in many aspects and understanding Japanese culture, etc: Dr. Lixiang Cheng, Dr. Jiayi Cai, Mr. Yutao Lu, Mr. Wei Fu, Mr. Yingchi Fang, Mr. Zhenghao Chen, and many friends outside Zhao laboratory, etc: Dr. Peipei Li and Dr. Fangwen Ge.

Yang Di
January, 2024

概要

コンファインド・コンクリート構造は、構造要素の延性を向上させるために導入され、建設業界で広く受け入れられています。この建築手法は、補強のための外部支持または拘束を通じて、コンクリート構造の性能を向上させます。初期に使用された拘束材料は鋼管であり、このように鋼管で覆われたコンクリートはコンクリート充填鋼管（CFST）として知られています。CFST の拘束メカニズムは、高い強度、剛性、そして延性を実現します。また、もう一つの一般的な拘束材料として繊維強化ポリマー（FRP）があり、これは耐食性に優れ、軽量で弾力性が高く、施工も容易です。

CFST 柱でも FRP 拘束コンクリート柱でも、軸耐力は構造工学において重要な安全設計の要素です。長年にわたり、多くの実験的及び理論的研究が進められています。これらの研究は、実験データの経験的解析に基づくモデルや、能動的拘束コンクリートの理論に基づくモデルが含まれています。能動的拘束コンクリートと異なり、受動的拘束コンクリートは軸方向応力の増加に伴い横方向応力も増加します。荷重過程で軸方向変形が増加すると、受動的拘束コンクリートのひび割れが進み、拘束応力も変化します。受動的拘束コンクリート柱の耐力モデルは、コンクリートと拘束材の相互作用メカニズムに基づいて確立されています。

鋼管や FRP ジャケットによるコンクリートの拘束は、本質的にエネルギー伝達プロセスです。この観点から、軸圧縮下で受動的に拘束されたコンクリート柱のエネルギー関係を詳細に分析し、ピーク強度でのエネルギー特性を比較することは、充填コンクリートと外部拘束材との相互作用の理解において重要です。

本研究では、受動的に拘束されたコンクリート柱のコンクリートと拘束材間の相互作用メカニズムをエネルギーの観点から初めて検討しました。拘束材とコンクリートの間のエネルギー関係を反映するエネルギーパス法を提案しました。また、エネルギー比は拘束材とコンクリートが吸収するエネルギーの相関関係を示します。ピーク応力時のエネルギー比を分析することで、受動的に拘束されたコンクリート柱のエネルギー分布状態を明らかにすることができます。本研究で得られた重要な結論を簡単にまとめると以下ようになります：

- 1) CFST 柱のコンクリートと鋼管の相互作用メカニズムを、エネルギーの観点から検討しました。
- 2) CFST 柱のエネルギー伝達経路を定義し、一軸圧縮強度や鋼材強度、 D/t 比などのパラメータを基に実験的に分析しました。
- 3) FRP 拘束コンクリート柱と FRP ジャケットの相互作用を、エネルギーの観点から調査しました。
- 4) 一軸圧縮強度や FRP 層数などのパラメータに基づき、FRP 拘束コンクリート柱のエネルギー伝達経路を提案し、実験的に検証しました。
- 5) 応力経路の分析に基づき、受動的拘束コンクリートの等価横応力を提案し、能動的拘束と受動的拘束のコンクリートの相関関係を明確にしました。
- 6) コンクリートと鋼管のエネルギー分布を考慮した、CFST 柱の耐力モデルを開発しました。

ABSTRACT

Confined concrete structures emerged for meeting the ductility prerequisites of structural elements, garnering considerable attention and extensive adoption within the construction sector. This architectural approach enhances concrete structure performance through the provision of supplementary external support or confinement.

The early material that was used as a constrained material was steel tube and the combined structure of concrete covered with steel tube was called concrete-filled steel tube (CFST) concrete. This confinement mechanism of CFST columns is responsible for the excellent properties, such as high strength, stiffness and ductility. Another common confinement material is fiber reinforced polymer (FRP), which is corrosion-resistant, lightweight, has a high modulus of elasticity, and is easy to construct.

No matter for the CFST columns or FRP-confined concrete columns, the axial capacity has long been the main concern for safety design in the field of structural engineering. Extensive experimental and theoretical studies have been conducted over the last several decades. These models are either developed through the empirical regression of experimental test data, or based on or adopted models of actively confined concrete. On the other hand, different from actively confined concrete in which the lateral stress is constant, the confined concrete, as passive confinement, experiences increasing lateral stress with increasing axial stress. During the loading process, with the increase of axial deformation, the passively confined concrete cracks start to develop gradually, and the confining stress of the passively confined concrete changes continuously with the cracks. As for passively confined concrete columns, the basis for a well-established load-bearing capacity model of is clear the interaction mechanism between the concrete and constrained material.

It is noteworthy that the confinement of concrete by a steel tube or FRP jacket is essentially an energy transfer process. From this point of view, a detailed analysis of the energy relations of passively confined concrete columns under axial compression and a comparison of the energy properties at peak strength are significant to understand the interaction mechanism between the infilled concrete and external constrained material.

In this research, the interaction mechanism between the concrete and constrained material of passively confined concrete columns was investigated from an energy relations perspective for the

ABSTRACT

The purpose of this investigation was to determine the effect of the type of concrete used in the construction of a bridge pier on the load-carrying capacity of the pier. The investigation was conducted using a series of tests on concrete piers of different heights and diameters. The results of the tests showed that the load-carrying capacity of the piers increased with the height of the pier and the diameter of the pier. The type of concrete used in the construction of the pier had a significant effect on the load-carrying capacity of the pier.

The results of the tests showed that the load-carrying capacity of the piers increased with the height of the pier and the diameter of the pier. The type of concrete used in the construction of the pier had a significant effect on the load-carrying capacity of the pier. The results of the tests showed that the load-carrying capacity of the piers increased with the height of the pier and the diameter of the pier. The type of concrete used in the construction of the pier had a significant effect on the load-carrying capacity of the pier.

The results of the tests showed that the load-carrying capacity of the piers increased with the height of the pier and the diameter of the pier. The type of concrete used in the construction of the pier had a significant effect on the load-carrying capacity of the pier. The results of the tests showed that the load-carrying capacity of the piers increased with the height of the pier and the diameter of the pier. The type of concrete used in the construction of the pier had a significant effect on the load-carrying capacity of the pier.

The results of the tests showed that the load-carrying capacity of the piers increased with the height of the pier and the diameter of the pier. The type of concrete used in the construction of the pier had a significant effect on the load-carrying capacity of the pier. The results of the tests showed that the load-carrying capacity of the piers increased with the height of the pier and the diameter of the pier. The type of concrete used in the construction of the pier had a significant effect on the load-carrying capacity of the pier.

The results of the tests showed that the load-carrying capacity of the piers increased with the height of the pier and the diameter of the pier. The type of concrete used in the construction of the pier had a significant effect on the load-carrying capacity of the pier. The results of the tests showed that the load-carrying capacity of the piers increased with the height of the pier and the diameter of the pier. The type of concrete used in the construction of the pier had a significant effect on the load-carrying capacity of the pier.

first time. An energy path method was proposed to reflect the energy relations between the constrained material and the concrete. On the other hand, the energy ratio represents the relative correlation between the energy absorbed by the constrained material and the concrete. The state of energy distribution in passively confined concrete columns can be derived by analyzing the energy ratio at peak stress condition. Several important conclusions obtained in this research are briefly summarized as follows:

- 1). The interaction mechanism between the concrete and steel tube of CFST column is investigated from an energy relations perspective.
- 2). The energy path of CFST column is proposed and analyzed experimentally from the column parameters such as unconfined concrete strength, steel strength and D/t ratio.
- 3). The interaction mechanism between the concrete and FRP jacket of FRP-confined concrete column is investigated from an energy relations perspective.
- 4). The energy path of FRP-confined concrete column is proposed and analyzed experimentally from the column parameters such as unconfined concrete strength and number of FRP layers.
- 5). The equivalent lateral stress of passively confined concrete is proposed from the analysis of stress path, which establishes a connection between the actively and passively confine concrete.
- 6). A load-bearing capacity model for axial loaded CFST column is proposed, considering the energy distribution relationship between the concrete and steel tube.

CHAPTER 1. INTRODUCTION

1.1. Background

Confined concrete structures find broad application across structural engineering with lateral reinforcement to increase the strength and ductility of these members. Behaviors of confined concrete columns have been extensively studied in previous research [1-2].

The early material that was used as a constrained material was steel tube and the combined structure of concrete covered with steel tube was called concrete-filled steel tube (CFST) concrete. CFST columns have the combined advantage of the tensile capacity of an external steel tube along with the compressive capacity of infilled concrete [3-4]. The external steel tube of CFST columns not only carries the compressive load but also confines the concrete. This confinement mechanism of CFST columns is responsible for the excellent properties, such as high strength, stiffness and ductility. Another common confinement material is fiber reinforced polymer (FRP), which is corrosion-resistant, lightweight, has a high modulus of elasticity, and is easy to construct. Due to the elastic nature of FRP material, its force state is simpler and easier to analyze theoretically [5].

No matter for the CFST columns or FRP-confined concrete columns, the axial capacity has long been the main concern for safety design in the field of structural engineering. Extensive experimental and theoretical studies have been conducted over the last several decades, and many calculated models were proposed to predict the load-bearing capacity of these confined concrete columns [6-7]. These models are either developed through the empirical regression of experimental test data, or based on or adopted models of actively confined concrete. The accuracy of the empirical formulas obtained based on the regression analysis of the test data results depends greatly on the reliability and comprehensiveness of the test results database [1]. On the other hand, different from actively confined concrete in which the lateral stress is constant, the confined concrete, as passive confinement, experiences increasing lateral stress with increasing axial stress. During the loading process, with the increase of axial deformation, the passively confined concrete cracks start to develop gradually, and the confining stress of the passively confined concrete changes continuously with the cracks. The constraint stress of actively confined concrete is externally provided and remains constant during the loading process, independent of crack development. Thus, reasonability of modelling the passively confined concrete by using the actively confined concrete is doubtful. As for passively confined

concrete columns, the basis for a well-established load-bearing capacity model of is clear the interaction mechanism between the concrete and constrained material.

It is noteworthy that the confinement of concrete by a steel tube or FRP jacket is essentially an energy transfer process [2]. Therefore, during the columns being subjected to axial loading, the energy transfer between the constrained material and the concrete is the intrinsic driving force for the lateral restraint effect, while the strength increase is the extrinsic manifestation. From this point of view, a detailed analysis of the energy relations of passively confined concrete columns under axial compression and a comparison of the energy properties at peak strength are significant to understand the interaction mechanism between the infilled concrete and external constrained material.

In this paper, the interaction mechanism between the concrete and constrained material of passively confined concrete columns was investigated from an energy relations perspective for the first time. An energy path method was proposed to reflect the energy relations between the constrained material and the concrete, which was defined as the trajectory of energy ratio absorbed by the constrained material and concrete with the compressive strength. On the other hand, the energy ratio represents the relative correlation between the energy absorbed by the constrained material and the concrete. The state of energy distribution in passively confined concrete columns can be derived by analyzing the energy ratio at peak stress condition. The load-bearing capacity model of passively confined concrete column can be established from the energy weight perspective. Surely, the precondition is the accurate confined concrete strength can be obtained.

1.2.Objectives and organization

The objectives of this paper would be:

- (1). To investigate the energy path of CFST columns and clarify interaction mechanism between the concrete and steel tube, establishing an energy path based compressive strength model;
- (2). To investigate the energy path of FRP-confined concrete columns and clarify interaction mechanism between the concrete and FRP jacket, establishing an energy path based compressive strength model;
- (3). To propose a load-bearing capacity models of CFST columns from the energy distribution relation perspective.

For the purpose, seven chapters will be covered in this dissertation. The organization can be seen in Fig. 1.1, and given as follows:

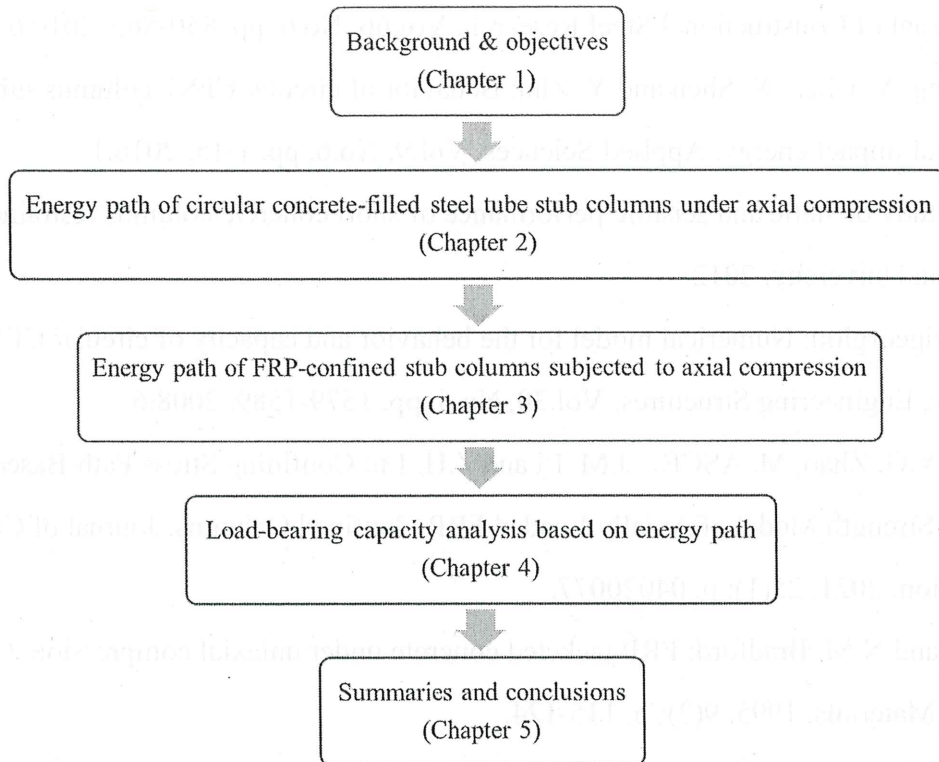


Fig. 1.1 Organization of this dissertation

For the purpose, seven chapters will be covered in this dissertation. The organization can be seen in Fig. 1.1, and given as follows:

In chapter two, experimental test with a total of 18 circular concrete loaded CFT stub columns subjected to axial compression was conducted, based on which the confinement path of concrete and its relationship with the compressive strength were investigated.

In chapter three, the confinement path of concrete in whole-section-loaded CFT columns and its relationship with the compressive strength were investigated, based on which a compressive model was proposed.

In chapter four, the equivalence lateral stress was proposed to establish a connection between actively and passively confined concrete, rationalizing the application of compressive strength models for actively confined concrete in strength calculations for passively confined concrete.

In chapter five, the conclusions will be summarized.

References

- [1] Z.H. Lu and Y.G. Zhao: Suggested empirical models for the axial capacity of circular CFT stub columns, *Journal of Constructional Steel Research*, Vol.66, No.6, pp. 850-862, 2010.6.
- [2] X.Y. Zhang, Y. Chen, X. Shen and Y. Zhu: Behavior of circular CFST columns subjected to different lateral impact energy, *Applied Sciences*, Vol.9, No.6, pp. 1-15, 2016.1.
- [3] D. Gan: Study of static and seismic performance of short concrete columns restrained by steel tubes, Lanzhou University, 2012.
- [4] G.D. Hatzigeorgiou: Numerical model for the behavior and capacity of circular CFT columns, Part I: Theory, *Engineering Structures*, Vol.30, No.6, pp. 1579-1589, 2008.6.
- [5] S.Q. Lin, Y.G. Zhao, M. ASCE, J.M. Li and Z.H. Lu: Confining Stress Path-Based Compressive Strength Model of Axially Loaded FRP-Confined Columns. *Journal of Composites for Construction*, 2021. 25(1): p. 04020077.
- [6] A. Nanni and N.M. Bradford: FRP jacketed concrete under uniaxial compression. *Construction and Building Materials*, 1995. 9(2): p. 115-124.
- [7] Y. Xiao and H. Wu, Compressive Behavior of Concrete Confined by Carbon Fiber Composite Jackets. *Journal of Materials in Civil Engineering*, 2000. 12(2): p. 139-146.

CHAPTER 2. ENERGY PATH OF CIRCULAR CONCRETE-FILLED STEEL TUBE STUB COLUMNS UNDER AXIAL COMPRESSION

2.1. Introduction

Concrete-filled steel tube (CFST) columns can be found in a wide range of buildings and infrastructure, from skyscrapers and factories to subways and parking garages [1-5]. CFST columns have the combined advantage of the tensile capacity of an external steel tube along with the compressive capacity of infilled concrete. The external steel tube of CFST columns not only carries the compressive load but also confines the concrete. This interaction between the core concrete and steel tube is responsible for the excellent properties of CFST columns, such as high strength, good ductility, and light weight [6-8].

The load-bearing capacity of CFST columns as support members have long been the main concern for safety design in the field of structural engineering. Extensive studies [9-14] have been conducted over the last several decades, based on which design codes from each country, such as AIJ [15], ACI [16], and AISC [17], were developed for predicting the load-bearing capacity of CFST columns. Researchers have also proposed many methods to analyze the axial behavior of CFST columns, such as the longitudinal fiber method [18-20], the finite element method [21-23], or the use of mechanical learning to organize and analyze experimental data. Ahmed et al. [19] proposed a unified numerical model with a new concrete constitutive relation to predict the ultimate strength of concrete-filled stainless-steel tubular (CFSST) columns and agree well with the experimental results. Patel [20] investigated the local and post-local buckling of round-ended concrete-filled steel tubular (RCFST) beam-columns through the nonlinear fiber-based strategy. These analysis methods were mostly based on accurate constitutive models of steel tubes and concrete and more focused on the matching with experimental results. Moreover, corresponding calculated models have been proposed to predict the load-bearing capacity of CFST columns. These proposed models usually show good agreement with some experiments, especially that were adopted to develop the model, but there is uncertainty as to whether they can provide satisfactory predictions or not in many other cases [2]. The reason may result from the insufficient understanding of the interaction mechanism between the infilled concrete and external steel tube of CFST columns.

It is noteworthy that the confinement of concrete by a steel tube is essentially an energy transfer

process. The process of core concrete expanding outward is the process of concrete making negative work to the outside, meanwhile, the energy will be transferred to the steel tube. Therefore, during the CFST columns being subjected to axial loading, the energy transfer between the steel tube and the concrete is the intrinsic driving force for the lateral restraint effect, while the strength increase is the extrinsic manifestation. From this point of view, a detailed analysis of the energy relations of CFST columns under axial compression and a comparison of the energy properties at peak strength are significant to understand the interaction mechanism between the infilled concrete and external steel tube of CFST columns. The prior stress-based analysis does not address the energy distribution relationship of CFST columns, and energy analysis methods are well suited for heterogeneous and discontinuous materials such as concrete. Moreover, the relative energy relationship between core concrete and steel tube reflects the common regularity of energy distribution and transfer in CFST columns and reduces the effect of the individual specimen's differentiation. According to the laws of thermodynamics, the respective stress-strain relationship of steel tube and concrete can reflect the energy condition of the structure [24, 25].

In this study, the interaction mechanism between the core concrete and external steel tube is investigated from the energy relations to establish an effective load-bearing capacity model of CFST columns. An energy path method is proposed to reflect the CFST column energy transfer that takes place between the steel tube and core concrete. The experiments of CFST stub columns under whole-section-loaded were conducted to perform a parametric analysis of the energy path. The response states of concrete and steel tubes during the process were analyzed by energy paths. Two quantitative metrics were introduced to characterize the energy path of the whole compression process and to discuss the limit form of the energy path. The results of a parametric study conducted on the energy path are discussed to connect the metric and the structural and material parameters. The interaction mechanism between the infilled concrete and external steel tube was further explained by comparing the energy path of CFST column and stress path of constrained concrete. Finally, a concrete compression strength model and a load-bearing capacity model of CFST columns were developed based on the analysis of the energy paths.

2.2. Experimental program

2.2.1. Definition and determination of the energy path

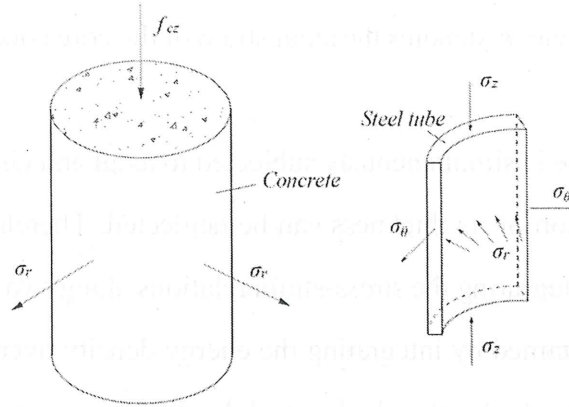


Fig. 2.1 Stress state of circular CFST column.

Owing to the large variation in the total energy absorbed by the steel tube and core concrete during the compression procedure of CFST columns, the energy variation rule by each cannot be analyzed separately. However, the proportion of energy gained by concrete to that by steel tube can reflect the relative relationship of energy. This ratio describes the process of energy transfer between the steel tube and concrete, meanwhile, the variation in this ratio can be used to investigate the forces state on the different components of the CFST column during axial compression. Moreover, the interaction mechanism of steel tube and core concrete can be informed by analyzing the variation trajectory of the energy ratio with compressive stress. This variation trajectory is defined as the energy path. The object of this paper belongs to the strengthened stress-strain relationship, and the softened stress-strain relationship will be analyzed in the subsequent study.

In a CFST column under whole section loading, the core concrete is subjected to forces from all three directions with two equal stresses along the horizontal directions, as shown in Fig. 2.1. In the vertical direction, the steel tube and concrete are cooperatively in deformation, ignoring the local buckling of the steel tube. The energy density of the core concrete is obtained by integrating the stress-strain relations along all three directions, and the work done by the external force is obtained by integrating the energy density over the volume of the concrete. Therefore, the energy absorbed by the concrete at each loading stage is given by

$$Q_c = A_c H U_c = A_c H \left(\int_0^{\varepsilon_c} f_{cz} d\varepsilon_c + 2 \int_0^{\varepsilon_r} \sigma_r d\varepsilon_r \right), \quad (2.1)$$

where Q_c denotes the energy that the concrete absorbed at each loading stage; A_c is the cross-sectional

area of the core concrete; H is the height of the CFST column; U_c represents the energy density of the core concrete; f_{cz} is the compressive stress generated in the core concrete; σ_r denotes the lateral stress generated in the core concrete; ε_c denotes the axial strain of the core concrete; and ε_r denotes the radial strain of the core concrete.

The external steel tube is simultaneously subjected to axial and circumferential stress; however, the stress along the direction of its thickness can be neglected. Therefore, the energy density of the steel tube is obtained by integrating the stress-strain relations along two directions, and the work done by the external force is obtained by integrating the energy density over the volume of the steel tube. Thus, the energy that the steel tube absorbed at each loading stage is given by

$$Q_s = A_s H U_s = A_s H \left(\int_0^{\varepsilon_z} \sigma_z d\varepsilon_z + \int_0^{\varepsilon_\theta} \sigma_\theta d\varepsilon_\theta \right), \quad (2.2)$$

where Q_s denotes the energy that the steel tube absorbed at each loading stage; A_s is the steel tube's cross-sectional area; U_s represents the steel tube's energy density; σ_z and σ_θ denote the axial stress and circumferential stress generated in the external steel tube; ε_z denotes the steel tube's axial strain; and ε_θ denotes the steel tube's circumferential strain.

As the stresses of the core concrete and steel tube obtained by the strains measured in the test are discontinuous values, the integration in Eqs. (2.1) and (2.2) is approximated as a superposition of the trapezoidal area below the line connecting adjacent stress values in the stress-strain relations. The variation of the energy ratio (Q_c/Q_s) with the compressive strength of constrained concrete (f_{cz}) normalized with respect to the strength of unconstrained concrete (f_c) gives the energy path of the CFST column. According to Eqs. (2.1) and (2.2), the stress-strain relations of the core concrete and steel tube are required to determine the energy path, as specified below.

The force equilibrium state can be used to calculate the lateral stress σ_r generated in core concrete, such that

$$\sigma_r = \frac{2t}{D-2t} \sigma_\theta, \quad (2.3)$$

where D represents the CFST column's diameter, and t represents the steel tube's wall thickness.

The compressive stress f_{cz} of concrete can be calculated using.

$$f_{cz} = \frac{N - \sigma_z A_s}{A_c}, \quad (2.4)$$

where N is the axial load applied to the CFST column. Next, the equations are presented for determining the axial stress and circumferential stress in the steel tube.

The von Mises stress (σ_e) in the steel tube is defined as

$$\sigma_e = \sqrt{\sigma_z^2 - \sigma_z \sigma_\theta + \sigma_\theta^2}. \quad (2.5)$$

During the elastic phase ($\sigma_e < f_y$), where f_y is the tensile strength of steel tube, the stress exerted on steel tube can be evaluated using modified version of Hooke's law:

$$\begin{Bmatrix} d\sigma_z \\ d\sigma_\theta \end{Bmatrix} = \frac{E_s}{1-\nu^2} \begin{bmatrix} 1 & \nu \\ \nu & 1 \end{bmatrix} \begin{Bmatrix} d\varepsilon_z \\ d\varepsilon_\theta \end{Bmatrix}, \quad (2.6)$$

where $d\varepsilon_z$ and $d\varepsilon_\theta$ denote the infinitesimal axial and circumferential strains, separately. The tangent modulus is denoted by E_s , and the Poisson's ratio is denoted by ν [26]. Note that the total axial/circumferential stress is determined by summing the measured components of the axial/circumferential strain at every loading stage.

During the plastic phase ($\sigma_e \geq f_y$), the stress in the steel tube can be evaluated using the Prandtl-Reuss flow criterion:

$$\begin{Bmatrix} d\sigma_z \\ d\sigma_\theta \end{Bmatrix} = \frac{E_s}{1-\nu^2} \begin{bmatrix} 1 & \nu \\ \nu & 1 \end{bmatrix} \begin{Bmatrix} d\varepsilon_z \\ d\varepsilon_\theta \end{Bmatrix} - \frac{Ed\gamma}{3(1-\nu^2)} \begin{bmatrix} 2-\nu & 2\nu-1 \\ 2\nu-1 & 2-\nu \end{bmatrix} \begin{Bmatrix} \sigma_z \\ \sigma_\theta \end{Bmatrix}, \quad (2.7)$$

such that the scalar $d\gamma$ is given by

$$d\gamma = \frac{9G(s_z de_z + s_r de_r + s_\theta de_\theta)}{2\sigma_e^2(H' + 3G)} \quad (2.8)$$

$$G = \frac{E}{2(1+\nu)}, \quad (2.9)$$

where s_i and e_i denote the i th components of the deviatoric stress and strain, separately; H' stands for the gradient of the corresponding plastic stress-strain curve for the steel tube during tensile testing; and G and E denote the shear and elastic moduli of steel, separately.

The compressive and lateral stresses in the core concrete can be calculated by substituting the values of the circumferential stress (σ_θ) and axial stress (σ_z) generated in the external steel tube at every loading stage in Eqs. (2.3) and (2.4), respectively. The energy absorbed by the core concrete and steel tube can be calculated by substituting the axial and lateral stresses generated in the core concrete in Eq. (2.1) and the axial and circumferential stresses generated in the steel tube in Eq. (2.2),

respectively. Consequently, the energy paths of CFST columns can be determined. Fig. 2.2 shows the flowchart for determining the energy absorbed by the core concrete and steel tube utilizing experimentally recorded axial and circumferential strains, along with the CFST column's structure parameters.

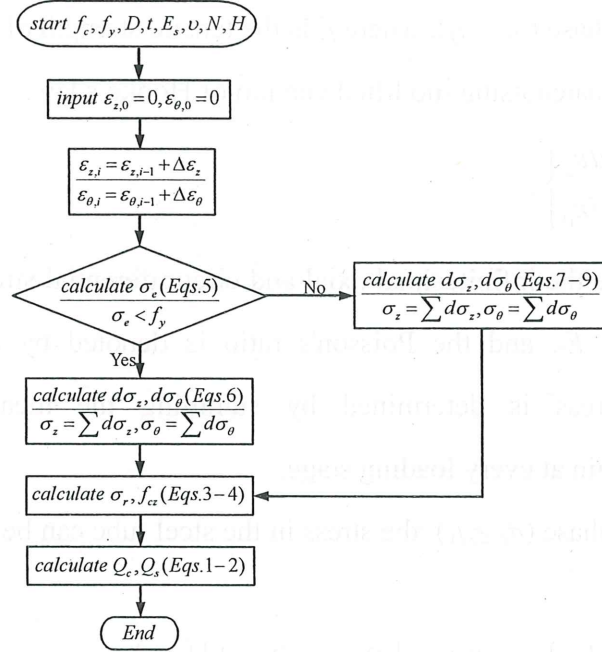


Fig. 2.2 Flowchart for determining the energy path of CFST column.

A canonical energy path of CFST column subjected to whole section loading is shown in Fig. 2.3 (corresponding to specimen 490-36-31-WL; see Table 2.1). Figs. 3 and 4 show the corresponding axial load-displacement and stress-strain curves, respectively. The energy path explains the variation in the energy ratio absorbed by the CFST column during the compression procedure, and it can be divided into four phases. The corresponding positions of OABCD on the energy path under the same force state are also marked on the load-displacement curve. Under the whole section loading condition, the steel tube and core concrete are simultaneously subjected to an external load during the initial phase (i.e., phase OA in Fig. 2.3). The degree of deformation of the CFST specimen owing to the external load is typically determined by parameters such as the flatness of the loading face and bonding between the steel tube and concrete. As the core concrete is poured directly in the steel tube, the two are naturally bonded before loading. With the axial loading acting on the steel tube and concrete at the same time, the steel tube and concrete will separate due to different lateral expansion caused by different Poisson's ratio. The energy path exhibits large fluctuations during the OA phase.

When the increasing trend of the energy ratio begins to weaken, the approximate location of point A can be given by combining the force state of the concrete. These reveal that the point A marks the onset of interaction between the core concrete and steel tube. At this stage, microcracks develop rapidly in the core concrete, and the concrete has a larger side swelling than the steel tube; consequently, the concrete experiences an increase in circumferential stress. A sharp decrease in the energy ratio at point B (at approximately $0.75 f_{cz}/f_c$) indicates that a large amount of external energy is absorbed by the steel tube via direct or indirect transfer, which is macroscopically manifested by the non-increase of concrete strength and the increase of steel tube strength. Therefore, the concrete's yield phase is located near point B. Note that the rate of decrease of the energy ratio decreases and the concrete strength increases, demonstrating that the steel tube begins to enter the yield phase. During phase BC, the energy ratio starts to increase gradually with the compressive stress, which implies that the energy absorbed by the steel tube starts to decline compared to that absorbed by the core concrete. This is because the axial and circumferential stresses in the steel tube do not increase sufficiently after the yield point, while the compressive strength grows considerably owing to external constraints; consequently, the rate of decrease in energy ratio starts to slow down. Point C marks the start of the steel tube's strain hardening phase. During phase CD, the energy ratio increases until the point of ultimate strength is reached at D. This is because the core concrete dissipates some of its energy owing to plastic deformation, and hence, less energy is transferred from the core concrete to the steel tube via side swelling.

In summary, the core concrete starts to develop microfractures at point A; whereas the steel tube starts to yield at point B, enters the hardening stage at point C, and achieves its limit strength by point D. The stress-strain curves and axial load-displacement of CFST column show that most of the elastic strain energy in the core concrete is accumulated during the AC phase, owing to which greatly improves the concrete's compressive strength. Moreover, as the steel tube starts to yield, the core concrete moves from the elastic to the plastic stage.

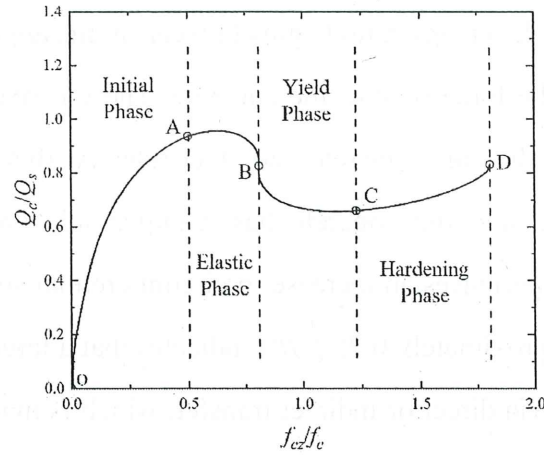


Fig. 2.3 Typical energy path of CFST column under whole section loading.

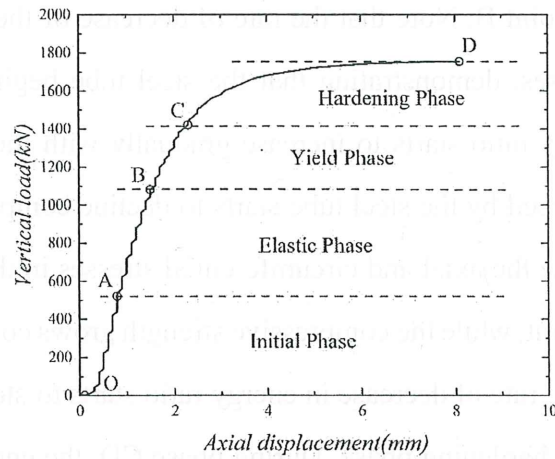


Fig. 2.4 Typical axial load-displacement curve of a CFST column.

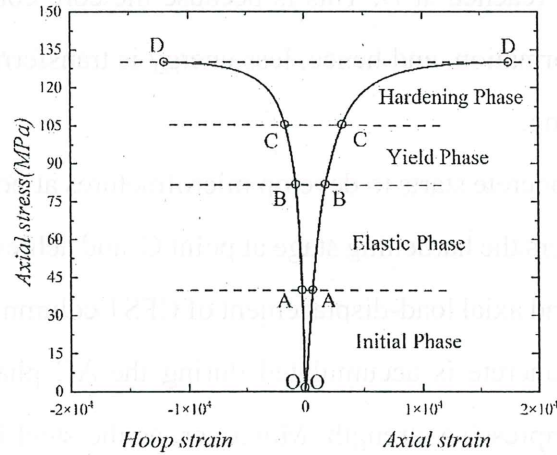


Fig. 2.5 Typical axial stress-strain curve of a CFST column.

2.2.2. Experimental setup

The energy path of CFST stub columns was analyzed parametrically under whole section loading. Seven sets of CFST columns were selected with two identical specimens in each set. The following parameters were varied during the experiments: (1) strength of unconstrained concrete f_c ; (2) strength of the steel tube at yield point f_y ; and (3) ratio of column diameter to steel tube thickness D/t . Two

types of core concretes with compressive strength 36 and 60 MPa were used for the experiments. Concrete cylinders measuring 100 mm by 200 mm were subjected to uniaxial compression testing to ascertain the compressive strength. The tubes used were made of two types of steel, STK400 and STK490. The mechanical qualities of the steel tubes were ascertained by performing tensile tests on coupons made before production from the corresponding steel plates. To mitigate the effects of slenderness ratio, each specimen's length was picked to be three times its diameter. In addition, the D/t ratio was set to 25, 33, and 45 to delay the occurrence of local buckling or reduce the local buckling deformation. Table 2.1 provides a list of the specifications of sample sets and various experimental parameters.

Table 2.1

Parameter settings and specifications of samples.

Specimens	D (mm)	t (mm)	D/t	f_y (MPa)	f_c (MPa)	f_u (MPa)	E_s (GPa)	η	N_{ue} (kN)	K	Ω
400-36-31-WL-1	140	4.5	31	365	41	455	203	1.64	1,474.2	1.04	0.51
400-36-31-WL-2	140	4.5	31	365	41	455	203	1.64	1,458.1	0.98	0.49
400-60-31-WL-1	140	4.5	31	365	68	455	203	2.65	1,880.9	1.20	0.55
400-60-31-WL-2	140	4.5	31	365	68	455	203	2.65	1,891.8	1.34	0.57
490-36-31-WL-1	140	4.5	31	463	41	550	192	1.23	1,771.1	0.63	0.39
490-36-31-WL-2	140	4.5	31	463	41	550	192	1.23	1,753.0	0.70	0.41
490-60-31-WL-1	140	4.5	31	463	68	550	192	2.14	2,268.3	1.27	0.56
490-60-31-WL-2	140	4.5	31	463	68	550	192	2.14	2,222.3	1.17	0.54
400-36-25-WL-1	114.3	4.5	25	440	41	476	200	1.09	1,161.0	0.56	0.36
400-36-25-WL-2	114.3	4.5	25	440	41	476	200	1.09	1,167.1	0.57	0.36
400-36-33-WL-1	165.2	5.0	33	416	41	441	200	1.53	2,035.4	1.03	0.51
400-36-33-WL-2	165.2	5.0	33	416	41	441	200	1.53	2,040.3	0.92	0.48
400-36-45-WL-1	165.2	3.7	45	383	41	462	200	2.28	1,692.3	1.35	0.57
400-36-45-WL-2	165.2	3.7	45	383	41	462	200	2.28	1,723.4	1.13	0.53

Fig. 2.6 displays the apparatus used in the experiment. Axial loads were applied to both the steel tube and the concrete core. Utilizing an all-purpose testing device with a 5000 kN maximum capacity,

uniaxial compression was applied to each specimen. To measure the axial and lateral strains, two sets of strain sensors were mounted on the exterior of the steel tube at chest level. Under whole section loading, the axial displacement of the column was roughly equivalent to that of the steel tube. Two identical specimens from each of the seven sample sets were tested. The numbers and letters in the specimen name indicate steel grade, concrete design grade, ratio of column diameter to steel tube thickness, loading mode, and specimen identifier, respectively.

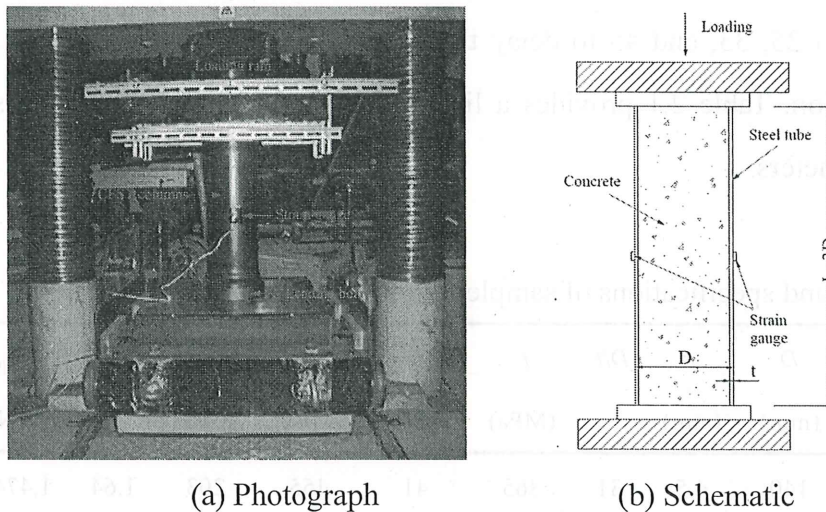


Fig. 2.6 Experimental settings.

2.2.3. Experimental results

Fig. 2.7 shows the axial stress as a function of the axial strain and circumferential strain of the CFST specimens. The total axial input energy can be obtained by integrating the axial stress and strain, and the total input energy-axial strain curves for different CFST samples are drawn in Fig. 2.8. The maximum load (N_{ue}) on all the specimens is listed in Table 2.1. As shown in Fig. 2.8(a), the external energy absorbed by the CFST column at peak stress increases with an increase in the steel strength, which implies that the area under the stress-strain curve increases. Thus, the effect of steel strength on the ultimate strength and peak strain of the CFST columns can be determined by comparing the areas under the corresponding stress-strain curves. Note that when the slopes of the total input energy curves are in similar cases, the magnitude of the total input energy indicates the strength and ductility of the components. Unlike steel strength, the overall amount of energy absorbed by the CFST columns is not significantly affected by concrete strength; by contrast, the energy growth rate clearly increases with increasing concrete strength as shown in Fig. 8(a). A higher concrete strength implies a smaller ultimate strain at peak stress, which in turn implies higher brittleness. Thus, specimens with higher

steel strength and lower concrete strength exhibit higher ductility. Fig. 2.8(b) shows that specimens with a lower D/t ratio tend to absorb more energy and have a larger area under their stress-strain curves; consequently, these specimens exhibit higher ductility. This is due to the increased steel content in specimens with a lower D/t ratio, and steel is normally more ductile than concrete.

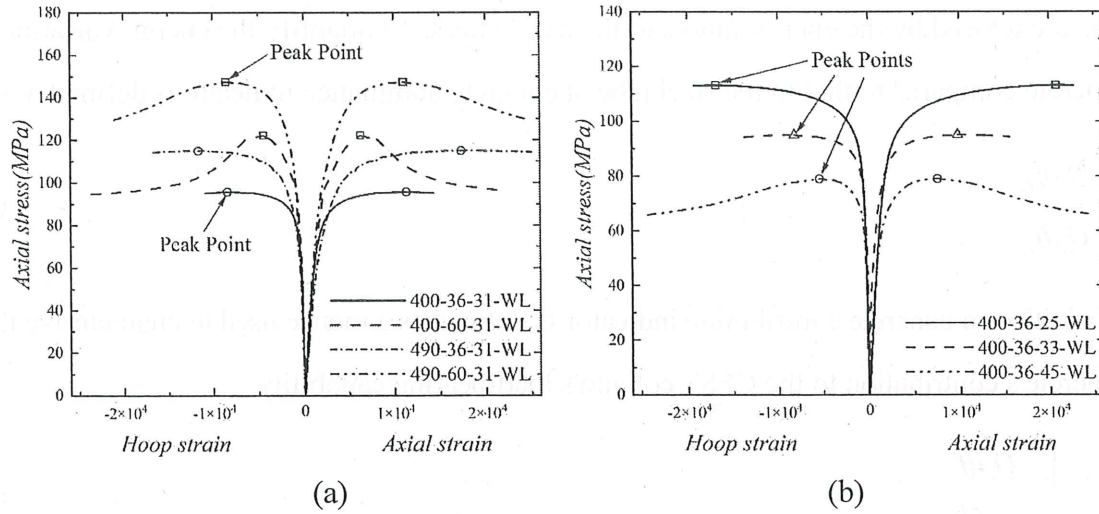


Fig. 2.7 Axial stress-strain profiles from different CFST samples.

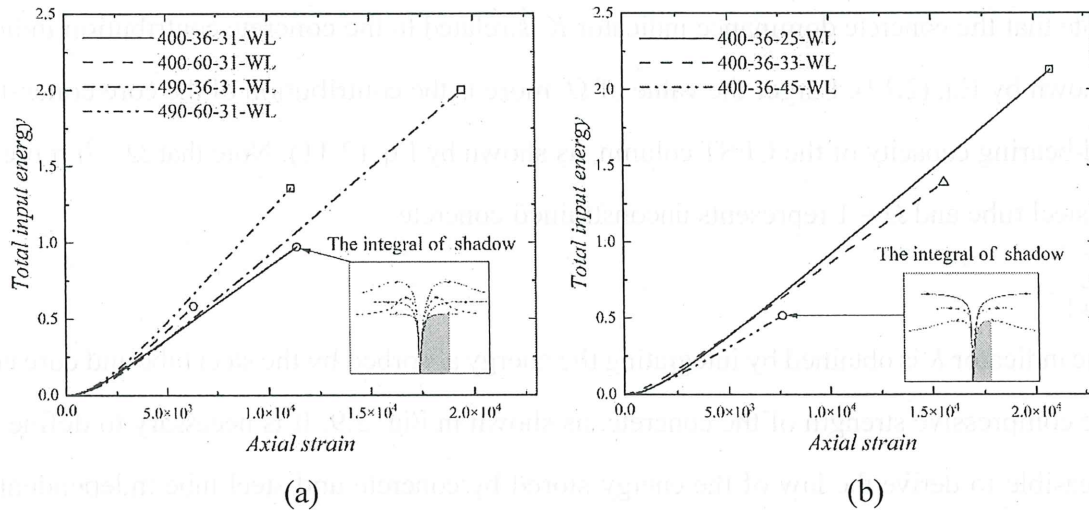


Fig. 2.8 Total input energy-axial strain profiles from different CFST samples.

The relationship between the energy absorbed by the core concrete and that absorbed by the external steel tube is discussed in the following section. In summary, the process outlined in Section 2.1 can be used to determine the energy path.

2.3. Investigation of the energy path

2.3.1. Evaluation indices of the energy path

The energy path is essentially the trajectory of the ratio of the energy absorbed by the core

concrete to that absorbed by the steel tube, with relation to the compressive strength of concrete. As energy transfer takes place continuously between steel tube and concrete, the energy path essentially indicates the change in energy contribution of the core concrete. The energy paths are variable for different column parameters, and the path characteristics during axial compression are represented by the area enclosed by the energy ratio and the axial stress. To quantify the energy variation in the core concrete compared to that in the steel tube, a concrete dominance indicator is defined as

$$K = \frac{\int_0^{f_{cz}} Q_c df_{cz}}{\int_0^{f_{cz}} Q_s df_{cz}}. \quad (2.10)$$

In addition, a concrete contribution indicator is defined as a metric used to characterize the core concrete's contribution to the CFST column's load-bearing capability.

$$\Omega = \frac{\int_0^{f_{cz}} Q_c df_{cz}}{\int_0^{f_{cz}} Q_s df_{cz} + \int_0^{f_{cz}} Q_c df_{cz}}. \quad (2.11)$$

Note that the concrete dominance indicator K is related to the concrete contribution indicator Ω , as shown by Eq. (2.12). Larger the value of Ω , more is the contribution of the core concrete to the load-bearing capacity of the CFST column, as shown by Eq. (2.11). Note that $\Omega = 0$ represents a hollow steel tube and $\Omega = 1$ represents unconstrained concrete.

$$\Omega = \frac{K}{K+1}. \quad (2.12)$$

The indicator K is obtained by integrating the energy absorbed by the steel tube and core concrete over the compressive strength of the concrete, as shown in Fig. 2.9. It is necessary to define K , as it is not feasible to derive the law of the energy stored by concrete and steel tube independently. The enlarged area in Fig. 2.9 indicates that under the whole section loading mode, the lateral expansion of steel tube may occur more than the concrete, which will lead to a small decrease in the compressive strength of concrete. Therefore, the inflection points will appear in the figure.

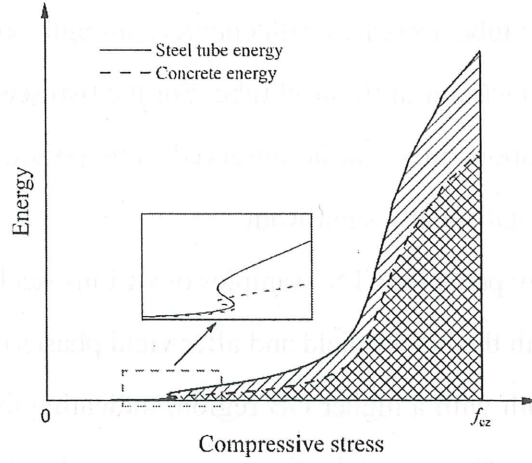


Fig. 2.9 Qualitative determination of the concrete dominance indicator K .

A higher value of K indicates that the core concrete absorbs more energy than the steel tube, as shown by Eq. (2.10). This demonstrates the importance of compressive stress in determining the energy paths of CFST columns.

2.3.2. Parametric analysis of the energy path

In this section, the effect of different parameters (i.e., f_c , f_y , and D/t) on the energy path of CFST columns under whole section loading is investigated. The energy paths exhibited different characteristics depending on the column parameter.

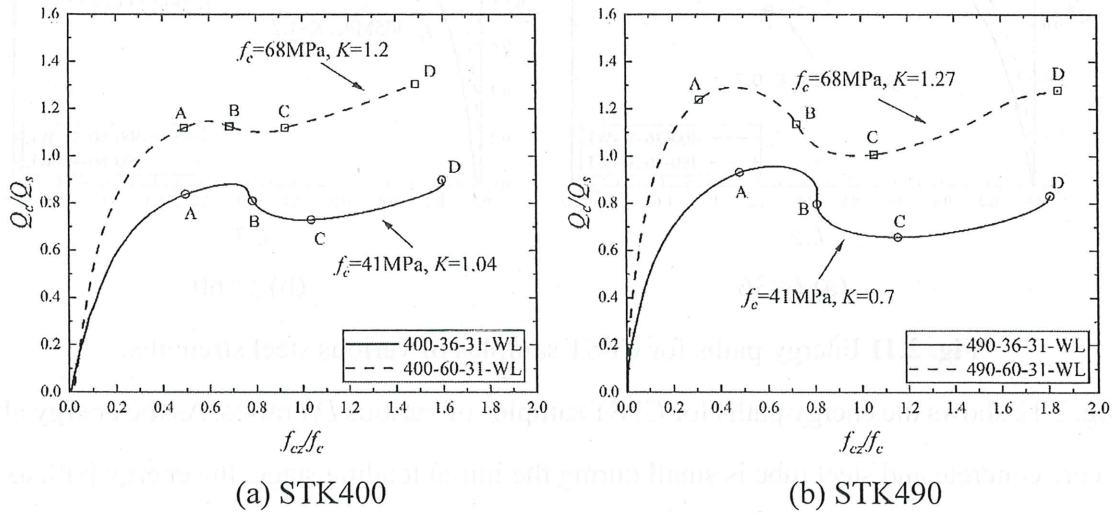


Fig. 2.10 Energy paths for CFST samples of various concrete strengths.

Fig. 2.10 shows the energy paths for CFST samples of various concrete strengths. It is observed that a higher concrete strength leads to a higher energy ratio, while the overall trend of the energy path remains the same. As the concrete strength increases, points A and C are shifted to lower compressive stress, indicating an increase in the brittleness of the concrete. Conversely, the proportion

of energy absorbed by the steel tube decreases with concrete strength, indicating that a high concrete strength leads to less efficient restraint of the steel tube. For the two sets of figures for different steel tube strengths, the same variation rules can be observed, thus proving that the effect of concrete strength on the energy path is statistically significant.

Fig. 2.11 shows the energy paths for CFST samples of various steel strengths. The steel strength has a significant impact on both the before yield and after yield phases of energy path. A higher steel strength leads to an energy path with a higher OB region, indicating that the core concrete absorbs more energy than the steel tube. Consequently, the core concrete develops microcracks at an earlier phase owing to the generation of lateral stress. Moreover, a higher steel strength leads to an energy path with a lower and more elongated BD region. This indicates a more efficient transfer of energy from the core concrete to the steel tube owing to lateral stress and a higher ductility of the constrained concrete. Similarly, for the two sets of figures for different concrete strengths, the statistically significant of effect of concrete strength on the energy path is proved.

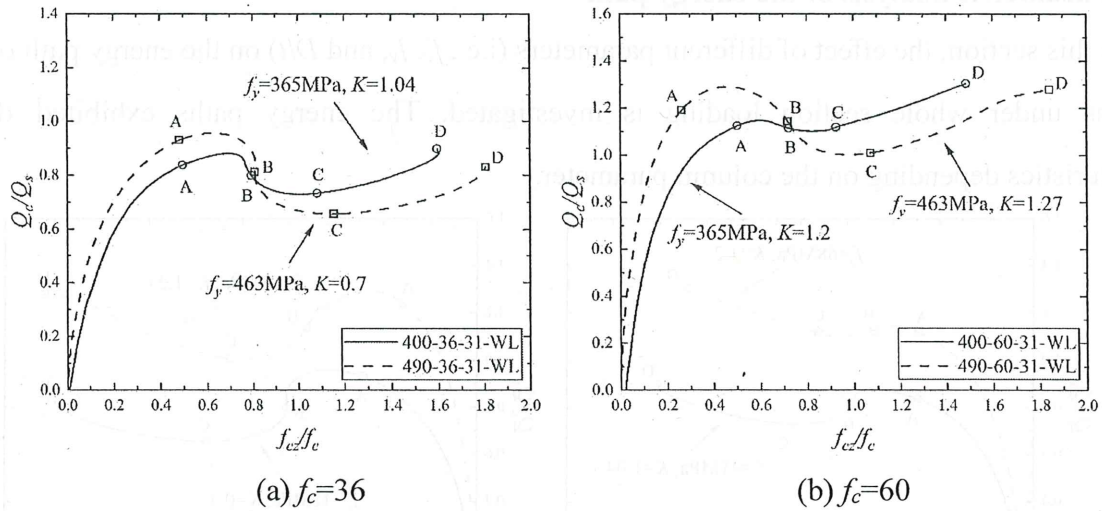


Fig. 2.11 Energy paths for CFST samples of various steel strengths.

Fig. 2.12 shows the energy paths for CFST samples of various D/t ratios. As the energy absorbed by the core concrete and steel tube is small during the initial loading stage, the energy path exhibits a lot of fluctuations. Moreover, minor differences in experimental conditions, such as the flatness of the loading face and cementation between the steel tube and concrete, affect the initial behavior of the energy path. The ratio of column diameter to steel tube thickness has the greatest impact on the AD stage and range of variation of the energy path, as seen in Fig. 2.12. Lower D/t ratio columns have a propensity to constrain the core concrete better because a larger portion of the energy is

absorbed by the steel tube. The sequential distribution of the energy paths for the three D/t ratios similarly demonstrates the generalizability of the effect rules.

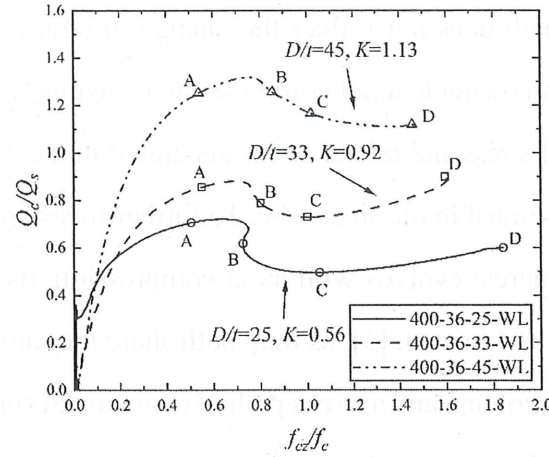


Fig. 2.12 Energy paths for CFST samples of various D/t ratios.

Interestingly, the D/t ratio and concrete strength seem to have a greater impact on the energy path than steel strength. However, the steadiness of the energy path is drastically impacted by the steel strength.

The energy path is represented by the concrete dominance indicator K , as discussed in Section 3.1. Table 2.1 presents an overview of the K values for all CFST specimens. The average values of K for different CFST samples are given in Figs. 8-10. As stated in Section 2.3, intrinsic or extrinsic causes may result in an increase in the load-bearing capability of CFST columns. For instance, an increase in the load-bearing capacity of CFST columns owing to the improved strength of concrete is an intrinsic factor, which also leads to an increase in the brittleness of the columns. Conversely, an increase in the load-bearing capacity owing to the confinement effect of the external steel tube is an extrinsic factor. For a given concrete strength, improving the D/t ratio and decreasing the steel strength decreases the total energy absorbed by the CFST column. This in turn decreases the overall ductility and strength but increases the concrete dominance indicator, indicating that the core concrete absorbs more energy than the steel tube. The total energy absorbed by the CFST column is not a suitable quantity for analyzing the energy path of the CFST column; hence, the concrete dominance indicator was used to represent the compressive strength of the CFST columns in this work.

2.3.3. Comparison of energy path and stress path

Stress-path-based analysis is a method proposed from Zhao [26] and Lin [3] to study the

confinement mechanism from variation of lateral pressure. To further clarify the force state of CFST during the energy path, the energy path of CFST columns was compared with their corresponding stress paths in this section, as they both share the same x-axis.

In general, the energy path does not reflect the change in stress experienced by the different components of a CFST column owing to axial compression. Conversely, the stress path describes the relationship between the axial stress and lateral stress generated in the constrained concrete but does not reflect the axial stress generated in the steel tube. To further investigate how the energy absorbed by the steel tube and core concrete evolves with axial compression, the energy path was compared with the stress path proposed by Lin et al. [3], as they both share the same x-axis. Fig. 2.13 compares a typical energy path of CFST column and a stress path of constrained concrete. While the axial stress in the concrete rises throughout the OA phase, the lateral stress does not adequately alter; consequently, the energy ratio increases with compressive stress. During the AB phase, the lateral stress in the concrete increases significantly while the axial stress increases only slightly; consequently, the energy ratio starts to decrease with compressive stress. During the BC phase, the lateral stress and axial stress exhibit opposite trends, indicating that the steel tube enters the yielding stage; consequently, the energy ratio starts to increase again. Finally, during the CD as steel hardening phase, both concrete lateral and axial stress increase; consequently, the energy ratio also increases with compressive stress. Thus, the energy state of the steel tube and concrete is significantly correlated with its force state.

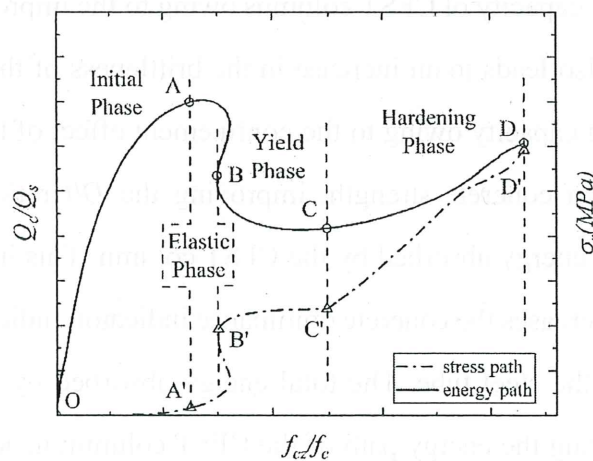


Fig. 2.13 Comparison with typical energy path of CFST column and stress path of constrained concrete.

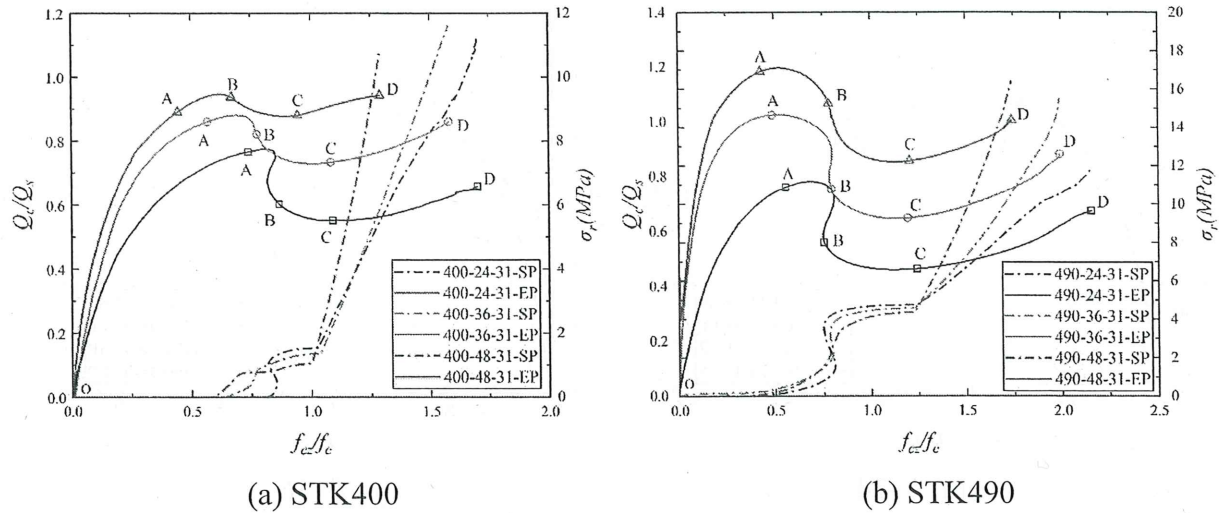


Fig. 2.14 Comparison of energy paths and stress paths for different concrete strengths.

Because the same column parameters (i.e., concrete strength, steel strength, and D/t ratio) affect both the energy and stress paths, the two paths for different CFST specimens are compared in Figs. 14-16. The numbers and letters in the specimen name indicate respectively steel grade, concrete design grade, D/t , and path mode (SP means stress path and EP means energy path). Fig. 2.14 shows that for the energy path, the energy ratio increases with increasing concrete strength; whereas, for the stress path, the slope of the steel hardening phase increases with concrete strength. This indicates that the energy path is more sensitive to concrete strength than the stress path. The change in energy ratio during the yielding and hardening stages of the steel tube is also consistent with the physical properties of steel.

Fig. 2.15 shows that there is an overlap between the energy paths for different steel strengths. In addition, the energy ratio fluctuates more for higher steel strengths, although the overall trend of the energy paths remains the same for different steel strengths. By contrast, the stress paths differ significantly for different steel strengths. This indicates that the stress path is more sensitive to steel strength than the energy path.

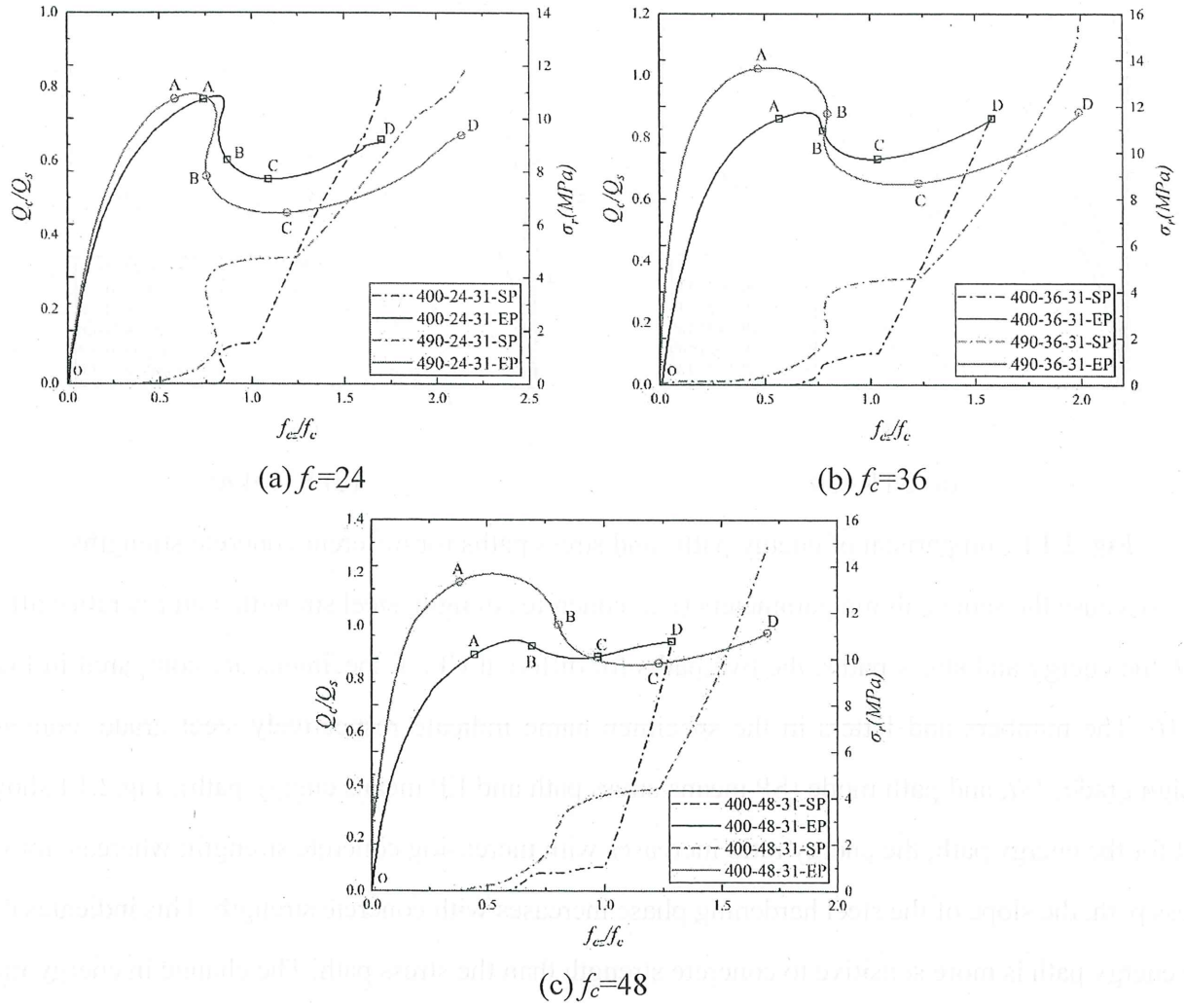


Fig. 2.15 Comparison of stress paths and energy paths for variable steel strengths.

Fig. 2.16 shows a comparison of the energy paths and stress paths for variable D/t ratios. The energy path is more sensitive to D/t ratio than the corresponding stress path for CFST columns under whole section loading, as shown in figure.

In addition, the effect of different parameters on energy paths are also consistent to the discussion in section 3.2 and exhibit statistical significance, as seen in Fig. 2.14-2.16.

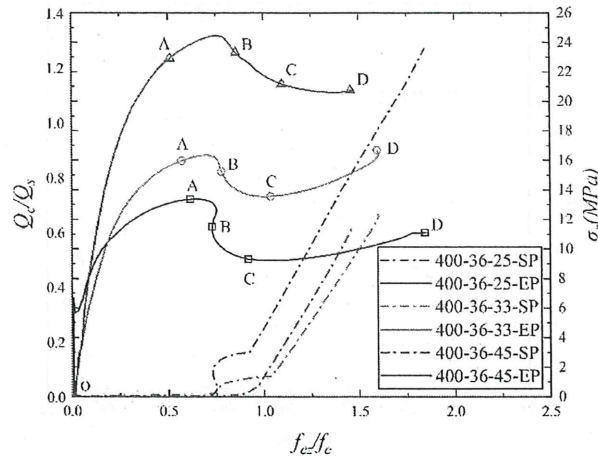


Fig. 2.16 Comparison of energy paths and stress paths for different D/t ratios.

2.4. Energy path-based load-bearing capacity of CFST columns

2.4.1. Effect of energy path on concrete compressive strength

Throughout this chapter, the effect of the energy path on constrained concrete compressive strength in CFST columns is investigated using the concrete dominance indicator K . Figs. 17 and 18 show K as a function of f_c/f_y and D/t , respectively.

Several studies have shown that the intrinsic relationships between the energy dissipation, energy released, ultimate strength, and abrupt structural failure of a CFST column are key to understanding the deformation processes in constrained concrete [27-29]. Thus, the compressive strength of constrained concrete is closely related to its energetics. Therefore, analysis of the energy absorbed by the core concrete can be used to develop a model for estimating the compressive strength of constrained concrete in CFST columns.

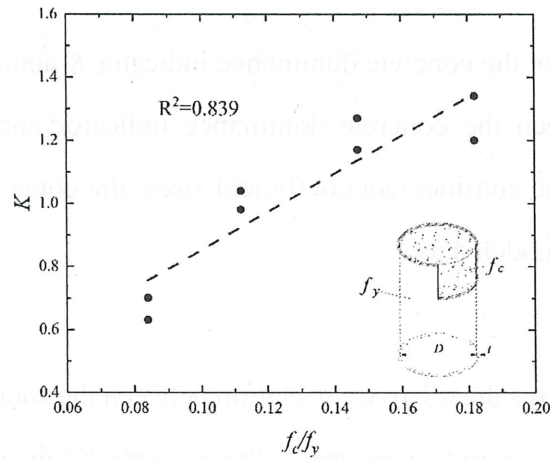


Fig. 2.17 Relation between the concrete dominance indicator K and f_c/f_y ratio.

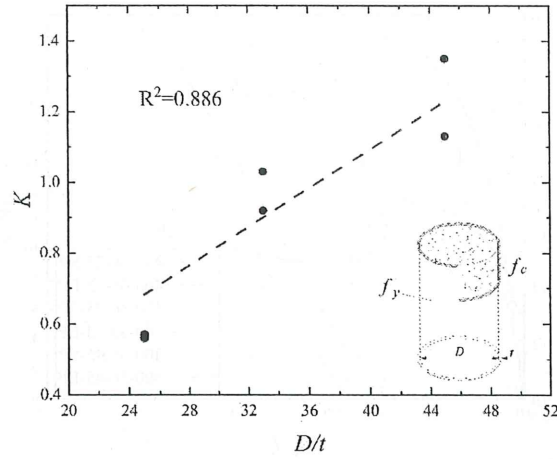


Fig. 2.18 Relationship between the concrete dominance indicator K and D/t ratio.

Energy path is known to be affected by column parameters from the study presented in Section 3.1, which in turn may determine the concrete dominance indicator. The following formula is used to define a confinement coefficient η that takes into account all the variables:

$$\eta = \frac{D-2t}{2t} \frac{f_c}{f_y} \quad (2.13)$$

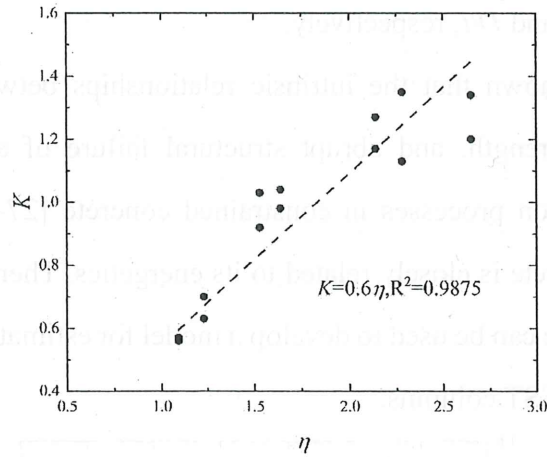


Fig.2.19 Relation between the concrete dominance indicator K and confinement coefficient η .

The relationship between the concrete dominance indicator and confinement coefficient is displayed in Fig. 2.19. As the confinement coefficient rises, the concrete dominance indicator also rises linearly, which can be modeled as:

$$K = 0.6\eta \quad (2.14)$$

The energy ratio represents the relative correlation between the energy absorbed by the steel tube and that absorbed by the core concrete; conversely, the concrete dominance indicator represents exact correlation between the two for a given structural composition. During the compression procedure, the energy accumulated by the CFST column reaches a maximum, which is called the energy storage

limit of the column [30-32]. The damage of CFST columns is ultimately a state instability phenomenon driven by energy. Concrete strength and lateral stress represent the factors affecting the strength improvement of different components respectively, and the effect of both is weighed by the concrete dominance indicator K . Based on the experimental results, a model to determine the compressive strength of constrained concrete in CFST columns under whole section loading is proposed, as follows:

$$f_{cz} = f_c + 0.4K^{0.2} f_c^{0.44} \sigma_r. \quad (2.15)$$

where K is given by Eq. (2.14). The effectiveness of the suggested model in comparison to the experimental findings is shown in Fig. 2.20. The suggested model had an R-squared value of 0.9864. The performance of the proposed model is in good agreement with the measured data. In summary, the indicator K derived from the energy relationship is accurate and easy to calculate, and the predicted concrete strength can be obtained from the basic parameters. Moreover, the expression of Eq. (2.15) is also quite simple, which can be conveniently used in the design of CFST columns and further theoretical studies on the energy relations of CFST columns.

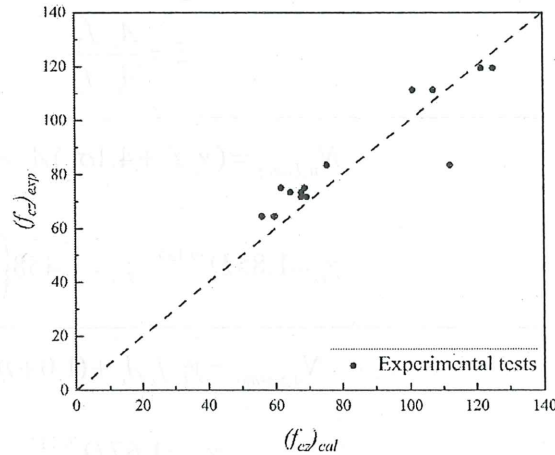


Fig. 2.20 Effectiveness of the suggested model.

2.4.2. Load-bearing capacity of CFST columns and verification

Based on the load superposition of steel tube and concrete, the model of load-bearing capacity of CFST column can be obtained as:

$$N_{cu} = f_{cz} A_c + f_{sz} A_s. \quad (2.16)$$

where f_{sz} is the axial stress of steel tube at peak state; f_{cz} is determined by Eq. (2.15).

Table 2.2

Typical load-bearing capacity formulas from existing design codes and empirical models

Design Codes	Formulas
AIJ[15]	$N_{u,AIJ} = 0.85 f_c A_c + (1.0 + \eta) f_y A_s$
ACI[16]	$N_{u,ACI} = 0.85 f_c A_c + f_y A_s$
AISC[17]	$N_{u,AISC} = \begin{cases} N_p & (\text{Compact}) \\ N_p - \frac{N_p - N_y}{(\lambda_r - \lambda_p)^2} (\lambda - \lambda_p)^2 & (\text{Noncompact}) \\ f_{cr} A_s + 0.7 f_{co} A_c & (\text{Slender}) \end{cases}$ $N_p = f_s A_s + 0.95 f_c A_c \quad N_y = f_s A_s + 0.7 f_c A_c$ $f_{cr} = \frac{0.72 f_y}{\left[\left(\frac{D}{t} \right) \frac{f_y}{E_s} \right]^{0.2}}$
Empirical Models	Formulas
Cai et al.[34]	$N_{u,Cai} = (1 + \sqrt{\xi} + \xi) f_c A_c$ $\xi = \frac{A_s f_y}{A_c f_c}$
Liang and Fragomeni[35]	$N_{u,Liang} = (\gamma_c f_c + 4.1 \sigma_r) A_c + \gamma_s f_y A_s$ $\gamma_c = 1.85 D^{-0.135} \quad \gamma_s = 1.458 \left(\frac{D}{t} \right)^{-0.1}$
Sakino et al.[33]	$N_{u,Sakino} = \gamma_U f_c A_c + (1.0 + \eta) f_y A_s$ $\gamma_U = 1.67 D^{-0.112}$

Based the experimental, theoretical and finite element analysis results, the circumferential stress σ_θ of the steel tube is taken as $0.6f_y$ [10], and according to Eq. (2.3), the lateral stress σ_r can be obtained. The concrete compressive strength f_{cz} can be obtained by taking the lateral stress σ_r , the concrete dominance indicator K and the concrete strength f_c into Eq. (2.15). Considering that the steel tube is generally in the hardening phase when the CFST column reaches the peak stress state, and combining with the analysis of Hatzigeorgiou et al. [11], the von Mises stress is taken 1.25 times of the steel strength. The value of f_{sz} can be given as $0.84f_y$ by Eq. (2.5). Therefore, the prediction model of this

paper can be proposed as below:

$$N_{cu} = f_{cu} A_c + 0.84 f_y A_s. \quad (2.17)$$

Table 2.3

Detailed information on the 157 published experimental data.

Ref.	Number of Specimens	f_y (Mpa)	f_c (Mpa)	D (mm)	t (mm)	D/t	N_u (kN)
Lin et al.[3]	18	371.9-462.9	26.88-49.92	140-216.3	4.5-8.2	26.4-48.1	1275.3-3800.3
Gardner et al.[36]	12	363.3-633.4	20.9-43.4	76.2-152.6	1.68-4.93	29.5-48.4	355.6-2911.6
Tang et al.[37]	11	232.4-433.5	20-46.6	92-210	1.5-4.5	24-84	504.7-1636.6
Lin et al.[34]	8	360.8	30.72-61.44	208-230	2.3-3.2	65-100	1901.8-3272.5
Sakino et al.[38]	12	249-283	21.3-43.6	174-179	3-9	19.8-58	1410-2730
M. Saisho et al.[39]	8	341-377.3	24.4-28.2	101.6-139.8	2.37-2.99	34.0-59.0	676.0-1107.0
O'Shea et al.[40]	15	185.7-363.3	41.0-108.0	165-190	0.86-2.82	58.5-220.9	1350.0-3360.0
Yamamoto et al.[41]	10	371-452	22.3-49.2	101.4-216.4	3.02-6.66	32.5-33.5	660.0-4023.0
Hiroaki et al.[42]	12	176-321	24.6-32.2	299.98-300.26	0.94-4.17	71.4-319.2	1957.0-4314.0
Chen et al.[43]	9	251.8-304.3	70.86-130.8	107.9-114.9	2.05-8.03	13.4-55.5	904-1748

Farid et al.[44]	6	300	44.0-60.0	114-167	3.1-5.6	20.4-53.9	1042.0-1873.0
Lai et al.[45]	6	365	29.1-114.3	114-168	5-10	13.9-33.6	1876.0-3408.0
Richard et al.[46]	7	308-428	49.5-166.6	114.3-219.1	3.6-6.3	18.1-43.8	2314.0-3118.0
Ye et al.[47]	2	287.5	24.1	165	2.37	69.6	996.0-1008.0
Talha et al.[48]	6	235-355	54.0-102.9	114.3	2.74-5.9	19.4-41.7	901.8-1989.9
Zhou et al.[49]	15	691-734	35.07-37.82	140.84-262.00	2.11-3.04	49.55-124.12	1550.0-4302.0

The proposed capacity prediction model in this paper is compared with the existing models, for verifying the accuracy and applicability of the model. Typical load-bearing capacity formulas from existing design codes and empirical models are listed in Table 2.2. Also, the model was evaluated using 157 specimen results and the data from the experiments used are displayed in Table 2.3. It should be noted that in some of the specimen results the concrete strengths were defined based on standard cube concrete strength f_{cu150} . To convert f_{cu150} to the equivalent standard cylinder concrete strength, the model proposed by L'Hermite [50] is used:

$$f_c = \left[0.76 + 0.2 \log_{10} \left(\frac{f_{cu150}}{19.6} \right) \right] f_{cu150}. \quad (2.18)$$

This paper uses two statistical indicators, the average value (AV) and the average absolute error (AAE) of N_{uc}/N_u , which are calculated according to Eqs. 2.19-2.20, for comparing the prediction effects of different models. The statistical indicators of different prediction models are exhibited in Table 2.4. The results of the comparison between the calculated and tested values of different prediction models are shown in Fig. 2.21. As seen from Table 2.4 and Fig. 2.21, the proposed model in this paper has a better fitting result, with an AE of 0.9979 and an AAE of 0.0820 of N_{uc}/N_u , which is more accurate, and the integral error between the calculated and tested values is basically controlled within 20%. It can be seen that, the load-bearing capacity model of CFST columns obtained by the

energy path is very effective, after clarifying the interaction mechanism between the concrete and steel tube.

It should be noted that the specimens tested in this paper are subjected to the quasi-static axial loading. As a good seismic structure, the study of the interaction mechanism between steel tube and concrete under dynamic or seismic loading for CFST columns is also important and significant. The energy paths and corresponding relations with the compressive strength of CFST columns under dynamic or seismic loading need to be further investigated.

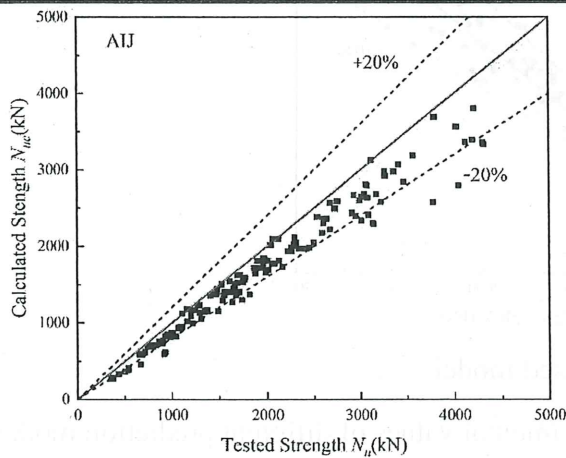
$$AV = \frac{\sum_{i=1}^n \frac{N_{uc}}{N_u}}{n} \quad (2.19)$$

$$AAE = \frac{\sum_{i=1}^n \left| \frac{N_{uc} - N_u}{N_u} \right|}{n} \quad (2.20)$$

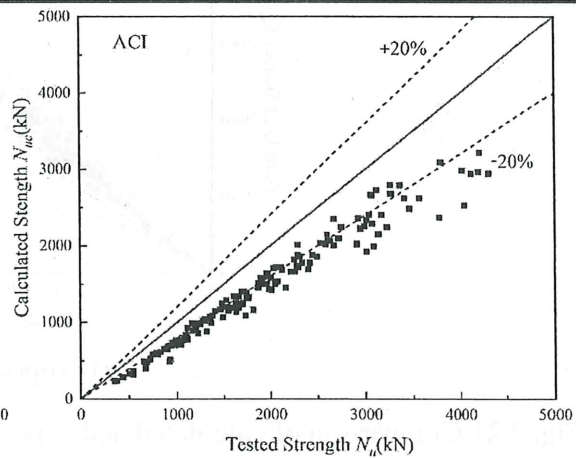
Table 2.4

Verification for the proposed model and existing models

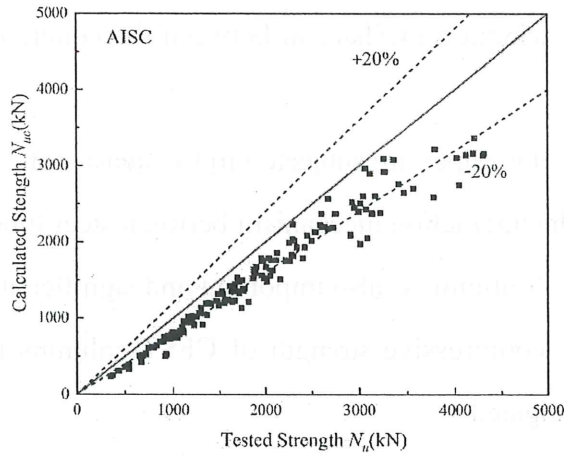
Assessment	AIJ	ACI	AISC	Cai et al.	Liang and	Sakino et	Proposed
Indicators	[15]	[16]	[17]	[34]	Fragomeni [35]	al. [33]	
AV	0.8723	0.7571	0.8031	1.2011	1.0735	0.9200	0.9979
AAE	0.1284	0.0700	0.2429	0.2072	0.1098	0.0869	0.0820



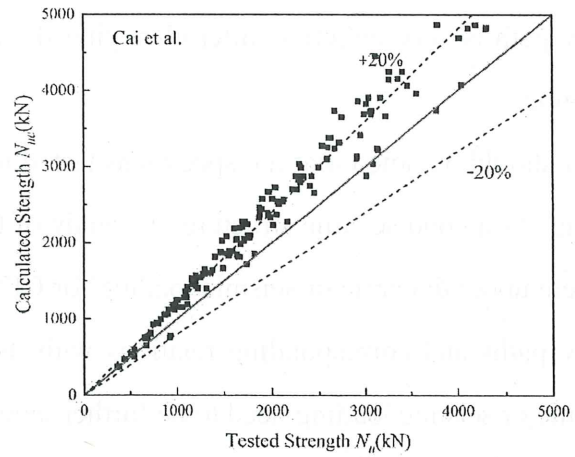
(a) AIJ



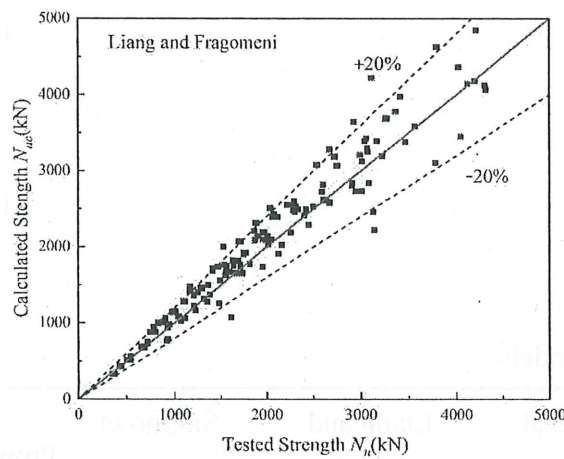
(b) ACI



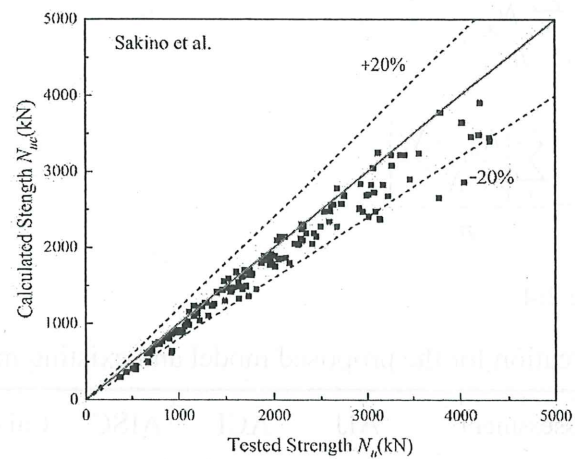
(c) AISC



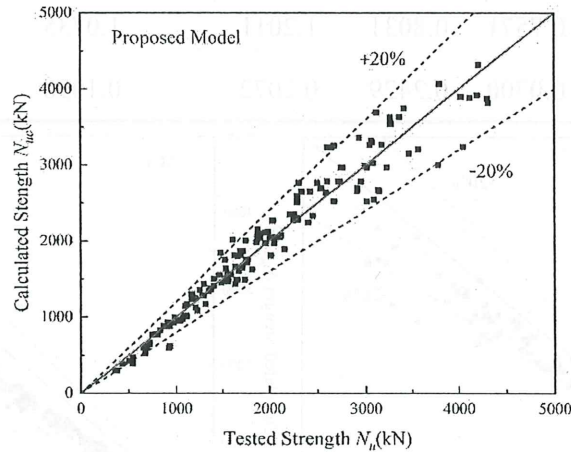
(d) Cai et al.



(e) Liang and Fragomeni



(f) Sakino et al.



(g) Proposed model

Fig. 2.21 Comparison of calculated and experimental values of different prediction models.

2.5. Conclusions

In this study, the interaction mechanism between external steel tube and internal concrete of circular CFST stub columns was theoretically and experimentally investigated using the energy paths

for the first time. The relative relationship between the energy absorbed by concrete and steel tube is visualized in the form of energy paths, reducing the effect of differences in experimental results. The two performance indices (i.e., the concrete dominance indicator K and the concrete contribution indicator Ω) were introduced to quantitatively characterize the energy paths. Based on the results and discussions in this study, the following findings were drawn:

1. The energy path represents the variation of the energy ratio (Q_c/Q_s) during the loading process, and the interaction mechanism between the components is investigated according to the regularity. After the initial phase, the energy ratio decreases indicating increased lateral expansion of the concrete, which means transferring energy to the external steel tube. Accordingly, the decrease in energy ratio begins to slacken after the steel tube enters the plastic phase. Finally, the energy ratio tends to stabilize during the hardening phase until the specimen reaches peak stress.
2. The energy path of CFST column is influenced by various parameters, namely, steel strength f_y , concrete strength f_c , and ratio of column diameter to steel tube thickness D/t . The energy paths for different test conditions were represented by the concrete dominance indicator K . The findings of the experiment revealed that the concrete dominance indicator K rose with f_c/f_y and D/t ratios, indicating the increased contribution of core concrete to the energy path compared to that of steel tube.
3. The force state of CFST columns during the loading process was further analyzed by comparing its energy path with stress path of constrained concrete. The energy paths were found to be more sensitive to D/t ratio and concrete strength f_c ; nevertheless, the stress paths were found to be more sensitive to the steel strength f_y .
4. One model for determining concrete compressive strength and load-bearing capacity of CFST columns under whole section loading was proposed from an energy relation perspective. The predictions by proposed model and the tested results agreed fairly well.

Appendix. A Simple Numerical Example for The Energy Path Calculation

The procedure for calculating the energy absorbed by the concrete Q_c is introduced as follows:

1. Based on the Eqs. (2.4) - (2.9), the stress-strain relationships in three directions of the concrete are obtained.
2. Select initial points on the stress-strain relationship: Vertical direction $U_{czi} = (f_{czi}, \varepsilon_{ci})_{i=1}$, Lateral

direction $U_{cri}=(\sigma_{ri}, \varepsilon_{ri})_{i=1}$.

3.The energy density in vertical direction of concrete U_{cz} :

$$U_{cz} = \int_0^{\varepsilon_c} f_{cz} d\varepsilon_c \approx \sum_{i=1}^j \frac{(f_{czi} + f_{czi+1})(\varepsilon_{czi+1} - \varepsilon_{czi})}{2}, i=1, 2 \dots j, \quad (2.21)$$

The energy density in lateral direction of concrete U_{cr} :

$$U_{cr} = 2 \int_0^{\varepsilon_r} \sigma_r d\varepsilon_r \approx 2 \sum_{i=1}^j \frac{(\sigma_{ri} + \sigma_{ri+1})(\varepsilon_{ri+1} - \varepsilon_{ri})}{2}, i=1, 2 \dots j, \quad (2.22)$$

j stands for the point of ultimate strength.

4.The total energy density of concrete U_c :

$$U_c = U_{cz} + U_{cr}. \quad (2.23)$$

5.Take Eqs. (2.23) into Eqs. (2.21), energy absorbed by the concrete Q_c is obtained. Each time steps 3-5 are calculated, Q_c corresponding to the compressive stress f_{cz} can be obtained.

The procedure for calculating the energy absorbed by the steel tube Q_s is introduced as follows:

6.Based on the Eqs. (2.3), (2.5) - (2.9), the stress-strain relationships in two directions of the steel tube are obtained.

7.Select initial points on the stress-strain relationship: Vertical direction $U_{szi} = (\sigma_{zi}, \varepsilon_{zi})_{i=1}$, Loop direction $U_{s\theta i} = (\sigma_{\theta i}, \varepsilon_{\theta i})_{i=1}$.

8.The energy density in vertical direction of concrete U_{sz} :

$$U_{sz} = \int_0^{\varepsilon_z} \sigma_z d\varepsilon_z \approx \sum_{i=1}^j \frac{(\sigma_{zi} + \sigma_{zi+1})(\varepsilon_{zi+1} - \varepsilon_{zi})}{2}, i=1, 2 \dots j, \quad (2.24)$$

The energy density in loop direction of concrete $U_{s\theta}$:

$$U_{s\theta} = \int_0^{\varepsilon_\theta} \sigma_\theta d\varepsilon_\theta \approx \sum_{i=1}^j \frac{(\sigma_{\theta i} + \sigma_{\theta i+1})(\varepsilon_{\theta i+1} - \varepsilon_{\theta i})}{2}, i=1, 2 \dots j, \quad (2.25)$$

j stands for the point of ultimate strength.

9.The total energy density of steel tube U_s :

$$U_s = U_{sz} + U_{s\theta}. \quad (2.26)$$

10.Take Eqs. (2.26) into Eqs. (2.2), energy absorbed by the steel tube Q_s is obtained. Each time steps 8-10 are calculated, Q_s corresponding to the compressive stress f_{cz} can be obtained.

In the end, the energy path of Q_c / Q_s versus f_{cz} / f_{co} is calculated.

References

- [1] S.Q. Lin, Y.G. Zhao, Z.H. Lu, Modified confining stress path dependent analytical model for axially loaded circular normal, high and ultra-high strength concrete-filled steel tube stub columns, *Compos Struct.* 2020, 242.
- [2] Z.H. Lu, Y.G. Zhao, Suggested empirical models for the axial capacity of circular CFT stub columns, *J Constr Steel Res.* 66.6(2010)850-862.
- [3] S.Q. Lin, Y.G. Zhao, L.S. He, Stress paths of confined concrete in axially loaded circular concrete-filled steel tube stub columns, *Eng Struct.* 173(2018)1019-1028.
- [4] X.F. Yan, Y.G. Zhao, S.Q. Lin, Compressive behaviour of circular CFST short columns with high- and ultrahigh-strength concrete, *Thin-Wall Struct.* 164(2021) 107898.
- [5] J.J. Zeng, Y.W. Zheng, F. Liu, Behavior of FRP Ring-Confined CFST columns under axial compression[J]. *Compos Struct.* 2020.
- [6] S. Morino, J. Kawaguchi, Research on and construction of the concrete-filled steel tube column system in Japan, *Int J of Steel Struct.* 5(2005)277-298.
- [7] B. Uy, Strength of short concrete filled high strength steel box columns, *J Constr Steel Res.* 57(2001)113-134.
- [8] M.C. Sundarraja, G.G. Prabhu, Experimental investigation on strengthening of CFST columns using CFRP composites, *Int J Earth Sci Eng.* 6(2013)15-20.
- [9] L.H. Han, S.L. Zhong, Study on the working mechanism and behavior of concrete filled steel tubular (CFST) members subjected to compression, bending and torsion, *J Build Struct.* 49(1995) 379-395.
- [10] D. Gan, Study of static and seismic performance of short concrete columns restrained by steel tubes, Lanzhou University (2012). [in Chinese].
- [11] G.D. Hatzigeorgiou, Numerical model for the behavior and capacity of circular CFT columns, Part I: Theory, *Eng Struct.* 30.6(2008)1579-1589.
- [12] MF Hassanein, AY Hamed, KA Cashell, YB Shao, Confinement-based direct design method for fibre reinforced polymer confined CFST short columns, *Thin-Walled Struct.* 192(2023) 111207.
- [13] MF Hassanein, AY Hamed, YB Shao, N Silvestre, Confinement-based direct design of circular steel tube confined concrete (STCC) short columns, *J Constr Steel Res.* 204(2023), 107871.
- [14] MF Hassanein, N Silvestre, New confining stress-based design for rubberised concrete-filled

- single/double-skin steel tubular short columns, *J Constr Steel Res.*197(2022), 107435.
- [15] AIJ. Standards for structural calculation of steel reinforced concrete structures 5th ed. Tokyo (Japan): Architectural Institute of Japan; 2001 [in Japanese].
- [16] ACI-318R (2005). Building code requirements for structural concrete and commentary. Farmington Hills, American Concrete Institute, MI, USA.
- [17] AISC (2005). Load and resistance factor design (LRFD) specification for structural steel buildings. American Institute of Steel Construction, Chicago, USA.
- [18] L.H. Han, X.L. Zhao, T. Zhong, Tests and mechanics model for concrete-filled SHS stub columns, columns and beam-columns, *Steel Compos Struct.* 1(2001)51-74.
- [19] M. Ahmed, Q.Q. Liang, VI Patel, A Hamoda, Unified numerical model for performance analysis of various cross-sections of concrete-filled stainless-steel tubular stub columns under axial loading, *Struct.* (2023).
- [20] VI Patel, Analysis of uniaxially loaded short round-ended concrete-filled steel tubular beam-columns, *Eng Struct.*205(2020) 110098.1-110098.13.
- [21] M. Shams, M.A. Saadeghvaziri, Nonlinear response of concrete-filled steel tubular columns under axial loading, *Struct J.* 96(1999)1009-1017.
- [22] S.P. Schneider, Axially loaded concrete-filled steel tubes, *J Struct Eng.* 124(1998)1125-1138.
- [23] S.M. Zhang, L.H. Guo, Z. Ye, Y.Y. Wang, Behavior of steel tube and confined high strength concrete for concrete-filled RHS tubes, *Adv Struct Eng.* 8(2005)101-116.
- [24] T. Nishiyama, Y. Chen, H. Kusuda, T. Ito, K. Kaneko, H. Kita, T. Sato, The examination of fracturing process subjected to triaxial compression test in Inada granite, *Eng Geol.* 2002.
- [25] M.J. Mccaveney, T.R. Davies, Surface energy is not one of the energy losses in rock comminution, *Eng Geol.* 109(2009)109-113.
- [26] Y.G. Zhao, S.Q. Lin, Z.H. Lu, T. Saito, L.S. He, Loading paths of confined concrete in circular concrete loaded CFST stub columns subjected to axial compression, *Eng Struct.* 156(2018)21-31.
- [27] H.P. Xie, L.Y. Li, R.D. Peng, Y. Ju, Energy analysis and criteria for structural failure of rocks, *J Rock Mech Geotech Eng*, 1(2009)11-20.
- [28] Rong C, Shi Q. Analysis constitutive models for actively and passively confined concrete, *Compos Struct* 2021; 256(4):113009.
- [29] L.M. Zhang, Y. Cong, F.Z. Meng, Z.Q. Wang, P. Zhang, S. Gao, Energy evolution analysis and

- failure criteria for rock under different stress paths, *Acta Geotech.* 16(2020)569-580.
- [30] G.Y. Zhao, B. Dai, L.J. Dong, C. Yang, Energy conversion of rocks in process of unloading confining pressure under different unloading paths, *T Nonferr Metal Soc.* 25(2015)1626-1632.
- [31] B.S. Institution, Amendment no. 6 To Bs 8110: Part 1: Structural use of concrete. Part 1: Code of practice for design and construction. 1985.
- [32] E. Standardization, Design of concrete structures. Part 1. General rules and rules for buildings (together with United Kingdom National Application Document), Eurocode 2. 1992.
- [33] K. Sakino, H. Nakahara, S. Morino, Behavior of Centrally Loaded Concrete-Filled Steel-Tube Short Columns, *J Struct Eng.* 130(2004)180-188.
- [34] S.Q. Lin, Y.G. Zhao, Ultimate Stress of the Steel Tube in Circular CFT Stub Columns Subjected to Axial Compression, *Inter J Eng Tech*, 10.4 (2018):315-319.
- [35] Q.Q. Liang, S. Fragomeni, Nonlinear analysis of circular concrete-filled steel tubular short columns under axial loading, *J Constr Steel Res.* 65.12 (2009): 2186-2196.
- [36] N. J. Gardner, E. R. Jacobson, Structural Behavior of Concrete Filled Steel Tubes, *aci Struct J.*
- [37] G.Z. Tang, B.Q. Zhao, H.X. Zhu, X.M. Shen, Study on the Fundamental Structural Behavior of Concrete Filled Steel Tubular Columns, *J Build Struct.* 1982.
- [38] K. Sakino, H. Hayashi, Behavior of concrete filled steel tubular stub columns under concentric loading. In: *Proceeding of the 3rd international conference on steel-concrete composite structures.* 1991. 25-30.
- [39] M. Saisho, T. Abe, K. Nakaya, Ultimate bending strength of high-strength concrete filled steel tube column, *J Struct and Construct Eng (Transactions of AIJ).* 523(1999)133-140.
- [40] M.D. O'Shea, R.Q. Bridge, Design of Circular Thin-Walled Concrete Filled Steel Tubes, *J Struct Eng.* 126(2000)1295-1303.
- [41] Y. Takamasa, K. Jun, M. Shosuke, Experimental study of the size effect on the behaviour of concrete filled circular steel tube columns under axial compression, *J Struct and Construct Eng (Transactions of AIJ).* 67(2002)237-244.
- [42] H. Kitoh, T. Koyabu, K. Sahara, K. Sonoda, Concrete filled circular steel tubular stubs with a large ratio of diameter to thickness under compression, *JSCE Proceedings.* 2010,25-36.
- [43] S.M. Chen, Z. Rui, L.J. Jia, Structural behavior of UHPC filled steel tube columns under axial loading, *Thin-Walled Struct.* 130(2018)550-563.

- [44]F. Abed, M. Alhamaydeh, S. Abdalla, Experimental and numerical investigations of the compressive behavior of concrete filled steel tubes (CFSTs), J Constr Steel Res. 80(2013)429–439.
- [45]M.H. Lai, J.C.M. Ho, Behaviour of uni-axially loaded concrete-filled-steel-tube columns confined by external rings, Struct. Des. Tall Spec. Build. 23(2014)403-426.
- [46]J.Y. Richard Liew, M.X. Xiong, D.X. Xiong, Design of Concrete Filled Tubular Beam-columns with High Strength Steel and Concrete, Struct. 2016,213-226.
- [47]Y. Ye, L.H. Han, T. Sheehan, Z.X. Guo, Concrete-filled bimetallic tubes under axial compression: Experimental investigation, Thin-Walled Struct. 2016.
- [48]Ekmekyapar, Talha, Al-Eliwi, Baraa, J.,M, Experimental behaviour of circular concrete filled steel tube columns and design specifications, Thin-Walled Struct. 2016.
- [49]S.M. Zhou, Q. Sun, X. Wu, Impact of D/t ratio on circular concrete-filled high-strength steel tubular stub columns under axial compression. Thin-Walled Struct.132(2018):461-474.
- [50] R.. L'Hermite, Idées actualles sur la technologie du béton, Documentation Technique du Bâtiment et des Travaux Publics, Paris, 1955.

CHAPTER 3. ENERGY PATH OF FRP-CONFINED CONCRETE STUB COLUMNS SUBJECTED TO AXIAL COMPRESSION

3.1. Introduction

Fiber-reinforced polymer (FRP) composites have been used in the construction sector for over three decades due to their properties, such as high strength-to-weight ratio, high tensile strength and modulus, corrosion resistance, and durability. One important application of FRP composites is as a confining material for concrete, particularly in the strengthening or seismic retrofit of existing reinforced concrete columns by the provision of an FRP jacket [1-9]. The mechanical behavior of FRP-confined concrete has long been the main concern for structural design in the field of engineering. Depending on the different type, strength and number of layers of FRP jacket, the stress-strain relationship of FRP-confined concrete will exhibit strain hardening behavior or strain softening behavior. A well-established ultimate strength is important for the investigation of the constitutive relationship of FRP-confined concrete [7, 10].

In the past few decades, a large number of researchers have been carried out on the ultimate conditions of FRP-confined concrete columns, leading to proposed of 68 compressive strength models [11]. These models were largely based on the design-oriented constitutive relationship and analysis-oriented constitutive relationship [9]. Many of these models were either empirically regressed from test results or adopted the actively confined concrete or steel-confined concrete models. These models generally well predicted the experimental results, especially that were adopted to develop the model, while in some other cases could lead to uncertain satisfactory accuracy [11]. The reason may result from the insufficient understanding of the interaction mechanism between the FRP jacket and the concrete of FRP-confined concrete [3].

Early in the 1980s, Mander et al. [12] proposed a new energy-balance based research method, which was mainly used to develop the ultimate strain model of confined concrete columns. This method assumes that the additional strain energy capacity of a confined concrete column relative to its unconfined counterpart is equal to the work done by the confining material up to its rupture [13-16]. Although, Matthys [17] and Pham [18, 19] have doubted the rationality of the energy balance method and made some corrections and improvements. These research focus more on the quantitative relationship between the additional strain energy and the strain energy of FRP jacket. In fact, during

the axial compression of FRP-confined concrete, the lateral expansion of the concrete makes the FRP jacket tensile in the hoop direction, which is itself an energy transfer process [20-22]. The variations for the strain energy of concrete and FRP jacket are closely related to their force and deformation states. However, the interaction mechanism between the FRP jacket and the concrete of FRP-confined concrete columns has not been investigated from the perspective of the energy relationship to date.

In this study, the interaction mechanism between the FRP jacket and the concrete of FRP-confined concrete columns was investigated from an energy relations perspective for the first time. The energy path method was proposed to reflect the relative energy relations between the FRP jacket and the concrete, which was defined as the trajectory of energy ratio absorbed by the FRP jacket and concrete with the compressive strength. Nine sets of axial compression tests on FRP-confined concrete columns were executed and the energy paths for each set were obtained from the measured data. The energy paths of FRP-confined concrete with different column parameters were investigated theoretically and experimentally, and the relationship between the energy paths and compressive strength of FRP-confined concrete was studied. Theoretical expression for the energy path was derived, and with the experimental results, an energy path-based compressive strength model was proposed for FRP-confined concrete. The developed model yielded more accurate predictions than existing models based on the results of this paper and previous tests.

3.2. Evaluation method of energy path

3.2.1. Definition of the energy path

The energy path was defined as the trajectory of energy ratio absorbed by the FRP jacket and concrete with the compressive strength. In an FRP-confined concrete column under whole section loading, the concrete is subjected to forces from all three directions with two equal stresses along the horizontal directions, as shown in Fig. 3.1. In the axial direction, the FRP jacket and concrete are cooperatively in deformation. The energy density of the concrete is obtained by integrating the stress-strain relations along all three directions, and the work done by the external force is obtained by integrating the energy density over the volume of the concrete. Therefore, the energy absorbed by the concrete at each loading stage is given by

$$Q_c = A_c H U_c = A_c H \left(\int_0^{\varepsilon_c} f_{cz} d\varepsilon_c + 2 \int_0^{\varepsilon_r} \sigma_r d\varepsilon_r \right), \quad (3.1)$$

where Q_c denotes the energy that the concrete absorbed at each loading stage; A_c is the cross-sectional area of the core concrete; H is the height of the CFST column; U_c represents the energy density of the core concrete; f_{cz} is the compressive stress generated in the core concrete; σ_r denotes the lateral stress generated in the core concrete; ε_c denotes the axial strain of the core concrete; and ε_r denotes the radial strain of the core concrete.

The FRP jacket is simultaneously subjected to hoop stress; however, the stress along the direction of its thickness can be neglected. Therefore, the energy density of the FRP jacket is obtained by integrating the stress-strain relations along one directions, and the work done by the external force is obtained by integrating the energy density over the volume of the FRP jacket. Thus, the energy that the FRP jacket absorbed at each loading stage is given by

$$Q_f = A_f H U_f = A_f H \int_0^{\varepsilon_\theta} \sigma_\theta d\varepsilon_\theta, \quad (3.2)$$

where Q_f denotes the energy that the FRP jacket absorbed at each loading stage; A_f is the FRP jacket's cross-sectional area; U_f represents the FRP jacket's energy density; σ_θ denote the hoop stress generated in the FRP jacket; and ε_θ denotes the FRP jacket's hoop strain.

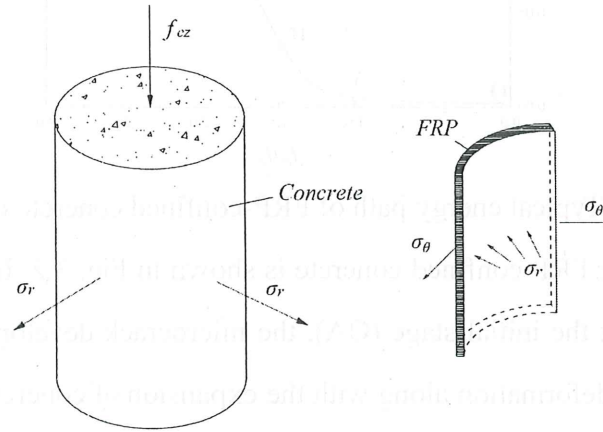


Fig. 3.1 Stress state of circular FRP-confined concrete column.

The variation of the energy ratio (Q_f/Q_c) with the compressive strength of constrained concrete (f_{cz}) normalized with respect to the strength of unconfined concrete (f_c) gives the energy path of the FRP-confined concrete column. According to Eqs. (3.1) and (3.2), the stress-strain relations of the concrete and FRP jacket are required to determine the energy path, as specified below.

For an axially loaded circular FRP-confined concrete, the compressive stress (f_{zc}) and lateral stress (σ_r) can be respectively given as follows:

$$f_{cz} = \frac{N}{A_c}, \quad (3.3)$$

$$\sigma_r = \frac{2t}{D} \sigma_\theta = \frac{2tE_f \varepsilon_\theta}{D}, \quad (3.4)$$

where N denotes the axial load; t denotes the thickness of the FRP jacket; E_f denotes the elastic modulus of the FRP jacket; D denotes the diameter of the concrete.

The energy absorbed by the concrete and FRP jacket can be calculated by substituting the axial and lateral stresses generated in the core concrete in Eq. (1) and the hoop stress generated in the FRP jacket in Eq. (2), respectively. Consequently, the energy paths of FRP-confined concrete columns can be determined.

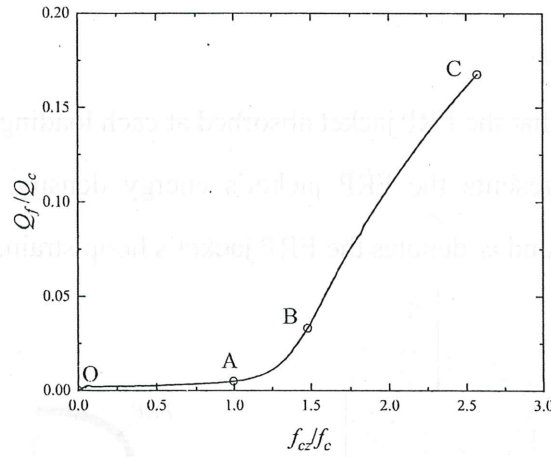


Fig. 3.2 Typical energy path of FRP-confined concrete column.

A typical energy path for FRP-confined concrete is shown in Fig. 3.2. In general, the energy path consists of three stages. At the initial stage (OA), the microcrack develops slowly in concrete, and FRP jacket suffers tensile deformation along with the expansion of concrete. As the deformations of concrete and FRP jacket are harmonized, the energy ratio varies little and close to a constant value during the OA phase. Therefore, the behavior of FRP-confined concrete at this stage is not significantly influenced by the lateral confinement but the inherent property of the concrete. When the axial stress exceeds the unconfined concrete strength, the energy path exhibits a transition stage (AB), during which microcracks start to develop rapidly and energy ratio increases. This indicates that the increased rate of energy absorbed by the FRP jacket is higher than the rate of energy absorbed by the concrete. As the lateral stress increases, more energy is transferred from the concrete to the FRP jacket. At the AB stage, both the property of the concrete and the FRP jacket influence the

behavior of FRP-confined concrete. With the increase in axial load, the concrete core extensively cracks, and the confinement of the FRP jacket causes the damage to be redistributed in the concrete. The rate of energy transfer from concrete to FRP jacket also stabilizes after stress redistribution, which leads to a near-linear branch (BC) of the energy path until the FRP jacket fractures. At this stage, the FRP jacket has a dominant contribution to the behavior of FRP-confined concrete [3].

3.2.2. Evaluation index of the energy path

The energy path is essentially the trajectory of the ratio of the energy absorbed by the concrete to that absorbed by the FRP jacket, with relation to the compressive strength of concrete. As energy transfer takes place continuously between FRP jacket and concrete, the energy path essentially indicates the change in energy contribution of the concrete. The energy paths are variable for different column parameters, and the path characteristics during axial compression are represented by the area enclosed by the energy ratio and the axial stress. To quantify the energy variation in the core concrete compared to that in the FRP jacket, a concrete dominance indicator is defined as

$$K = \frac{\int_0^{f_{cz}} Q_c df_{cz}}{\int_0^{f_{cz}} Q_f df_{cz}}, \quad (3.5)$$

In addition, a concrete contribution indicator is defined as a metric used to characterize the concrete's contribution to the FRP-confined concrete column's load-bearing capability.

$$\Omega = \frac{\int_0^{f_{cz}} Q_c df_{cz}}{\int_0^{f_{cz}} Q_f df_{cz} + \int_0^{f_{cz}} Q_c df_{cz}}, \quad (3.6)$$

Note that the concrete dominance indicator K is related to the concrete contribution indicator Ω , as shown by Eq. (7). Larger the value of Ω , more is the contribution of the core concrete to the load-bearing capacity of the FRP-confined concrete column, as shown by Eq. (6). Note that $\Omega = 0$ represents a hollow FRP jacket and $\Omega = 1$ represents unconfined concrete.

$$\Omega = \frac{K}{K+1}, \quad (3.7)$$

A higher value of K indicates that the concrete absorbs more energy than the FRP jacket, as shown by Eq. (5). This demonstrates the importance of compressive stress in determining the energy paths of the FRP-confined concrete columns.

3.3. Experimental programs

3.3.1. Details of the specimens and test

A total of 18 specimens were prepared and tested to investigate the energy paths, and the relationship between the energy paths and compressive strengths of FRP-confined concrete columns. All specimens were stub columns 150 mm in diameter and 300 mm in height. Three concrete grades were used in the test and the compressive strengths were measured using 150 mm× 300 mm concrete cylinders, which on the test day were 33, 46, and 56 MPa, respectively.

The cured cylinder concrete columns were strengthened by a high-strength carbon FRP (CFRP) with an overlap of that was a quarter of the perimeter. According to the manufacturer, the CFRP has a nominal thickness of 0.25 mm/ply, a tensile strength (f_t) of 3,760 MPa, an elastic modulus (E_f) of 237 GPa, and an ultimate strain (ϵ_{fu}) of 0.01586. A mixture of epoxy resin and hardener at a ratio of 2:1 was used as an adhesive to bond the CFRP sheets onto the specimens. The concrete specimens for each strength grade were confined by the CFRP with one, two, and three layers. Two identical specimens were prepared for repeatability verification. The details of all specimens are summarized in Table 3.1 and can be divided into three groups according to the concrete strength. The specimens were identified as: FRP type + concrete design strength + FRP jacket layers + specimen number. For example, C36-1-1 indicates the first specimen confined by a single layer CFRP sheet with a concrete design strength of 36 MPa. To measure the hoop strains, three strain gauges, distributed at 120° along the perimeter, were placed at the midheight of the specimen. One was attached at the overlap zone, and the other two were located away from the overlap. The detailed arrangement of the strain gauges is shown in Fig. 3.3. All specimens were tested on a universal testing machine with a capacity of 5,000 kN. The axial deformation of the column was read directly from the testing equipment.

Table 3.1

Parameter settings and specifications of samples.

Specimens	f_c (MPa)	t (mm)	ϵ_{rup}	k_e	f_{cc} (MPa)	K	Ω
C24-1-1	33	0.25	0.010187	0.64	58.3	12.36	0.93
C24-1-2	33	0.25	0.011209	0.49	62.5	12.41	0.93
C24-2-1	33	0.5	0.008141	0.51	84.9	8.81	0.90

C24-2-2	33	0.5	0.009314	0.59	80.1	8.63	0.90
C24-3-1	33	0.75	0.011476	0.72	109.8	5.69	0.85
C24-3-2	33	0.75	0.012024	0.76	97.7	4.14	0.81
C36-1-1	46	0.25	0.009434	0.42	72	18.52	0.95
C36-1-2	46	0.25	0.006163	0.39	61.8	23.15	0.96
C36-2-1	46	0.5	0.011592	0.73	91.7	10.17	0.91
C36-2-2	46	0.5	0.007429	0.46	88.8	12.77	0.93
C36-3-1	46	0.75	0.011115	0.70	106.4	4.82	0.83
C36-3-2	46	0.75	0.011505	0.72	115.1	5.81	0.85
C48-1-1	56	0.25	0.006127	0.38	76.4	21.46	0.96
C48-1-2	56	0.25	0.005008	0.32	72.5	30.86	0.97
C48-2-1	56	0.5	0.008421	0.53	96.2	17.73	0.95
C48-2-2	56	0.5	0.010989	0.69	94	11.89	0.92
C48-3-1	56	0.75	0.008563	0.91	126.9	13.37	0.93
C48-3-2	56	0.75	0.010386	0.65	113.2	8.57	0.90

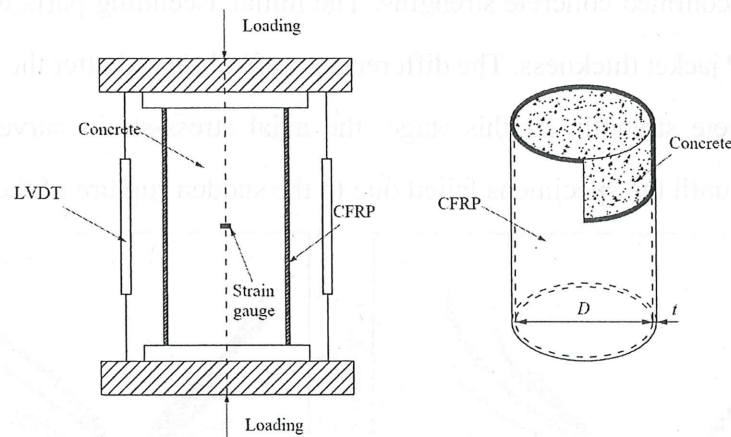


Fig. 3.3 Experimental settings.

3.3.2. Experimental results

The typical failure mode of the tested FRP-confined concrete is shown in Fig. 3.4. In general, the specimens failed due to the rupture of the FRP jacket at or near the midheight of the column followed by a sudden explosive crushing of concrete, which is consistent with the observations in previous studies [23-26]. This was probably because the ends of the axially loaded columns yielded smaller

deformation that resulted from the restrictions of the testing equipment. Therefore, for uniformly wrapped columns, the midheight section was relatively weaker than the ends of specimens, which led to failure in this zone.

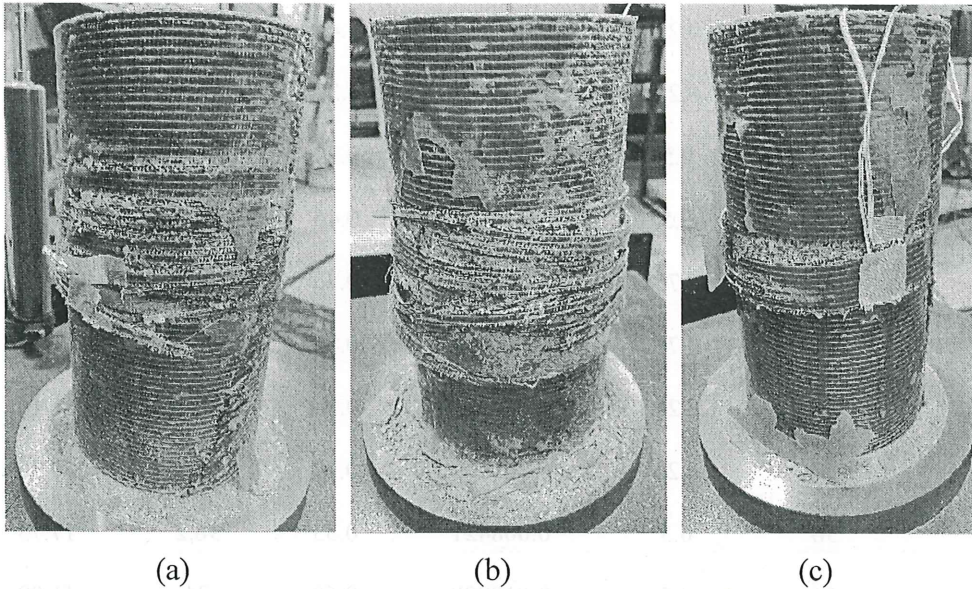
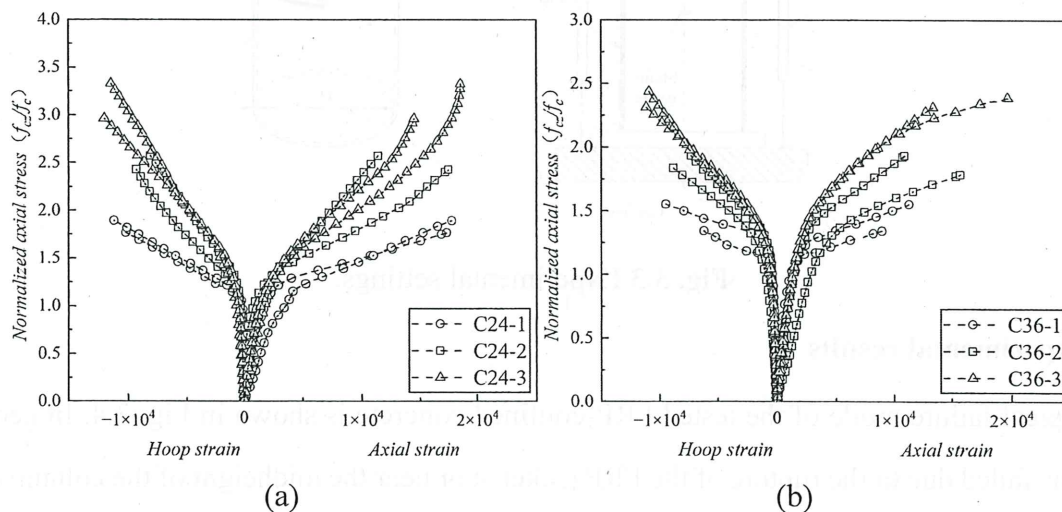
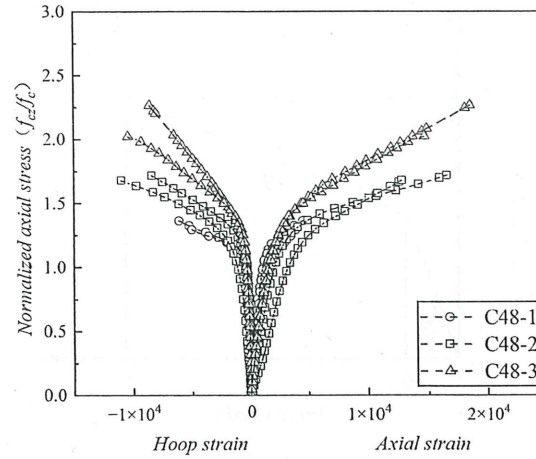


Fig. 3.4 Typical failure mode of FRP-confined concrete: (a) 24-1; (b) C36-1; and (c) C48-1.

The axial stress-strain curves for FRP-confined specimens with a concrete design strength of 24, 36, and 48 MPa are shown in Figs. 3.5(a-c), respectively. The axial stresses for all the specimens were normalized for the unconfined concrete strengths. The initial ascending parts were not significantly influenced by the FRP jacket thickness. The differences were observed after the axial stress exceeded the unconfined concrete strength. At this stage, the axial stress-strain curves for the specimens continued to increase until the specimens failed due to the sudden rupture of the FRP jackets.





(c)

Fig. 3.5 Axial stress-strain curves of FRP-confined concrete: (a) C24; (b) C36; and (c) C48.

3.4. Investigation of energy path

In this section, the energy paths of FRP-confined concrete during whole loading process are investigated theoretically. Then, the energy paths of different specimens, which were determined based on the test results of this paper, are discussed. It is noted that imperfections, such as voids and debonding, might affect the bond integrity between the concrete and the FRP jacket, which could probably influence the energy path of FRP-confined concrete. However, the influence of these imperfections is not considered in this paper.

3.4.1. Theoretical study on energy path

The bilinear stress-strain curves appeared more frequently in the subsequent studies on FRP-confined concrete [5, 27]. Behavior of FRP-confined concrete was simply represented by a bilinear curve defined by a transition point (f_c, ϵ_c) near the location of the unconfined concrete peak stress and a final point (f_{cz}, ϵ_{cu}) at the ultimate condition, as shown in Fig. 3.6. For convenient calculation, the strength enhancement due to the confinement at the transition point was ignored and the strength and strain of unconfined concrete can be taken as the transition point value.

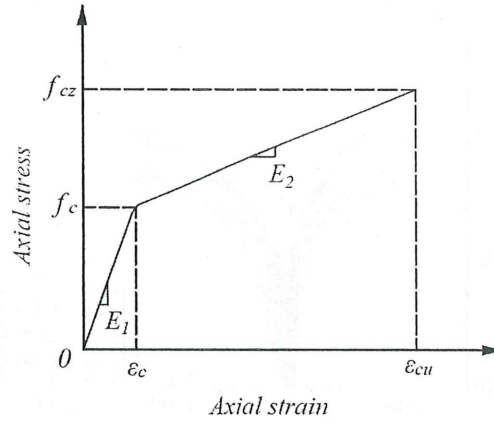


Fig. 3.6. Bilinear stress-strain curve of FRP-confined concrete

For the bilinear stress-strain curves of FRP-confined concrete, the area under the stress-strain curve represents the total energy absorption capacity per unit volume of FRP-confined concrete. Therefore, the areas under the first slope curve and the second slope curve are approximated as the areas of a triangle and a rectangle, respectively, as shown in Fig. 3.7. The energy absorption capacity of an axial loaded FRP-confined concrete column is given by

$$U_1 = V_c \int_0^{\epsilon_c} f_{cz} d\epsilon_{cz} = 0.5 V_c f_{cz} \epsilon_{cz}, (\epsilon_{cz} \leq \epsilon_c) \quad (3.8)$$

$$U_2 = V_c \int_{\epsilon_c}^{\epsilon_{cu}} f_{cz} d\epsilon_{cz} = 0.5 V_c (f_c + f_{cz}) (\epsilon_{cz} - \epsilon_c), (\epsilon_c \leq \epsilon_{cz} \leq \epsilon_{cu}) \quad (3.9)$$

where f_{cz} and ϵ_{cz} are the axial stress and strain of FRP-confined concrete at one moment, respectively; V_c is the volume of the concrete column; U_1 and U_2 donate the energy absorbed by the confined concrete at one slope section and second slope section, respectively; ϵ_{cu} is the ultimate strain of FRP-confined concrete; f_c and ϵ_c are the compressive strength and strain of unconfined concrete, respectively.

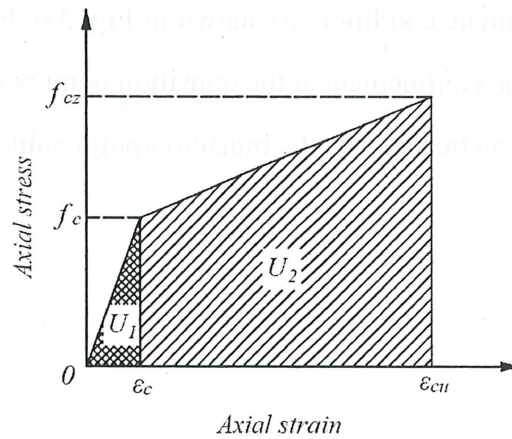


Fig. 3.7 The energy absorption of FRP-confined concrete

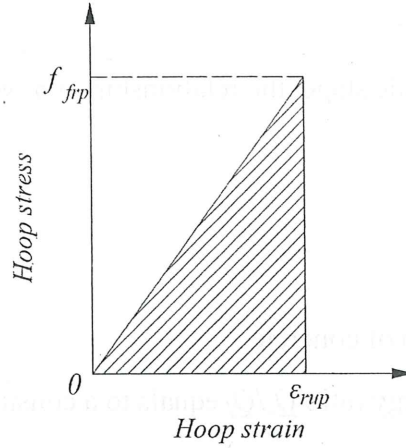


Fig. 3.8 The energy absorption of FRP jacket

The work done by FRP jacket at any moment can be calculated by integration of its stress-strain curve (as seen in Fig. 3.8)

$$U_{frp} = \frac{4t}{D} V_c \int_0^{\varepsilon_{rup}} f_{frp} d\varepsilon_{frp} = \frac{2t}{D} V_c f_{frp} \varepsilon_{frp}, (\varepsilon_{frp} \leq \varepsilon_{rup}) \quad (3.10)$$

where f_{frp} and ε_{frp} are the stress and strain of FRP jacket at one moment, respectively; ε_{rup} is the ultimate strain of FRP jacket.

Based on the calculation before, ignored the energy dissipation, the energy ratio of the concrete versus FRP jacket at first slope section is given by

$$\frac{Q_c}{Q_f} \Big|_{\varepsilon_{cz} \leq \varepsilon_c} = \frac{U_1 - U_{frp}}{U_{frp}} \quad (3.11)$$

Similarly, when the axial stress f_{cz} passed the unconfined concrete compressive strength f_c , the energy ratio of the concrete versus FRP jacket at section slope section is given by

$$\frac{Q_c}{Q_f} \Big|_{\varepsilon_c \leq \varepsilon_{cz} \leq \varepsilon_{cu}} = \frac{U_1 \Big|_{f_{cz}=f_c} + U_2 - U_{frp}}{U_{frp}} \quad (3.12)$$

Based on the deformation compatibility and force equilibrium conditions in the cross section, the following equations are derived

$$\sigma_r = \frac{2t}{D} f_{frp} \quad (3.13)$$

Combined with the Hooke's law, substituting Eqs. (3.8), (3.10), and (3.13) into Eq. (3.11), the energy ratio in the first slope section can be given by

$$\frac{Q_c}{Q_f} \Big|_{\varepsilon_{cz} \leq \varepsilon_c} = \frac{t}{D} \frac{E_f}{E_1} \left(\frac{f_{cz}}{\sigma_r} \right)^2 - 1 \quad (3.14)$$

where E_f and E_1 donate elastic modulus of FRP jacket and the first slope of FRP-confined concrete,

respectively.

According to Lin et al. [3], at elastic stage, the relationship of σ_r versus f_{cz} is linear and can be taken by

$$\frac{f_{cz}}{\sigma_r} = \frac{1 - \nu_c + (E_1/E_f)(D/2t)}{\nu_c} \quad (3.15)$$

where ν_c donates the Poisson's ratio of concrete.

Based on the Eqs. (3.14), the energy ratio Q_c/Q_f equals to a constant at elastic stage. For the plastic stage, substituting Eqs. (3.8) - (3.10), and (3.13) into Eq. (3.12), the energy ratio in the second slope section can be given by

$$\left. \frac{Q_c}{Q_f} \right|_{\varepsilon_c \leq \varepsilon_{cz} \leq \varepsilon_{cu}} = \frac{t}{D} \frac{E_f (E_2 - E_1)}{E_1 E_2} \left(\frac{f_c}{\sigma_r} \right)^2 + \frac{t}{D} \frac{E_f}{E_2} \left(\frac{f_{cz}}{\sigma_r} \right)^2 - 1 \quad (3.16)$$

where E_2 donates the second slope of FRP-confined concrete.

According to Eq. (3.16), the energy ratio Q_c/Q_f is exponentially correlated with the axial stress f_{cz} . The energy ratio is exponentially correlated with the axial stress. This also proves the existence of a deterministic relationship between the energy ratio and the compressive strength and provides a theoretical basis for the subsequent proposal of an energy path-based compressive strength model.

3.4.2. Experimental observation of energy path

The theoretical study suggested that the energy path might be affected by column parameters (e.g., concrete strength, D/t ratio, E_1 , E_2 , E_f). In this section, the relationship between these parameters and confining stress paths during the entire loading process is investigated based on the test results from this paper.

The influence of the D/t ratio on the energy path for specimens with unconfined concrete strength of 33, 46, and 56 MPa are shown in Figs. 9(a-c), respectively. The elastic parts for specimens ($f_c = 46$ MPa) are enlarged and given in Fig. 3.9. At the elastic stage, it was observed experimentally that the energy ratios were constant value as that indicated by the theoretical results presented in the previous section. That is, the higher D/t ratio, the smaller the energy ratio of the energy path. However, it is noted that because the concrete barely expanded at this stage, the lateral stress was quite small. Therefore, the influence of the D/t ratio was insignificant, which led to similar energy paths at this stage. At the AB stage, with the D/t ratio decreased, the energy path reached point A earlier and point

B later, which means the transition stage was longer and smoother. This indicated that the stronger confinement effect makes the FRP-confined concrete smoother during the stress redistribution stage. Although there exhibited different rules in the BC stage in Fig. 3.9(c), the common rule was larger D/t ratio and smaller energy ratio, which means the confinement effect of the specimen with lighter confinement (i.e., larger D/t ratio), was less effective. Hence, a longer and smoother BC branch, which indicated a more effective confinement effect, was yielded in the specimen with a smaller D/t ratio.

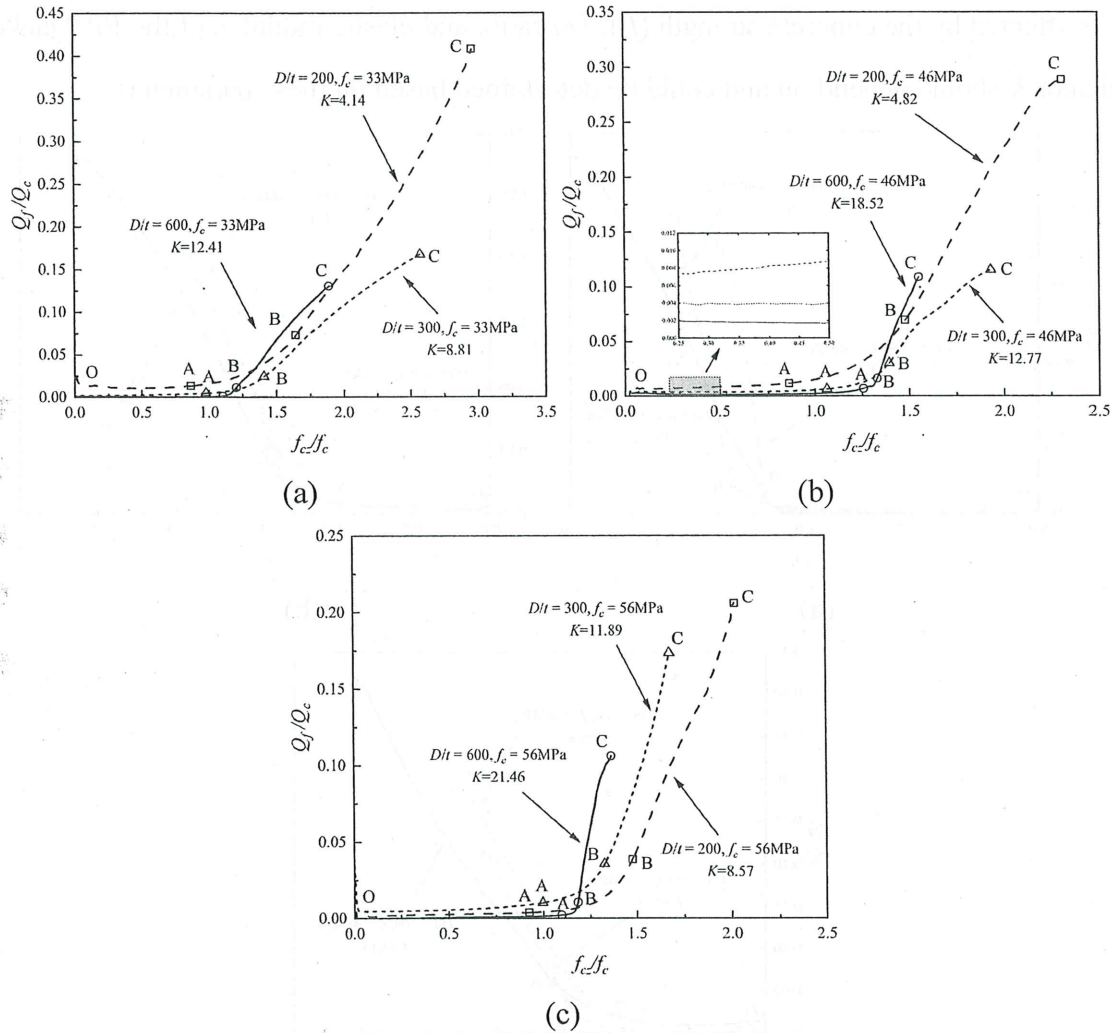


Fig. 3.9 Influence of D/t ratio on energy paths: (a) $f_c = 33$ MPa; (b) $f_c = 46$ MPa; (c) $f_c = 56$ MPa.

The influence of concrete strength on the energy path of specimens confined by FRP jackets with D/t ratios of 600, 300, and 200 are shown in Figs. 10(a-c), respectively. It can be seen that the overall trend of energy paths with different concrete strength is similar. The OA stage and AB stage were closely under different concrete strength, which means that under the same confinement effect, the weights of energy distribution are similar for different concrete strength during the initial period redistribution period of stress. For the BC stage, in general, the specimen with a smaller concrete

strength had a longer BC phase, while the slope is similar. This means that the FRP jacket of lower concrete strength specimen took up a more proportion of the energy and exerted a more efficient confinement.

As discussed previously, the energy paths of FRP-confined concrete columns were influenced by the column parameters. The energy path of FRP-confined concrete is characterized by concrete dominance indicator K . The K results for each specimen are summarized in Table 3.1. Since the energy is affected by the concrete strength (f_c), D/t ratio, and elastic modulus of the FRP jacket (E_f), the indicator K should depend on and could be determined based on these parameters.

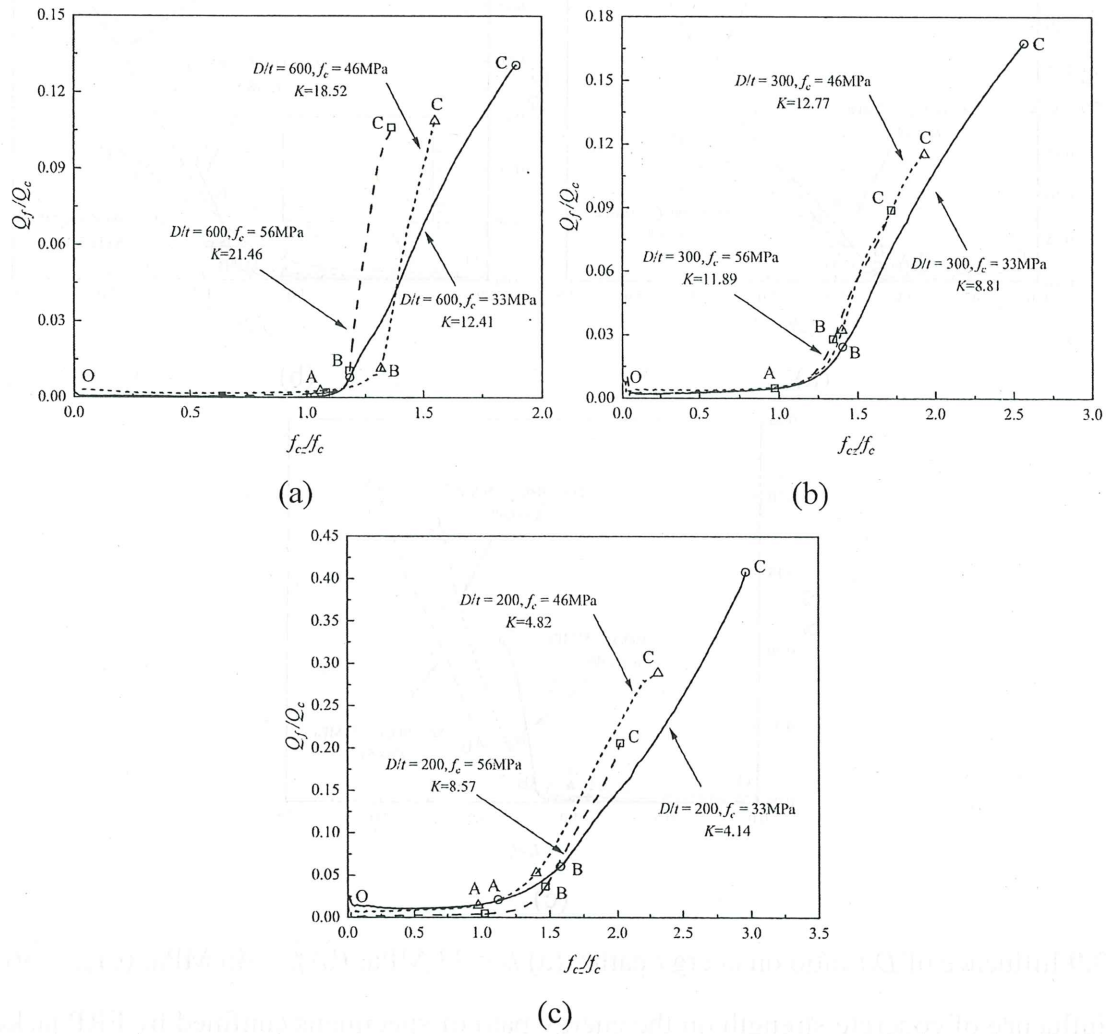


Fig. 3.10 Influence of concrete strength on energy paths: (a) $D/t = 600$; (b) $D/t = 300$; (c) $D/t = 200$.

The parameter D/t ratio and elastic modulus of the FRP jacket (E_f) can be indicated by the nominal ultimate lateral stress (f_{ru})

$$f_{ru} = \frac{2t}{D} E_f \varepsilon_{fu} = \frac{2t}{D} f_t \quad (3.17)$$

where f_t and ε_{fu} dominate the tensile strength and ultimate strain of FRP jacket, respectively.

The relationships of K versus f_c and K versus f_{ru} are shown in Figs. 11(ab), respectively. It can be seen that the indicator K increased with f_c but decreased with f_{ru} . Based on the test results, a model for indicator K is regressed as follows

$$K = 5.8 \frac{f_c}{f_{ru}} \quad (3.18)$$

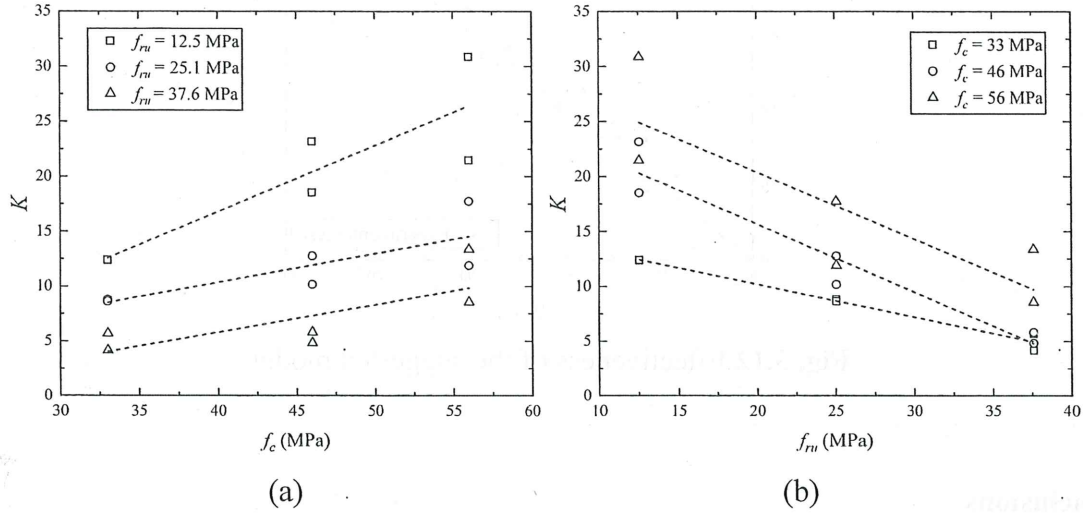


Fig. 3.11 Relationship between K and column parameters: (a) K versus f_c ; (b) K versus f_{ru} .

3.4.3. Relationship between energy path and compressive strength

In this section, the relationship between the energy path and the compressive strength of the FPR-confined concrete is discussed. The energy ratio represents the relative correlation between the energy absorbed by the FRP jacket and that absorbed by the concrete; conversely, the concrete dominance indicator represents exact correlation between the two for a given structural composition. The damage of FPR-confined concrete columns is ultimately a state instability phenomenon driven by energy. Concrete strength and lateral stress represent the factors affecting the strength improvement of different components respectively, and the effect of both is weighed by the concrete dominance indicator K . Based on the experimental results, a compressive strength model of FPR-confined concrete columns under axial loading is proposed, as follows:

$$f_{cz} = f_c + 29.23K^{0.34}f_c^{-0.83}\sigma_r \quad (3.19)$$

The indicator K is given by Eq. (3.18). The effectiveness of the suggested model in comparison to the experimental findings is shown in Fig. 3.12. The suggested model had an R-squared value of 0.9946. The performance of the proposed model is in good agreement with the measured data. In summary, the indicator K derived from the energy relationship is accurate and easy to calculate, and

the predicted concrete strength can be obtained from the basic parameters. Moreover, the expression of Eq. (3.19) is also quite simple, which can be conveniently used in the design of FRP-confined concrete columns and further theoretical studies on the energy relations.

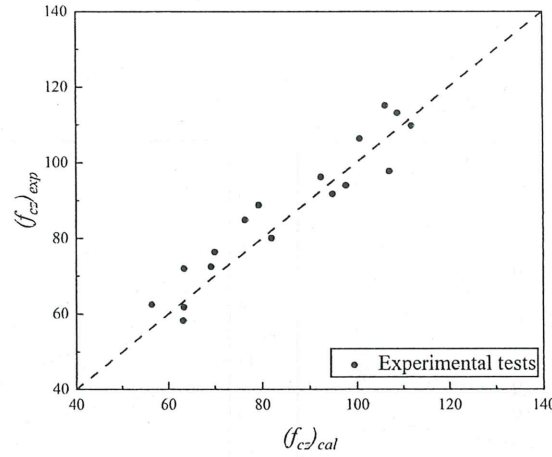


Fig. 3.12 Effectiveness of the suggested model.

3.5. Conclusions

In this study, the interaction mechanism between the FRP jacket and the concrete of the FRP-confined concrete columns was theoretically and experimentally investigated using the energy paths for the first time. The relative relationship between the energy absorbed by concrete and FRP jacket is visualized in the form of energy paths, reducing the effect of differences in experimental results. The two performance indices (i.e., the concrete dominance indicator K and the concrete contribution indicator Ω) were introduced to quantitatively characterize the energy paths. Based on the results and discussions in this study, the following findings were drawn:

1. The energy path represents the variation of the energy ratio (Q_f/Q_c) during the loading process, and the interaction mechanism between the components is investigated according to the regularity. At the initial stage, as the deformations of concrete and FRP jacket are harmonized, the energy ratio varies little and close to a constant value. When the axial stress exceeds the unconfined concrete strength, the energy path exhibits a transition stage, during which microcracks start to develop rapidly and energy ratio increases. The rate of energy transfer from concrete to FRP jacket also stabilizes after stress redistribution, which leads to a near-linear branch of the energy path until the FRP jacket fractures.
2. The energy path of FRP-confined concrete column is influenced by column parameters, namely,

concrete strength f_c , and ratio of column diameter to FRP jacket thickness D/t . The energy paths for different test conditions were represented by the concrete dominance indicator K . The findings of the experiment revealed that the concrete dominance indicator K increased with f_c but decreased with f_{ru} , indicating the confinement effective of FRP jacket was more significant for the specimen with a smaller K .

3. One model for determining concrete compressive strength of FRP-confined concrete columns under axial loading was proposed from an energy relation perspective. The predictions by proposed model and the tested results agreed well.

References

- [1] Jiang, T. and J.G. Teng, Analysis-oriented stress-strain models for FRP-confined concrete. *Engineering Structures*, 2007. 29(11): p. 2968-2986.
- [2] Xiao, Y., Applications of FRP Composites in Concrete Columns. *Advances in Structural Engineering*, 2004. 7(4): p. 335-343.
- [3] Lin, S., et al., Confining Stress Path-Based Compressive Strength Model of Axially Loaded FRP-Confined Columns. *Journal of Composites for Construction*, 2021. 25(1): p. 04020077.
- [4] Tang, H., et al., Experimental investigation of FRP-confined concrete-filled stainless steel tube stub columns under axial compression. *Thin-Walled Structures*, 2020. 146: p. 106483.
- [5] Nanni, A. and N.M. Bradford, FRP jacketed concrete under uniaxial compression. *Construction and Building Materials*, 1995. 9(2): p. 115-124.
- [6] Samaan, M., A. Mirmiran, and M. Shahawy, Model of Concrete Confined by Fiber Composites. *Journal of Structural Engineering*, 1998. 124(9): p. 1025-1031.
- [7] Lorenzis, L.D. and R. Tepfers, Comparative Study of Models on Confinement of Concrete Cylinders with Fiber-Reinforced Polymer Composites. *Journal of Composites for Construction*, 2003. 7(3): p. 219-237.
- [8] Xiao, Y. and H. Wu, Compressive Behavior of Concrete Confined by Various Types of FRP Composite Jackets. *Journal of Reinforced Plastics and Composites*, 2003. 22(13): p. 1187-1201.
- [9] Teng, J.G. and L. Lam, Behavior and Modeling of Fiber Reinforced Polymer-Confined Concrete. *Journal of Structural Engineering*, 2004. 130(11): p. 1713-1723.
- [10] Karbhari, V.M. and Y. Gao, Composite Jacketed Concrete under Uniaxial Compression—

- Verification of Simple Design Equations. *Journal of Materials in Civil Engineering*, 1997. 9(4): p. 185-193.
- [11] Ozbakkaloglu, T., J.C. Lim, and T. Vincent, FRP-confined concrete in circular sections: Review and assessment of stress–strain models. *Engineering Structures*, 2013. 49: p. 1068-1088.
- [12] Mander, J.B., M.J.N. Priestley, and R. Park, Theoretical Stress-Strain Model for Confined Concrete. *Journal of Structural Engineering*, 1988. 114(8): p. 1804-1826.
- [13] Tijani, I.A., Y.F. Wu, and C.W. Lim, Energy balance method for modeling ultimate strain of fiber-reinforced polymer-repaired concrete. *Structural Concrete*, 2019. 21(2): p. 1-17.
- [14] Mai, A.D., M.N. Sheikh, and M.N.S. Hadi, Strain model for discretely FRP confined concrete based on energy balance principle. *Engineering Structures*, 2021. 241: p. 112489.
- [15] Qasrawi, Y., P.J. Heffernan, and A. Fam, Dynamic behaviour of concrete filled FRP tubes subjected to impact loading. *Engineering Structures*, 2015. 100: p. 212-225.
- [16] Yu-Fei, W. and C. Yugui, Energy Balance Method for Modeling Ultimate Strain of Confined Concrete. *ACI Struct. J.* 114(2).
- [17] Matthys, S., H. Toutanji, and L. Taerwe, Stress–Strain Behavior of Large-Scale Circular Columns Confined with FRP Composites. *Journal of Structural Engineering*, 2006. 132(1): p. 123-133.
- [18] Pham, T.M. and M.N.S. Hadi, Strain Estimation of CFRP-Confined Concrete Columns Using Energy Approach. *Journal of Composites for Construction*, 2013. 17(6): p. 04013001.
- [19] Pham, T.M. and M.N.S. Hadi, Confinement model for FRP confined normal- and high-strength concrete circular columns. *Construction and Building Materials*, 2014. 69: p. 83-90.
- [20] McSaveney, M.J. and T.R. Davies, Surface energy is not one of the energy losses in rock comminution. *Engineering Geology*, 2009. 109(1): p. 109-113.
- [21] Nishiyama, T., et al., The examination of fracturing process subjected to triaxial compression test in Inada granite. *Engineering Geology*, 2002. 66(3): p. 257-269.
- [22] Cao, Y.-G., Y.-F. Wu, and X.-Q. Li, Unified model for evaluating ultimate strain of FRP confined concrete based on energy method. *Construction and Building Materials*, 2016. 103: p. 23-35.
- [23] Campione, G. and N. Miraglia, Strength and strain capacities of concrete compression members reinforced with FRP. *Cement and Concrete Composites*, 2003. 25(1): p. 31-41.
- [24] Berthet, J.F., E. Ferrier, and P. Hamelin, Compressive behavior of concrete externally confined by composite jackets. Part A: experimental study. *Construction and Building Materials*, 2005. 19(3):

p. 223-232.

[25] Li, G., Experimental study of FRP confined concrete cylinders. *Engineering Structures*, 2006. 28(7): p. 1001-1008.

[26] Realfonzo, R. and A. Napoli, Concrete confined by FRP systems: Confinement efficiency and design strength models. *Composites Part B: Engineering*, 2011. 42(4): p. 736-755.

[27] Xiao, Y. and H. Wu, Compressive Behavior of Concrete Confined by Carbon Fiber Composite Jackets. *Journal of Materials in Civil Engineering*, 2000. 12(2): p. 139-146.

CHAPTER 4. LOAD-BEARING CAPACITY ANALYSIS BASED ON ENERGY PATH

4.1. Introduction

The strengthening of existing reinforced concrete (RC) columns using steel tube or fiber-reinforced polymer (FRP) jacket is based on a well-established fact that lateral confinement of concrete can substantially enhance its axial compressive strength [1-6]. Consequently, various models for predicting the compressive strength and the stress-strain behavior have been developed theoretically and experimentally on the confined concrete structures and an accurate compressive strength model is important for a well-established constitutive relationship.

In early studies of confined concrete columns, the compressive strength models of Richard and Mander for actively confined concrete were widely used in the research of CFST columns and FRP-confined concrete columns. The predicted compressive strength models can be divided into two categories: (a) the design-oriented models; (b) the analysis-oriented models. In a design-oriented model, an explicit expression is used to calculate the ultimate strain, which is empirically regressed from test results. The accuracy of the model depends heavily on the reliability and comprehensiveness of the database of test results. With an analysis-oriented model, the ultimate strain is calculated through an incremental procedure to consider the interaction between the external confining structure and the internal concrete core, which is a combination of empirical and analytical approaches. For investigating the effect of the stress path on the compressive strength, Chen et al. [7] compared the hoop-axial strain curves and axial stress-strain curves of actively confined concrete and FRP-confined concrete. For the axial stress-strain curves, the axial stress of passively confined concrete is less than that of actively confined concrete for the same axial strain, confinement ratio, and transverse strain, indicating that the axial stress of confined concrete is related to the stress path.

Most of the theoretical studies of confined concrete, it was assumed that the axial stress of confined concrete in CFST column is identical to the actively confined concrete stress for a given set of axial strain and lateral stress [8, 9]. This is equivalent to assuming that the stress-strain relationship of confined concrete is stress path independent or, in other words, the history of hoop strain. In fact, this assumption ignores the progressive development of tensile splitting cracks in confined concrete, since active lateral stress applied in the laboratory test is hydraulically provided by external source and able

to remain steadily during the test, while passive confining requires the dilation of concrete core due to axial compression and the development of splitting crack for activation. Because of the progressive development of tensile splitting crack as the axial strain increases, the extent of splitting crack at a given lateral stress in passively confined concrete should be larger and hence larger axial deformation or strain. Equivalently, it indicates that at the same axial strain and lateral stress, passively confined concrete should have a smaller axial stress than that in the actively confined concrete. Therefore, it is doubtful that the compressive strength models of actively confined concrete directly applied to the compressive strength calculation of passively confined concrete [10, 11]. In general, whereas for the actively confined concrete compressive strength model, the main influencing parameter other than the plain concrete strength is the lateral stress.

This paper aims to investigate the relationship between actively confined concrete and passively confined concrete on the stress path. The concept of equivalent lateral stress is proposed by analyzing the stress path of passively confined concrete. The stress path of passively confined concrete is transformed into an alternative stress path of actively confined concrete. In turn, the strength model of actively confined concrete can be rationalized and applied to the strength calculation of passively confined concrete. Separate discussions are made for different constraint types such as steel tube and FRP jacket, and a uniform lateral stress expression are obtained. Finally, the equivalent lateral stress was substituted into the actively confined concrete strength models and the adjusted models were verified by comparison with experimental test results.

4.2. Confining action of the steel tube and FRP jacket

4.2.1. Confining action of the CFST column

As a typical confined concrete structures, the compressive capacity of the CFST columns as well as the load-displacement curves have been the focus of attention in the structural design. Depending on the loading position, it can be divided into whole-section loaded mode and concrete loaded mode, as seen in Fig. 4.1. Under the whole-section loaded mode, the concrete and steel tube are jointly subjected to the axial load. The sides of the concrete are confined by the steel tube and the concrete is subjected to a three-direction force state, and correspondingly, the steel tube is squeezed by the expansion of the concrete and subjected to a two-direction force state. In the initial stage of loading, because the Poisson ratio of the concrete is smaller than that of the steel tube, no lateral stress occurred

for the core concrete. When the compressive stress exceeds near $0.8f_c$, microcracks develop rapidly in the concrete, and its lateral expansion becomes larger than that of the steel tube, causing the lateral stress to develop smoothly. A sudden lateral expansion due to the fracture of concrete leads to a sharp increase in lateral stress. As the loading increases, the steel tube yields and the lateral stress keeps constant. After exhibiting a short plateau, the lateral stress continues to increase because of strain hardening of the steel tube, until reaching the ultimate state. This is basic condition of stress path of CFST columns under whole-section loaded mode.

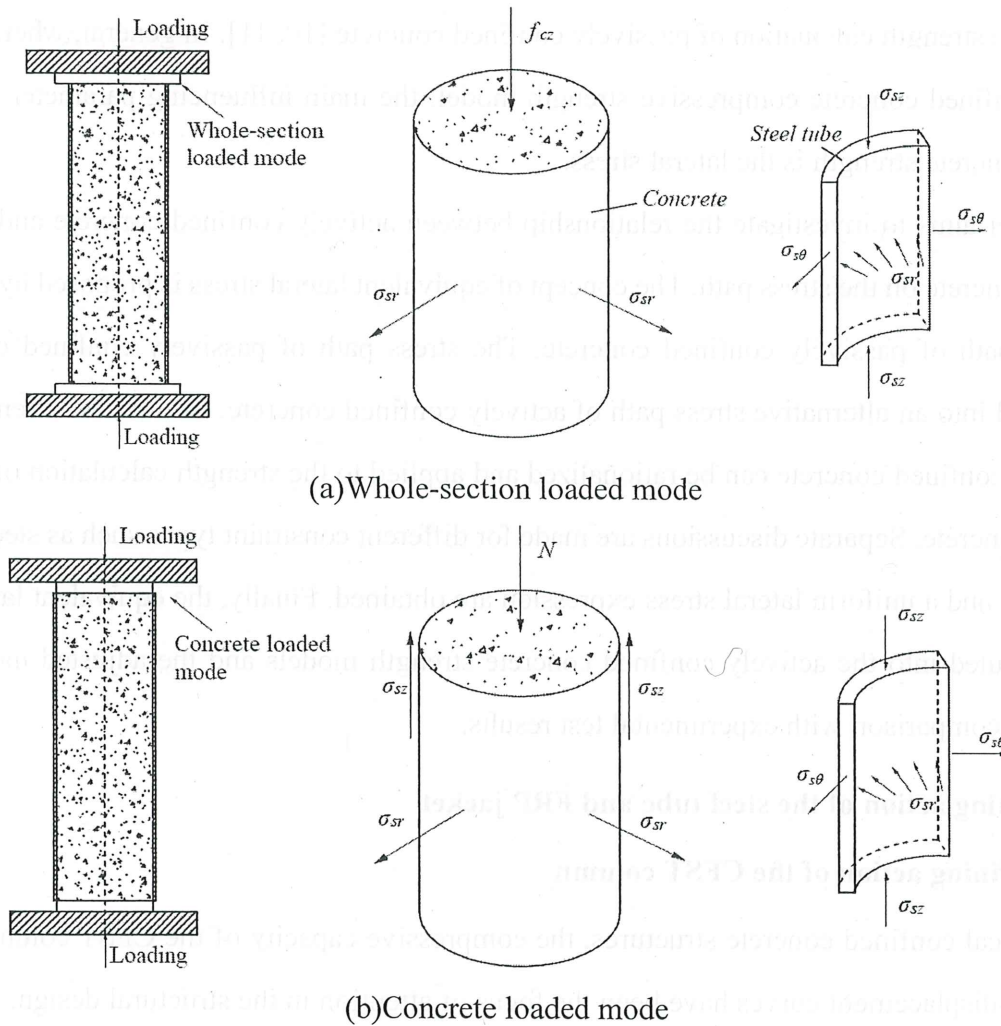


Fig. 4.1 Force state of CFST column under different loading mode.

As for the concrete loaded CFST column, the axial load is only subjected to the core concrete, the axial strain of the concrete is larger than that of the steel tube. The steel tube is also subjected to a two-direction force state because of the friction between the steel tube and concrete.

4.2.2. Confining action of the FRP-confined concrete column

With the development of FRP materials, its corrosion-resistant and lightweight properties have led

to its increasing use in confined concrete. As an elastic material, the stress-strain relationship of FRP jacket was simple and easy to investigate stress path of FRP-confined concrete columns. The force state of FRP-confined concrete column was shown in Fig. 4.2. At the initial stage, the microcrack develops slowly in concrete, and the lateral lateral stress is insignificant because of the small concrete dilation. Therefore, the behavior of FRP-confined concrete at this stage is not significantly influenced by the lateral confinement but the inherent property of the concrete core. When the axial stress exceeds the unconfined concrete strength, the microcracks start to develop rapidly and significant lateral stress is induced. Both the property of the concrete and the lateral confinement influence the behavior of FRP-confined concrete. With the increase in axial load, the concrete core extensively cracks, and the confinement of the FRP jacket causes the damage to be redistributed in the concrete. At this stage, the lateral confinement has a dominant contribution to the behavior of FRP-confined concrete.

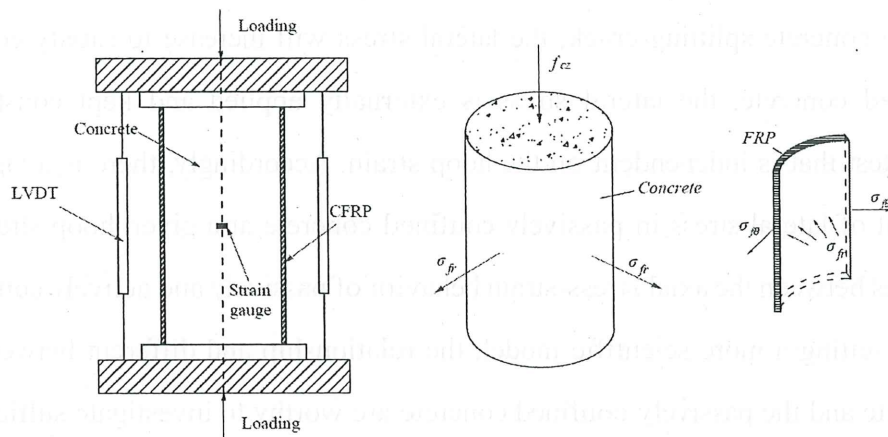


Fig. 4.2 Force state of FRP-confined concrete column.

4.3. The stress path of actively and passively confined concrete

The build-up of lateral stress in confined concrete is known as stress path. Stress path varies depending on the confinement material and confinement technique as shown in Fig. 4.3. Early proposed analysis-oriented models were developed based on assumption of stress path independence. This assumes that axial stress of a confined concrete is similar to that of actively confined concrete with the same confining pressure and deformation.

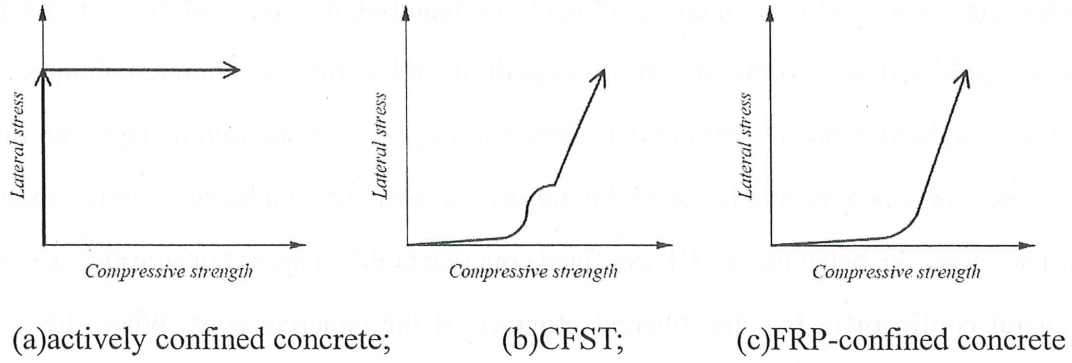


Fig. 4.3 Stress paths of different confined concrete.

Traditionally, the passively confined concrete stress evaluation follows the axial stress of the respective hoop strain of the actively confined concrete, which is equivalent to say that the development of passively confined concrete stress is lateral stress path independent [12-15]. However, there were arguments against this assumption [16, 17]. It is because the lateral stress in passively confined concrete will solely be developed by a change in hoop strain. When the axial/hoop strain increases due to concrete splitting crack, the lateral stress will increase to satisfy compatibility. In actively confined concrete, the lateral stress is externally applied and kept constant artificially throughout the test that is independent on the hoop strain. Accordingly, there is a lagging effect on the development of lateral stress in passively confined concrete at a given hoop strain, which may cause differences between the axial stress-strain behavior of passively and actively confined concrete. With a view to setting a more scientific model, the relationship and different between the actively confined concrete and the passively confined concrete are worthy to investigate sufficiently.

4.4. Equivalent lateral stress of passively confined concrete

4.4.1. Equivalent lateral stress of steel-confined concrete

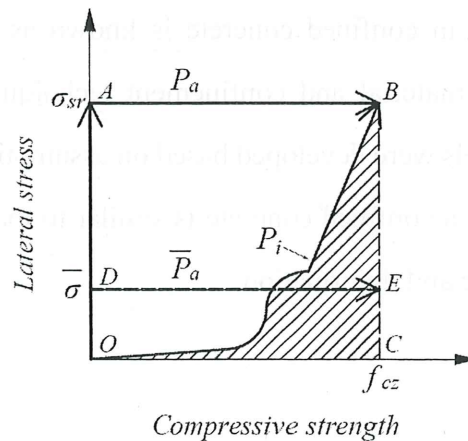


Fig. 4.4 Stress paths of actively confined and steel-confined concrete.

To investigate the stress path of confined concrete and its effect upon the compressive strength, Lin [18] and Zhao [19] proposed a lateral stress domination index SI to expressing the dominance degree of the lateral stress. Considering the typical stress paths of steel-confined concrete in Fig. 4.4, the stress path of steel-confined concrete could be indicated by path P_i (OB). Accordingly, the stress path of actively confined concrete was indicated by path P_a (OAB), which's constant lateral stress is equal to the ultimate lateral stress of passively confined concrete. From the figure, it can be known that the lateral stress for path P_a is significant during the whole loading process. Therefore, when path P_i gets closer to path P_a , the lateral stress for path P_i becomes more significant and will be in a more dominant state. The lateral stress domination index $SI(P_i)$ was defined as

$$SI(P_i) = \frac{S(P_i)}{S(P_a)} \quad (4.1)$$

where $S(P_i)$ is the area enclosed by path P_i and x-axis (OBC); $S(P_a)$ is the area enclosed by path P_a and x-axis (OABC). The boundary condition of the lateral stress domination index is $SI(P_a) = 1$.

Based on investigation of Lin [18] and Zhao [19], for the stress path with a small lateral stress domination index (stress path is “far away” from path P_a), the influence on the compressive strength is significantly different from that of path P_a . As the lateral stress domination index increases (the path gets closer to path P_a), the path-dependent effect becomes less significant. Besides, no matter for the whole-section loaded or concrete loaded CFST columns, there is a threshold value of the lateral stress domination index to distinguish weather the compressive strength is stress path dependent or not. This threshold value is defined by μ , indicating that when the $S(P_i)$ area is less than $\mu S(P_a)$, the compressive strength is stress path dependent. For the whole-section loaded or concrete loaded CFST columns, μ equals 0.5 according to Lin [3].

According to the features of the passively stress path P_i (OB), the compressive strength of the concrete is f_{cz} and the lateral stress is σ_{sr} at the peak stress state. Assume that there exists an actively stress path \bar{P}_a (ODE) such that the compressive strength of the confined concrete similarly reaches f_{cz} . Then the stress path \bar{P}_a is the equivalent actively stress path of the passively stress path P_i , and the lateral stress corresponding to the stress path \bar{P}_a is defined as equivalent lateral stress $\bar{\sigma}$. Thus, the following equation can be obtained by

$$S(P_i) = S(\bar{P}_a) \quad (4.2)$$

where $S(\bar{P}_a)$ is the area enclosed by path \bar{P}_a and x-axis (ODEC).

Considering the threshold value μ , the $S(\bar{P}_a)$ can be calculated by

$$S(\bar{P}_a) = \mu \bar{\sigma} f_{cz} \quad (4.3)$$

Submitted the Eqs. (4.2), and (4.3) into Eq. (1), the equivalent lateral stress $\bar{\sigma}$ is obtained by

$$\bar{\sigma} = \frac{SI(P_i) \sigma_{sr}}{\mu} \quad (4.4)$$

4.4.2. Equivalent lateral stress of FRP-confined concrete

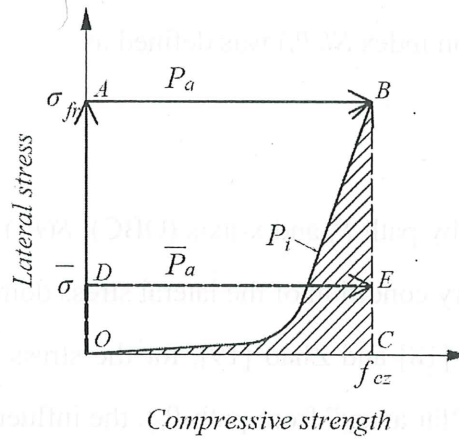


Fig. 4.5 Stress paths of actively confined and FRP-confined concrete.

Similarly, Lin [3] also proposed a lateral stress domination index SI to expressing the dominance degree of the lateral stress of FRP-confined concrete. Considering the typical stress paths of steel-confined concrete in Fig.4.5, the stress path of FRP-confined concrete could be indicated by path P_i (OB). Accordingly, the stress path of actively confined concrete was indicated by path P_a (OAB), which's constant lateral stress is equal to the ultimate lateral stress of passively confined concrete. From the figure, it can be known that the lateral stress for path P_a is significant during the whole loading process. Therefore, when path P_i gets closer to path P_a , the lateral stress for path P_i becomes more significant and will be in a more dominant state. The lateral stress domination index $SI(P_i)$ was defined as same as that in steel-confined concrete.

Based on investigation of Lin [3], for the stress path with a small lateral stress domination index (stress path is “far away” from path P_a), the influence on the compressive strength is significantly different from that of path P_a . As the lateral stress domination index increases (the path gets closer to

path P_a), the path-dependent effect becomes less significant. Besides, for the FRP-confined concrete column, there is also a threshold value of the lateral stress domination index to distinguish whether the compressive strength is stress path dependent or not. This threshold value is defined by μ , indicating that when the $S(P_i)$ area is less than $\mu S(P_a)$, the compressive strength is stress path dependent. For the FRP-confined concrete column, μ equals 0.34 according to Lin [3].

According to the features of the passively stress path P_i (OB), the compressive strength of the concrete is f_{cz} and the lateral stress is σ_{fr} at the peak stress state. Assume that there exists an actively stress path \bar{P}_a (ODE) such that the compressive strength of the confined concrete similarly reaches f_{cz} . Then the stress path \bar{P}_a is the equivalent actively stress path of the passively stress path P_i , and the lateral stress corresponding to the stress path \bar{P}_a is defined as equivalent lateral stress $\bar{\sigma}$. Thus, the following equation can be obtained by

$$S(P_i) = S(\bar{P}_a) \quad (4.5)$$

where $S(\bar{P}_a)$ is the area enclosed by path \bar{P}_a and x-axis (ODEC).

Considering the threshold value μ , the $S(\bar{P}_a)$ can be calculated by

$$S(\bar{P}_a) = \mu \bar{\sigma} f_{cz} \quad (4.6)$$

Submitted the Eqs. (4.5) and (4.6) into Eq. (4.1), the equivalent lateral stress $\bar{\sigma}$ is obtained by

$$\bar{\sigma} = \frac{SI(P_i)\sigma_{fr}}{\mu} \quad (4.7)$$

Based on the analysis, the passively confined concrete can be treated as an actively confined concrete with an equivalent lateral stress $\bar{\sigma}$.

4.5. Application for the equivalent lateral stress and verification

4.5.1. Application for the equivalent lateral stress of passively confined concrete

Many compressive strength models of actively confined concrete have been developed, and the most famous are that proposed by Richard [5] and Mander [6]. Both models are associated with the unconfined concrete strength f_c and the lateral stress σ_r . As the passively confined concrete can be treated as an actively confined concrete with an equivalent lateral stress $\bar{\sigma}$, submitted the equivalent lateral stress into the Richard model and Mander model respectively, the adjusted models are as follows

$$f_{cz-R} = f_c + 4.1\bar{\sigma} \quad (4.8)$$

$$f_{cz-M} = f_c \left(-1.254 + 2.254 \sqrt{1 + \frac{7.94\bar{\sigma}}{f_c} - \frac{2\bar{\sigma}}{f_c}} \right) \quad (4.9)$$

The equivalent lateral stress establishes a connection between actively and passively confined concrete, rationalizing the application of compressive strength models for actively confined concrete in strength calculations for passively confined concrete.

4.5.2. Verification for the equivalent lateral stress of passively confined concrete

Many tests have been conducted on passively confined concrete. In the present study, a database containing the test results of 50 CFST column specimens and 36 FRP-confined concrete column specimens was assembled from an extensive survey of the open literature (Table 4.1 and 4.2). There are 18 specimens of CFST columns under concrete loaded mode and 32 specimens under whole-section loaded mode.

Table 4.1

Parameter settings and specifications of CFST columns.

Source of data	Specimens	D (mm)	t (mm)	f_y (MPa)	f_c (MPa)	N_{ue} (kN)	SI	σ_{sr} (MPa)	$\bar{\sigma}$ (MPa)	K
Yang et al.	400-36-31-WL-1	140	4.5	365	41	1,474.2	0.20	12.5	4.3	1.04
[20]	400-36-31-WL-2	140	4.5	365	41	1,458.1	0.20	14.9	5.6	0.98
	400-60-31-WL-1	140	4.5	365	68	1,880.9	0.14	13.0	4.7	1.2
	400-60-31-WL-2	140	4.5	365	68	1,891.8	0.14	16.9	6.4	1.34
	490-36-31-WL-1	140	4.5	463	41	1,771.1	0.24	9.8	5.1	0.63
	490-36-31-WL-2	140	4.5	463	41	1,753.0	0.24	9.7	6.6	0.7
	490-60-31-WL-1	140	4.5	463	68	2,268.3	0.16	17.1	10.2	1.27
	490-60-31-WL-2	140	4.5	463	68	2,222.3	0.16	21.1	8.8	1.17
	400-36-25-WL-1	114.3	4.5	440	41	1,161.0	0.26	23.6	13.7	0.56
	400-36-25-WL-2	114.3	4.5	440	41	1,167.1	0.26	20.0	15.6	0.57
	400-36-33-WL-1	165.2	5.0	416	41	2,035.4	0.21	16.9	6.4	1.03
	400-36-33-WL-2	165.2	5.0	416	41	2,040.3	0.21	14.0	5.6	0.92

	400-36-45-WL-1	165.2	3.7	383	41	1,692.3	0.15	9.2	2.7	1.35
	400-36-45-WL-2	165.2	3.7	383	41	1,723.4	0.15	11.5	4.1	1.13
Lin et al.	400-24-31WL-1	140	4.5	374	28	1275.3	0.24	11.1	5.3	0.56
[18]	400-24-31WL-2	140	4.5	374	28	1294.5	0.20	11.3	4.5	0.49
	400-36-31WL-1	140	4.5	374	39	1406.4	0.18	11.2	4.0	0.84
	400-36-31WL-2	140	4.5	374	39	1405	0.17	12.0	4.1	0.80
	400-48-31WL-1	140	4.5	374	52	1524.3	0.13	10.8	2.8	0.91
	400-48-31WL-2	140	4.5	374	52	1530.4	0.14	11.5	3.2	0.98
	490-24-31WL-1	140	4.5	463	28	1646.7	0.34	11.8	8.0	0.58
	490-24-31WL-2	140	4.5	463	28	1662.3	0.38	10.7	8.1	0.60
	490-36-31WL-1	140	4.5	463	39	1763.9	0.30	15.5	9.3	0.76
	490-36-31WL-2	140	4.5	463	39	1753.8	0.35	9.7	6.8	0.70
	490-48-31WL-1	140	4.5	463	52	1865.2	0.24	16.4	7.9	0.92
	490-48-31WL-2	140	4.5	463	52	1871.6	0.25	17.3	8.7	0.92
	400-36-26WL-1	216	8.2	381	41	3788.4	0.23	14.4	6.6	0.74
	400-36-26WL-2	216	8.2	381	41	3800.3	0.20	14.5	5.8	0.75
	400-36-36WL-1	191	5.3	383	41	2530.3	0.16	10.8	3.4	1.06
	400-36-36WL-2	191	5.3	383	41	2544.8	0.23	14.1	6.5	1.00
	400-36-48WL-1	216	4.5	372	41	2740.4	0.19	9.6	3.6	1.38
	400-36-48WL-2	216	4.5	372	41	2751.2	0.17	9.2	3.1	1.37
Zhao et al.	400-24-31CL-1	140	4.5	374	28	-	0.38	24.1	18.3	-
[19]	400-24-31CL-2	140	4.5	374	28	-	0.40	25.0	20.0	-
	400-36-31CL-1	140	4.5	374	39	-	0.30	24.6	14.7	-
	400-36-31CL-2	140	4.5	374	39	-	0.29	23.4	13.6	-
	400-48-31CL-1	140	4.5	374	52	-	0.21	20.2	8.5	-
	400-48-31CL-2	140	4.5	374	52	-	0.21	20.4	8.6	-
	490-24-31CL-1	140	4.5	463	28	-	0.52	35.0	36.3	-
	490-24-31CL-2	140	4.5	463	28	-	0.48	37.3	35.8	-
	490-36-31CL-1	140	4.5	463	39	-	0.40	35.9	28.7	-

490-36-31CL-2	140	4.5	463	39	-	0.40	36.6	29.3	-
490-48-31CL-1	140	4.5	463	52	-	0.35	34.3	24.0	-
490-48-31CL-2	140	4.5	463	52	-	0.35	38.1	26.6	-
400-36-26CL-1	216.3	8.2	381	41	-	0.29	28.5	16.6	-
400-36-26CL-2	216.3	8.2	381	41	-	0.28	27.3	15.3	-
400-36-36CL-1	190.7	5.3	381	41	-	0.21	18.6	7.8	-
400-36-36CL-2	190.7	5.3	381	41	-	0.24	19.5	9.4	-
400-36-48CL-1	216.3	4.5	372	41	-	0.19	10.4	3.9	-
400-36-48CL-2	216.3	4.5	372	41	-	0.12	6.2	1.5	-

Table 4.2

Parameter settings and specifications of FRP-confined concrete columns.

Source of data	Specimens	D (mm)	t (mm)	f_{frp} (MPa)	f_c (MPa)	SI	σ_{fr} (MPa)	$\bar{\sigma}$ (MPa)
Yang et al.	C24-1-1	150	0.25	3760	33	0.21	8	4.9
	C24-1-2	150	0.25	3760	33	0.21	6.2	3.8
	C24-2-1	150	0.5	3760	33	0.28	12.9	10.6
	C24-2-2	150	0.5	3760	33	0.3	14.7	13.0
	C24-3-1	150	0.75	3760	33	0.35	27.2	28.0
	C24-3-2	150	0.75	3760	33	0.29	28.5	24.3
	C36-1-1	150	0.25	3760	46	0.15	5.3	2.3
	C36-1-2	150	0.25	3760	46	0.13	4.9	1.9
	C36-2-1	150	0.5	3760	46	0.22	18.3	11.8
	C36-2-2	150	0.5	3760	46	0.26	11.5	8.8
	C36-3-1	150	0.75	3760	46	0.25	26.3	19.3
	C36-3-2	150	0.75	3760	46	0.31	27.2	24.8
	C48-1-1	150	0.25	3760	56	0.12	4.8	1.7
	C48-1-2	150	0.25	3760	56	0.12	4	1.4
	C48-2-1	150	0.5	3760	56	0.17	13.3	6.7

	C48-2-2	150	0.5	3760	56	0.18	17.4	9.2
	C48-3-1	150	0.75	3760	56	0.23	34.1	23.1
	C48-3-2	150	0.75	3760	56	0.17	24.6	12.3
Lin et al. [3]	C24-1-1	150	0.25	3760	32.1	0.18	9.5	5.0
	C24-1-2	150	0.25	3760	32.1	0.15	8.5	3.8
	C24-2-1	150	0.5	3760	32.1	0.25	30.8	22.6
	C24-2-2	150	0.5	3760	32.1	0.24	36.2	25.6
	C24-3-1	150	0.75	3760	32.1	0.33	32.5	31.5
	C24-3-2	150	0.75	3760	32.1	0.32	41.3	38.9
	C36-1-1	150	0.25	3760	43.3	0.12	8.3	2.9
	C36-1-2	150	0.25	3760	43.3	0.11	11	3.6
	C36-2-1	150	0.5	3760	43.3	0.24	24.4	17.2
	C36-2-2	150	0.5	3760	43.3	0.22	20.7	13.4
	C36-3-1	150	0.75	3760	43.3	0.27	30.4	24.1
	C36-3-2	150	0.75	3760	43.3	0.22	32.9	21.3
	C48-1-1	150	0.25	3760	53.7	0.08	12.3	2.9
	C48-1-2	150	0.25	3760	53.7	0.09	11.8	3.1
	C48-2-1	150	0.5	3760	53.7	0.15	23.1	10.2
	C48-2-2	150	0.5	3760	53.7	0.17	25.3	12.7
	C48-3-1	150	0.75	3760	53.7	0.23	26.6	18.0
	C48-3-2	150	0.75	3760	53.7	0.26	25.7	19.7

The data from Tables 4.1 and 4.2 were taken into Richard's model and the results of the comparison between the calculated and measured values of the compressive stresses are shown in Fig.4.6. It can be seen that the compressive strength prediction results are more accurate for CFST, and the prediction accuracy values are large for FRP-confined concrete.

And the data from Tables 4.1 and 4.2 were taken into Mander's model and the results of the comparison between the calculated and measured values of the compressive stresses are shown in Fig.4.7. It can be seen that the compressive strength prediction results are accurate for both of CFST and FRP-confined concrete.

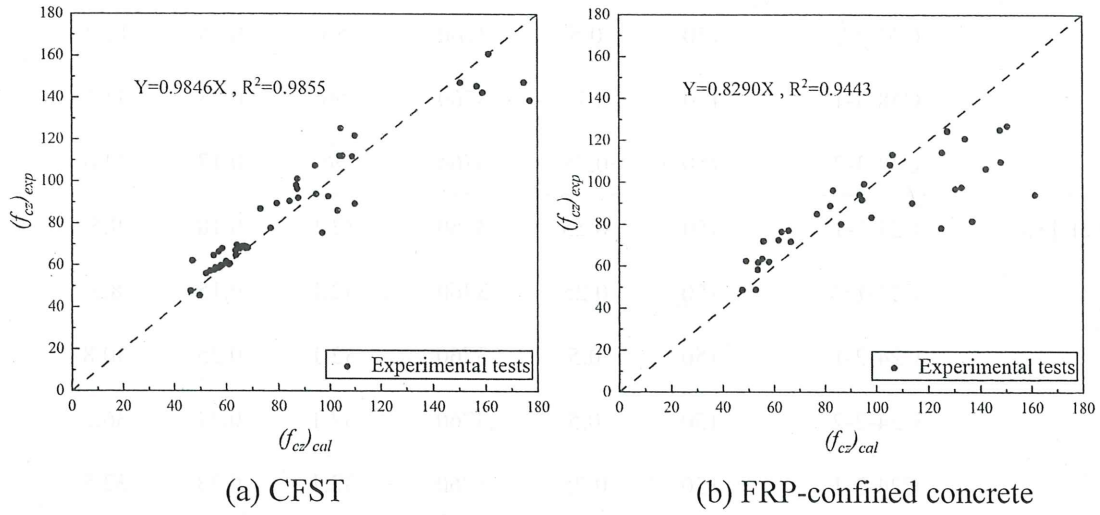


Fig. 4.6 Performance of Richard model: (a) CFST; (b) FRP-confined concrete

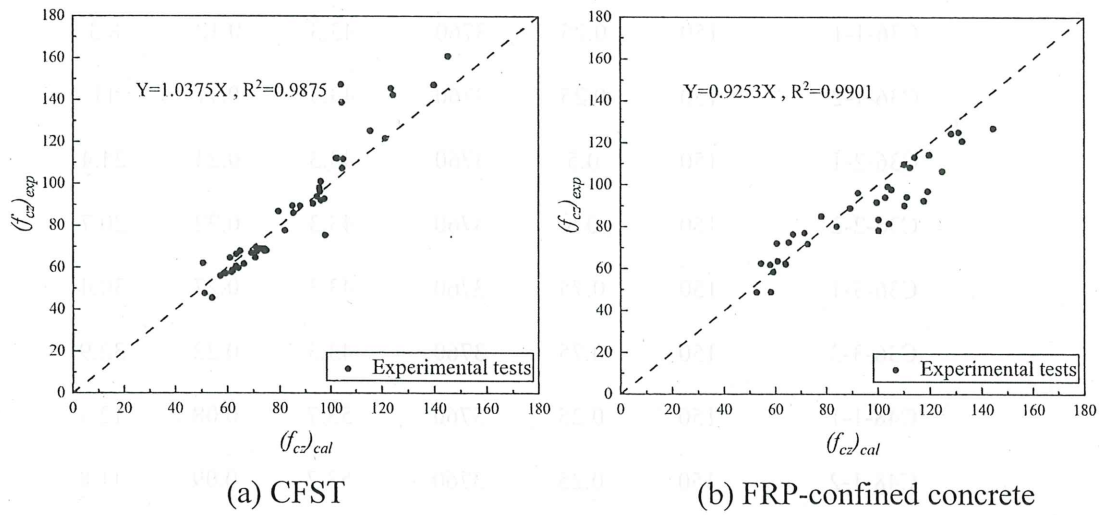


Fig. 4.7 Performance of Mander model: (a) CFST; (b) FRP-confined concrete

4.5.3. The load-bearing capacity model of CFST column based on energy path

The prediction of load-bearing capacity has been one of the main concerns of research for CFST columns. Therefore, it is necessary to establish an accurate load-bearing capacity model for CFST columns under whole-section loaded mode. Based on the analysis of the energy path for CFST column in Chapter 2, the energy path represents the trajectory of the energy absorbed by the steel tube and the concrete, then the energy ratio at the peak stress state can represent the proportion of the energy absorbed by the steel tube and the concrete.

Based on superposition of the loads on the steel tube and the concrete, the model of the axial capacity of CFST column is obtained as

$$N_{uc} = N_c + N_s \quad (4.10)$$

where N_c is the concrete's axial capacity calculated as $f_{cz}A_c$, and N_s is the steel tube's axial capacity.

The energy ratio represents the relative correlation between the energy absorbed by the steel tube and that absorbed by the core concrete; conversely, the concrete dominance indicator represents the exact correlation between the two for a given structural composition. The damage of CFST columns is ultimately a state instability phenomenon driven by energy. The concrete dominance indicator captures the weights for the contributions of the steel tube and the concrete to the axial capacity. For the steel tube, its axial capacity can be deduced from the accurately calculated axial capacity of the concrete and the concrete dominance indicator K . For the concrete, the main contribution of its absorbed energy is to the axial bearing capacity, while the energy absorbed by the steel tube resists both axial pressure and circumferential tension. Based on experimental, theoretical, and finite-element analysis results, under the peak state the circumferential stress σ_θ of the steel tube is taken as $0.6f_y$, and according to Von Mises yield criterion, the axial stress σ_z can be obtained as $0.55f_y$. Therefore, the axial capacity of the steel tube is introduced with a subdivision factor of 0.55 and is expressed as

$$N_s = 0.55 \frac{N_c}{K} \quad (4.11)$$

and so the prediction model proposed in this paper is

$$N_{uc} = f_{cz} A_c \left(1 + \frac{0.55}{K} \right) \quad (4.12)$$

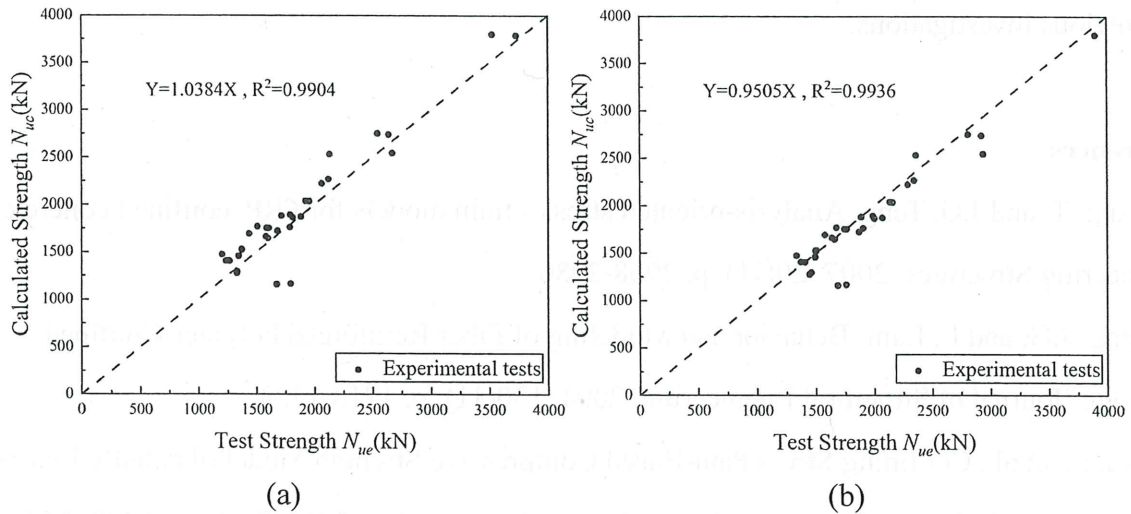


Fig. 4.8 Comparison between experimental values and those calculated by proposed model

To verify its accuracy and applicability, the calculated results are compared with experimental ones in Fig.4.8. Fig.4.8 contains graphs (a) and (b), representing the results of load-bearing capacity

calculations taken into account by the Richard strength model and the Mander strength model, respectively. The load-bearing capacity model of a CFST column as obtained from the energy relations is very effective.

4.6. Conclusions

In this study, the relationship between the actively confined concrete and passively confined concrete was clarified from the confining mechanism. The equivalence lateral stress was proposed to establish a connection between actively and passively confined concrete, rationalizing the application of compressive strength models for actively confined concrete in strength calculations for passively confined concrete.

1. The equivalent lateral stress was proposed from the analysis of stress path of passively confined concrete, namely CFST and FRP-confined concrete. The applicability of the active confined concrete strength models, which consist of Richard's and Mander's models, is verified by experimental data.
2. The axial capacity contribution is investigated by analyzing the energy ratio and leads to a load-bearing capacity model of CFST columns. The vertical capacity contribution of the steel tube is replaced by a weighted value of the axial capacity of the concrete and the concrete dominance indicator K . The predictions of the proposed model agreed well with experimental results from previous investigations.

References

- [1] Jiang, T. and J.G. Teng, Analysis-oriented stress-strain models for FRP-confined concrete. *Engineering Structures*, 2007. 29(11): p. 2968-2986.
- [2] Teng, J.G. and L. Lam, Behavior and Modeling of Fiber Reinforced Polymer-Confined Concrete. *Journal of Structural Engineering*, 2004. 130(11): p. 1713-1723.
- [3] Lin, S., et al., Confining Stress Path-Based Compressive Strength Model of Axially Loaded FRP-Confined Columns. *Journal of Composites for Construction*, 2021. 25(1): p. 04020077.
- [4] Popovics, S., A numerical approach to the complete stress-strain curve of concrete. *Cement and Concrete Research*, 1973. 3(5): p. 583-599.

- [5] Richart, F.E., A. Brandtæg, and R.L. Brown, A study of the failure of concrete under combined compressive stresses. University of Illinois. Engineering Experiment Station. Bulletin; no. 185, 1928.
- [6] Mander, J.B., M.J.N. Priestley, and R. Park, Theoretical Stress-Strain Model for Confined Concrete. *Journal of Structural Engineering*, 1988. 114(8): p. 1804-1826.
- [7] Lim, J.C. and T. Ozbakkaloglu, Confinement Model for FRP-Confined High-Strength Concrete. *Journal of Composites for Construction*, 2014. 18(4): p. 04013058.
- [8] Lam, L. and J.G. Teng, Design-oriented stress-strain model for FRP-confined concrete. *Construction and Building Materials*, 2003. 17(6): p. 471-489.
- [9] Lu, Z.-H. and Y.-G. Zhao, Suggested empirical models for the axial capacity of circular CFT stub columns. *Journal of Constructional Steel Research*, 2010. 66(6): p. 850-862.
- [10] Lai, M.H. and J.C.M. Ho, A theoretical axial stress-strain model for circular concrete-filled-steel-tube columns. *Engineering Structures*, 2016. 125: p. 124-143.
- [11] Lai, M.H., et al., A path dependent stress-strain model for concrete-filled-steel-tube column. *Engineering Structures*, 2020. 211: p. 110312.
- [12] Attard, M.M. and S. Setunge, Stress-Strain Relationship of Confined and Unconfined Concrete. *ACI Materials Journal*. 93(5).
- [13] Nanni, A. and N.M. Bradford, FRP jacketed concrete under uniaxial compression. *Construction and Building Materials*, 1995. 9(2): p. 115-124.
- [14] Samaan, M., A. Mirmiran, and M. Shahawy, Model of Concrete Confined by Fiber Composites. *Journal of Structural Engineering*, 1998. 124(9): p. 1025-1031.
- [15] Xiao, Y. and H. Wu, Compressive Behavior of Concrete Confined by Carbon Fiber Composite Jackets. *Journal of Materials in Civil Engineering*, 2000. 12(2): p. 139-146.
- [16] Lim, J.C. and T. Ozbakkaloglu, Unified Stress-Strain Model for FRP and Actively Confined Normal-Strength and High-Strength Concrete. *Journal of Composites for Construction*, 2015. 19(4): p. 04014072.
- [17] Shayanfar, J., J.A. Barros, and M. Rezazadeh, Unified model for fully and partially FRP confined circular and square concrete columns subjected to axial compression. *Engineering Structures*, 2022. 251: p. 113355.
- [18] Lin, S., Y.-G. Zhao, and L. He, Stress paths of confined concrete in axially loaded circular

concrete-filled steel tube stub columns. *Engineering Structures*, 2018. 173: p. 1019-1028.

[19] Zhao, Y.-G., et al., Loading paths of confined concrete in circular concrete loaded CFT stub columns subjected to axial compression. *Engineering Structures*, 2018. 156: p. 21-31.

[20] Yang, D. and Y.-G. Zhao, Energy path of circular concrete-filled steel tube stub columns under axial compression. *Journal of Constructional Steel Research*, 2024. 213: p. 108350.

CHAPTER 5. SUMMARIES

In this research, the interaction mechanism between the concrete and constrained material of passively confined concrete columns was investigated from an energy relations perspective for the first time. An energy path method was proposed to reflect the energy relations between the constrained material and the concrete, which was defined as the trajectory of energy ratio absorbed by the constrained material and concrete with the compressive strength. On the other hand, the energy ratio represents the relative correlation between the energy absorbed by the constrained material and the concrete. The state of energy distribution in passively confined concrete columns can be derived by analyzing the energy ratio at peak stress condition. The load-bearing capacity model of passively confined concrete column can be established from the energy weight perspective. The conclusions obtained in this research will be briefly summarized as follows:

Chapter 2. Energy path of circular concrete-filled steel tube stub columns under axial compression

1). The energy path represents the variation of the energy ratio (Q_c/Q_s) during the loading process, and the interaction mechanism between the components is investigated according to the regularity. After the initial phase, the energy ratio decreases indicating increased lateral expansion of the concrete, which means transferring energy to the external steel tube. Accordingly, the decrease in energy ratio begins to slacken after the steel tube enters the plastic phase. Finally, the energy ratio tends to stabilize during the hardening phase until the specimen reaches peak stress.

2). The energy path of CFST column is influenced by various parameters, namely, steel strength f_y , concrete strength f_c , and ratio of column diameter to steel tube thickness D/t . The energy paths for different test conditions were represented by the concrete dominance indicator K . The findings of the experiment revealed that the concrete dominance indicator K rose with f_c/f_y and D/t ratios, indicating the increased contribution of core concrete to the energy path compared to that of steel tube.

3). The force state of CFST columns during the loading process was further analyzed by comparing its energy path with stress path of constrained concrete. The energy paths were found to be more sensitive to D/t ratio and concrete strength f_c ; nevertheless, the stress paths were found to be more sensitive to the steel strength f_y .

4). One model for determining concrete compressive strength and load-bearing capacity of CFST columns under whole section loading was proposed from an energy relation perspective. The predictions by proposed model and the tested results agreed fairly well.

Chapter 3. Energy path of FRP-confined concrete stub columns subjected to axial compression

1). The energy path represents the variation of the energy ratio (Q_f/Q_c) during the loading process, and the interaction mechanism between the components is investigated according to the regularity. At the initial stage, as the deformations of concrete and FRP jacket are harmonized, the energy ratio varies little and close to a constant value. When the axial stress exceeds the unconfined concrete strength, the energy path exhibits a transition stage, during which microcracks start to develop rapidly and energy ratio increases. The rate of energy transfer from concrete to FRP jacket also stabilizes after stress redistribution, which leads to a near-linear branch of the energy path until the FRP jacket fractures.

2). The energy path of FRP-confined concrete column is influenced by column parameters, namely, concrete strength f_c , and ratio of column diameter to FRP jacket thickness D/t . The energy paths for different test conditions were represented by the concrete dominance indicator K . The findings of the experiment revealed that the concrete dominance indicator K increased with f_c but decreased with D/t , indicating the confinement effective of FRP jacket was more significant for the specimen with a smaller K .

3). One model for determining concrete compressive strength of FRP-confined concrete columns under axial loading was proposed from an energy relation perspective. The predictions by proposed model and the tested results agreed well.

Chapter 4. Numerical study of the behaviors of axially loaded large-diameter CFT stub columns

1). The equivalent lateral stress was proposed from the analysis of stress path of passively confined concrete, namely CFST and FRP-confined concrete. The applicability of the active confined concrete strength models, which consist of Richard's and Mander's models, is verified by experimental data.

2). The axial capacity contribution is investigated by analyzing the energy ratio and leads to a load-bearing capacity model of CFST columns. The vertical capacity contribution of the steel tube is

replaced by a weighted value of the axial capacity of the concrete and the concrete dominance indicator K . The predictions of the proposed model agreed well with experimental results from previous investigations.

International Conference

- [1] H. Yang and Y. Gao, "Effect of concrete strength on the load-carrying capacity of reinforced concrete columns," *Journal of Bridge Engineering*, vol. 1, no. 1, pp. 1-10, 1996.
- [2] H. Yang and Y. Gao, "Effect of concrete strength on the load-carrying capacity of reinforced concrete columns," *Journal of Bridge Engineering*, vol. 1, no. 1, pp. 1-10, 1996.
- [3] H. Yang and Y. Gao, "Effect of concrete strength on the load-carrying capacity of reinforced concrete columns," *Journal of Bridge Engineering*, vol. 1, no. 1, pp. 1-10, 1996.
- [4] H. Yang and Y. Gao, "Effect of concrete strength on the load-carrying capacity of reinforced concrete columns," *Journal of Bridge Engineering*, vol. 1, no. 1, pp. 1-10, 1996.
- [5] H. Yang and Y. Gao, "Effect of concrete strength on the load-carrying capacity of reinforced concrete columns," *Journal of Bridge Engineering*, vol. 1, no. 1, pp. 1-10, 1996.
- [6] H. Yang and Y. Gao, "Effect of concrete strength on the load-carrying capacity of reinforced concrete columns," *Journal of Bridge Engineering*, vol. 1, no. 1, pp. 1-10, 1996.
- [7] H. Yang and Y. Gao, "Effect of concrete strength on the load-carrying capacity of reinforced concrete columns," *Journal of Bridge Engineering*, vol. 1, no. 1, pp. 1-10, 1996.
- [8] H. Yang and Y. Gao, "Effect of concrete strength on the load-carrying capacity of reinforced concrete columns," *Journal of Bridge Engineering*, vol. 1, no. 1, pp. 1-10, 1996.
- [9] H. Yang and Y. Gao, "Effect of concrete strength on the load-carrying capacity of reinforced concrete columns," *Journal of Bridge Engineering*, vol. 1, no. 1, pp. 1-10, 1996.
- [10] H. Yang and Y. Gao, "Effect of concrete strength on the load-carrying capacity of reinforced concrete columns," *Journal of Bridge Engineering*, vol. 1, no. 1, pp. 1-10, 1996.

Domestic Conference

- [1] H. Yang and Y. Gao, "Effect of concrete strength on the load-carrying capacity of reinforced concrete columns," *Journal of Bridge Engineering*, vol. 1, no. 1, pp. 1-10, 1996.
- [2] H. Yang and Y. Gao, "Effect of concrete strength on the load-carrying capacity of reinforced concrete columns," *Journal of Bridge Engineering*, vol. 1, no. 1, pp. 1-10, 1996.
- [3] H. Yang and Y. Gao, "Effect of concrete strength on the load-carrying capacity of reinforced concrete columns," *Journal of Bridge Engineering*, vol. 1, no. 1, pp. 1-10, 1996.
- [4] H. Yang and Y. Gao, "Effect of concrete strength on the load-carrying capacity of reinforced concrete columns," *Journal of Bridge Engineering*, vol. 1, no. 1, pp. 1-10, 1996.
- [5] H. Yang and Y. Gao, "Effect of concrete strength on the load-carrying capacity of reinforced concrete columns," *Journal of Bridge Engineering*, vol. 1, no. 1, pp. 1-10, 1996.
- [6] H. Yang and Y. Gao, "Effect of concrete strength on the load-carrying capacity of reinforced concrete columns," *Journal of Bridge Engineering*, vol. 1, no. 1, pp. 1-10, 1996.
- [7] H. Yang and Y. Gao, "Effect of concrete strength on the load-carrying capacity of reinforced concrete columns," *Journal of Bridge Engineering*, vol. 1, no. 1, pp. 1-10, 1996.
- [8] H. Yang and Y. Gao, "Effect of concrete strength on the load-carrying capacity of reinforced concrete columns," *Journal of Bridge Engineering*, vol. 1, no. 1, pp. 1-10, 1996.
- [9] H. Yang and Y. Gao, "Effect of concrete strength on the load-carrying capacity of reinforced concrete columns," *Journal of Bridge Engineering*, vol. 1, no. 1, pp. 1-10, 1996.
- [10] H. Yang and Y. Gao, "Effect of concrete strength on the load-carrying capacity of reinforced concrete columns," *Journal of Bridge Engineering*, vol. 1, no. 1, pp. 1-10, 1996.

List of Publications

Journal papers

- [1] Di Yang and Yan-Gang Zhao, Energy path of circular concrete-filled steel tube stub columns under axial compression. *Journal of Constructional Steel Research*, 2024. 213: p. 108350.
- [2] Di Yang and Yan-Gang Zhao, Energy path of FRP-confined concrete stub columns subjected to axial compression. (Draft in preparation)
- [3] Di Yang and Yan-Gang Zhao, Strength models for circular steel-confined concrete based on equivalent lateral stress. (Draft in preparation)

International Conference:

- [4] Di Yang and Yan-Gang Zhao, Energy method of confined concrete in axially compressed circular concrete-filled steel tube columns, *International Symposium on Emerging Developments and Innovative Applications of Reliability Engineering and Risk Managements (EDIARR 2022)* (Taipei, China, 2022.10)
- [5] Di Yang and Yan-Gang Zhao, Confinement mechanism discussion in circular concrete-filled steel tube columns under axial compression, *3rd International Joint Conference on Energy, Electrical and Power Engineering (CoEEPE 2024)* (Melbourne, Australia, 2023.11)

Domestic Conference:

- [6] Di Yang, Hai-Zhong Zhang and Yan-Gang Zhao, Preparation and mechanical research on artificial transversely isotropic rock, *Summaries of Technical Papers of Annual Meeting, AIJ 2021*, pp. 317-318, East Sea.
- [7] Di Yang, Hai-Zhong Zhang and Yan-Gang Zhao, Compressive strength model for confined concrete in circular CFT stub columns based on energy method, *Summaries of Technical Papers of Annual Meeting, AIJ 2022*, pp. 1147-1148, Hokkaido.
- [8] Di Yang and Yan-Gang Zhao, Discussion on lateral stress of confined concrete in circular CFT stub columns, *Summaries of Technical Papers of Annual Meeting, AIJ 2023*, pp. 1275-1276, Kyoto.

[9] Di Yang and Yan-Gang Zhao, Interaction mechanism of components in circular concrete-filled steel tube columns under axial compression, International Forum on Reliability Engineering and Management (IFRERM 2023) (Kanagawa, Japan, 2023.02)